Universidad de Concepción

Facultad de Ingeniería

Departamento de Ingeniería Química

DEVELOPMENT AND VALIDATION OF A CONDUCTIVE HYDROGEL AS A WOUND HEALING ACCELERATOR

POR

ISLEIDY DE LA CARIDAD RUÍZ PÉREZ

Tesis para optar al grado de Doctor en Ciencias de la Ingeniería con mención en Ingeniería Química

TUTORA: Prof. Katherina Fernández Elgueta, PhD
Departamento de Ingeniería Química
Universidad de Concepción

CONCEPCIÓN, CHILE 2025

DEDICATORIA

A mi esposo y mi familia, por su amor incondicional, su paciencia y apoyo constante, y por ser siempre ejemplo de esfuerzo, fe y fortaleza que me inspiraron a seguir adelante.

AGRADECIMIENTOS

Mis más sinceros agradecimientos quiero expresarlos:

A mi esposo, por acompañarme en cada paso de este camino, celebrar mis logros y sostenerme en los momentos de mayor cansancio. Tu comprensión, paciencia y fortaleza fueron la base sobre la que construí este sueño.

A mi familia, especialmente a mi mamá Glennys, mis abuelos Teresa y Víctor, mi hermano Víctor, y mis suegros Maira y Jeovanis mi cuñada Ivettsy, por su amor incondicional, su paciencia y comprensión en los momentos de mayor exigencia, por su cariño y apoyo constante durante todo este proceso, por motivarme a seguir adelante incluso en los días más difíciles, y por ser siempre ejemplo de esfuerzo, fe y perseverancia en cada uno de mis pasos.

A mi tutora, Dra. Katherina Fernández Elgueta, por su guía, exigencia y acompañamiento en este arduo camino del doctorado, tanto en mi trabajo académico como en mi formación profesional.

Al Dr. Claudio Aguayo Tapia, por su dedicación, orientación y apoyo constante.

A mi familia cubana en Chile, con la que he compartido momentos inolvidables durante estos años. En especial, a mis queridos amigos Martha, Karel y Jenny, por abrirme las puertas de su casa desde el primer día, brindarme su amistad sincera y su ayuda desinteresada; por haber sido mi familia en la distancia y estar siempre ahí. Agradezco también a mis amigos Daviel, Maray, Luisbel, Yenisleidy, Libet, Eduardo, Pablo, Maidelys, Dailenys y Jessica, por los lindos momentos compartidos, las risas y el apoyo constante que hicieron de esta etapa una experiencia más amena y memorable.

Agradezco profundamente al Prof. Dr. Guilherme Ferreira Caetano por su guía, apoyo y dedicación durante mi pasantía en el University Center of Hermínio Ometto Foundation (FHO), Araras, Brasil. Extiendo mi gratitud a la Prof. Maria

Esméria Corezola do Amaral y a las alumnas Julia S., Cintia, Julia G. y Victoria, por su compromiso, colaboración y valiosa ayuda durante mi estadía en el laboratorio, que contribuyó significativamente al desarrollo de este trabajo.

Asimismo, agradezco de corazón a la familia de la señora Ignez, por haberme recibido con tanto cariño, acogiéndome en su hogar y haciéndome sentir parte de su familia durante aquellos meses en Brasil.

A todos mis compañeros de doctorado, por su apoyo constante, colaboración y amistad a lo largo de estos años. Gracias por compartir conmigo no solo las actividades académicas y de investigación, sino también los desafíos y las alegrías de esta etapa, dejando recuerdos imborrables.

A todos los profesores y personal del Departamento de Ingeniería Química (DIQ), quienes con su dedicación, enseñanza y amabilidad aportaron significativamente a mi formación profesional y personal.

Finalmente, todo el sacrificio que implicó dejar a mi familia, mis amigos y mi país ha sido recompensado con esta invaluable experiencia en Chile, tanto en lo personal como en lo profesional.

A todos, mi más sincero y eterno agradecimiento.

CONTENT

List of Abbreviations

DNA – Deoxyribonucleic acid

cDNA – Complementary deoxyribonucleic acid

$AgNO_3$ – Silver nitrate

Arg1 – Arginase 1

RNA – Ribonucleic acid

CCD – Central Composite Design

CD68 – CD68 glycoprotein

Cl^- – Chloride ion

COL I – Type I collagen

COL III – Type III collagen

COOH – Carboxyl group (carboxylic acid)

CONH – Secondary amide group

$CONH_2$ – Primary amide group

CS – Chitosan

DA – Dopamine

DMEM – Dulbecco's Modified Eagle Medium

DMSO – Dimethyl sulfoxide

FBS – Fetal bovine serum

FDA – Food and Drug Administration

FTIR – Fourier Transform Infrared Spectroscopy

GAPDH – Glyceraldehyde-3-phosphate dehydrogenase

GO – Graphene oxide

HDF – Human dermal fibroblast cell line

HCl – Hydrochloric acid

H_2O_2 – Hydrogen peroxide

H_3PO_4 – Phosphoric acid

H_2SO_4 – Sulfuric acid

hUC-MSC – Human umbilical cord–derived mesenchymal stem cells

H&E – Hematoxylin and eosin

IL-1β – Interleukin 1β

IL-1rn – Interleukin-1 receptor antagonist

IL-6 – Interleukin 6

IL-10 – Interleukin 10

K+ – Potassium ion

$KMnO_4$ – Potassium permanganate

L929 – Mouse fibroblast cell line

ECM – Extracellular matrix

MPO – Myeloperoxidase

MTT – 3-(4,5-Dimethylthiazol-2-yl)-2,5-diphenyltetrazolium bromide

Na+ – Sodium ion

NaOH – Sodium hydroxide

NH_2 – Amino group

OH – Hydroxyl group

PDA – Polydopamine

PDGF – Platelet-derived growth factor

PEG – Polyethylene glycol

PF (PEO–PPO–PEO) – Pluronic F-127 (polyethylene oxide–polypropylene oxide–polyethylene oxide)

PCL – Polycaprolactone

PLA – Poly(lactic acid)

TEER / PTE – Transepithelial electrical resistance / Potential

PVA – Poly(vinyl alcohol)

PVP – Poly(vinylpyrrolidone)

PBS – Phosphate-buffered saline

rGO – Reduced graphene oxide

ROS – Reactive oxygen species

RSM – Response Surface Methodology

RT-qPCR – Reverse transcription–quantitative polymerase chain reaction

R^2 – Coefficient of determination

SEM – Scanning electron microscopy

SO_3H – Sulfonic acid group (sulfonate group)

TGF-β – Transforming growth factor beta

Tris – Tris(hydroxymethyl)aminomethane

XRD – X-ray diffraction

VEGF – Vascular endothelial growth factor

List of Figures

List of Tables

Abstract

Chronic and slow-healing wounds present a clinical challenge, as they are associated with persistent inflammatory processes, infections, and impaired tissue regeneration. In this context, hydrogels have become established as an innovative therapeutic strategy due to their ability to maintain a moist microenvironment and promote tissue regeneration. This research aimed to develop and evaluate a hydrogel composed of chitosan (CS), reduced graphene oxide (rGO), and Pluronic F127 (PF), with the hypothesis that the inclusion of rGO would improve the material's physicochemical properties and provide a suitable microenvironment to accelerate skin healing. The hydrogel was optimized using a factorial experimental design and characterized from a physicochemical perspective, confirming that the incorporation of rGO increased stiffness, polymer network stability, and electrical conductivity, while PF contributed to flexibility and thermal stability. In vitro assays demonstrated significant antibacterial activity against Gram-positive and Gram-negative bacteria, high cell viability in dermal fibroblasts, and stimulation of cell migration. In murine models, the tannin-loaded hydrogel (TA) promoted faster and more organized wound closure than controls, accompanied by an early transition from the inflammatory to the proliferative phase, greater deposition of type I and III collagen, sustained angiogenesis, and abundant granulation tissue. Molecular analyses (RT-qPCR and Western blot) showed a decrease in the expression of proinflammatory mediators (IL-6, IL-1β), an increase in anti-inflammatory cytokines (IL-10, IL-1rn), and macrophage polarization toward the M2 phenotype (Arg1), which favored the resolution of inflammation and tissue regeneration. In the porcine model, which more closely resembles human physiology, the developed hydrogel achieved complete wound closure in 21 days, with results comparable to a commercial dressing (Nexcare™), but with additional advantages in dermal tissue organization, skin

appendage regeneration, and absence of fibrosis. In conclusion, the results confirm the hypothesis: the incorporation of rGO into chitosan-Pluronic F127 hydrogels confers physicochemical and biological properties that enhance skin healing, positioning the CS-rGO-PF hydrogel as a promising biomaterial for clinical applications in advanced wound treatment.

Resumen

Las heridas crónicas y de difícil cicatrización representan un desafío clínico, ya que se asocian con procesos inflamatorios persistentes, infecciones y una regeneración tisular deficiente. En este contexto, los hidrogeles se han consolidado como una estrategia terapéutica innovadora por su capacidad para mantener un microambiente húmedo y favorecer la regeneración de tejidos. La presente investigación tuvo como objetivo desarrollar y evaluar un hidrogel compuesto por quitosano (CS), óxido de grafeno reducido (rGO) y Pluronic F127 (PF), con la hipótesis de que la inclusión de rGO mejoraría las propiedades fisicoquímicas del material y proporcionaría un microambiente adecuado para acelerar la cicatrización cutánea. El hidrogel fue optimizado mediante un diseño experimental factorial y caracterizado desde el punto de vista fisicoquímico, confirmando que la incorporación de rGO aumentó la rigidez, la estabilidad de la red polimérica y la conductividad eléctrica, mientras que el PF contribuyó a la flexibilidad y estabilidad térmica. Los ensayos *in vitro* evidenciaron actividad antibacteriana significativa frente a bacterias Gram positivas y Gram negativas, alta viabilidad celular en fibroblastos dérmicos y estimulación de la migración celular. En modelos murinos, el hidrogel cargado con Tanino (TA) promovió un cierre de heridas más rápido y organizado que los controles, acompañado de una transición temprana de la fase inflamatoria a la proliferativa, mayor deposición de colágeno tipo I y III, angiogénesis sostenida y abundante tejido de granulación. Los análisis moleculares (RT-qPCR y Western blot) mostraron una disminución en la expresión de mediadores proinflamatorios (IL-6, IL-1β), incremento de citocinas antiinflamatorias (IL-10, IL-1rn) y polarización de macrófagos hacia el fenotipo M2 (Arg1), lo que favoreció la resolución de la inflamación y la regeneración tisular. En el modelo porcino, más cercano a la fisiología humana, el hidrogel desarrollado logró un cierre completo de heridas en 21 días, con

resultados comparables a un apósito comercial (Nexcare™), pero con ventajas adicionales en la organización del tejido dérmico, regeneración de anexos cutáneos y ausencia de fibrosis. En conclusión, los resultados confirman la hipótesis planteada: la incorporación de rGO en hidrogeles de quitosano-Pluronic F127 confiere propiedades químico-físicas y biológicas que potencian la cicatrización cutánea, posicionando al hidrogel CS-rGO-PF como un biomaterial prometedor para aplicaciones clínicas en el tratamiento avanzado de heridas.

Introduction

Cutaneous wounds, particularly those that are chronic or difficult to heal, represent a significant clinical challenge due to persistent inflammation, a high risk of infection, and the impaired tissue regeneration that characterizes these conditions[1,2]. Such lesions not only compromise patients' quality of life but also impose a substantial and growing healthcare burden worldwide, owing to prolonged treatment durations, recurrent hospitalizations, and intensive use of clinical resources[3,4]. Consequently, there is increasing interest in the development of advanced biomaterials capable of modulating the wound microenvironment, promoting functional tissue regeneration, and shortening healing times[5].

Among the most promising therapeutic strategies, hydrogels have emerged as valuable systems due to their ability to maintain a moist environment, absorb exudates, allow gas exchange, and serve as versatile platforms for the incorporation of bioactive agents[6,7]. However, conventional hydrogels often exhibit mechanical limitations, low structural stability, and limited intrinsic bioactivity, which restrict their effectiveness in more complex clinical contexts[8,9]. In this regard, the incorporation of conductive nanomaterials, such as reduced graphene oxide (rGO), has shown remarkable potential to enhance the physicochemical and biological properties of polymeric matrices[10]. rGO increases the rigidity, stability, and electrical conductivity of the material, attributes that support cell migration, tissue organization, and the restoration of the natural bioelectrical signals of injured skin[11]. Pluronic F-127 (PF), a triblock copolymer, contributes to the flexibility, thermal stability, and three-dimensional structuring of the hydrogel, generating a more robust and functional polymeric network[12]. Chitosan (CS), used as the primary matrix, provides biocompatibility, inherent antimicrobial activity, and the ability to interact with extracellular matrix proteins essential for wound healing[13,14].

The combination of CS, rGO, and PF thus results in a hybrid hydrogel with optimized physicochemical properties, designed to modulate the wound microenvironment and enhance cutaneous regeneration[15]. This system can be further strengthened through the incorporation of bioactive compounds such as tannins (TA), natural polyphenols widely distributed in plants—particularly in barks, leaves, fruits, and seeds—known for their ability to form stable complexes with proteins and polysaccharides, a property underlying their astringent effects and traditional medicinal applications[16].

From a biomedical perspective, tannins have gained increasing attention due to their notable antioxidant, anti-inflammatory, antimicrobial, and wound-healing activities[17]. Their structure, rich in hydroxyl groups, enables them to neutralize reactive oxygen species, modulate immune responses, and protect tissues against microbial and oxidative damage[18,19]. These characteristics position tannins as promising bioactive agents for incorporation into wound dressings and advanced biomaterials aimed at tissue regeneration[20].

Taking the above premises into consideration, the following hypotheses and objectives are proposed.

Hypothesis

The incorporation of reduced graphene oxide into chitosan–Pluronic F127-based hydrogels will enhance the stiffness and fluid absorption properties of these materials in simulated human fluids and provide electrical conductivity, thereby creating a suitable microenvironment for orderly cell migration and ultimately accelerating the skin wound-healing process.

General Objective

- To develop hydrogels based on chitosan-pluronic F127 and reduced graphene oxide (CS-PF-rGO), evaluating their conductive, physicochemical, and functional properties for their potential application in the skin healing process.

Specific Objectives

- To evaluate the influence of modifying the proportions of rGO and PF on the conductive and physicochemical properties of the CS-PF-rGO hydrogel.
- To determine the absorption kinetics of the previously synthesized hydrogels in simulated human fluids.
- To evaluate the cytotoxicity of the hydrogels in cell models (*in vitro*).
- To validate the healing and irritant effects of the hydrogels in animal models (*in vivo*).

Chapter 1: Background

1.1 The Skin

The skin is the largest organ of the human body and constitutes the first line of defense against external aggressions[21–23]. When its integrity is compromised by trauma, surgical interventions, or disease, a complex physiological process known as wound healing is triggered to restore the structure and function of the damaged tissue[24]. This process involves a sequence of cellular and molecular events organized into four main phases: hemostasis, inflammation, proliferation, and remodeling (**Figure 1.1A**)[25].

Hemostasis (coagulation): This phase occurs immediately after injury to stop blood loss. Platelets are activated and release growth factors such as PDGF (platelet-derived growth factor) and TGF-β (transforming growth factor beta), which promote cellular activation and the formation of a fibrin network that serves as a provisional matrix for cell migration[26,27].

Inflammation: During this stage, which may last between 24 and 72 hours, neutrophils and macrophages migrate to the wound site to eliminate pathogens, dead cells, and cellular debris. Macrophages also secrete cytokines and growth factors that regulate the transition to the proliferative phase[28,29].

Proliferation: This phase is characterized by the migration and proliferation of fibroblasts, keratinocytes, and endothelial cells. Fibroblasts produce collagen and other extracellular matrix components, while keratinocytes re-epithelialize the injured surface. Angiogenesis also occurs during this stage, restoring oxygen and nutrient supply to the regenerating tissue[30,31].

Remodeling (maturation): This phase may last weeks or months, depending on the type and extent of the wound. The initially deposited type III collagen is replaced by type I collagen, which provides greater mechanical strength to the

tissue. Additionally, the extracellular matrix is reorganized, and excessive vascularization is reduced[32,33].

The healing process can be compromised by various intrinsic factors, such as advanced age, metabolic diseases (e.g., diabetes mellitus), or vascular disorders, and extrinsic factors, such as local infections, tissue dehydration, or hypoxia in the affected area[6,7]. These factors can slow down or even halt tissue repair, giving rise to chronic or non-healing wounds, which significantly increase the risk of complications such as secondary infections, necrosis, or persistent ulcerations [34,35]. In response to these challenges, biomedical research has focused on developing new therapeutic strategies capable of providing a favorable microenvironment for each phase of the healing process[36].

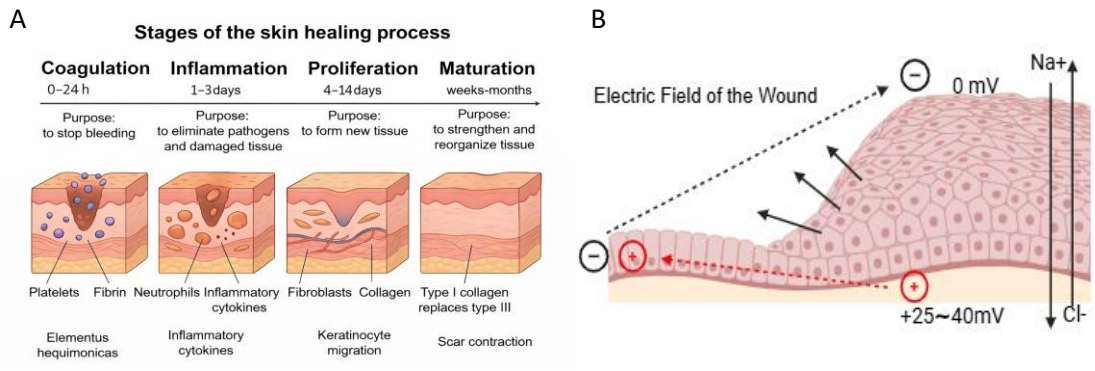

Figure 1.1. (A) diagram of the stages of the epithelial regeneration process: coagulation, inflammation, proliferation, and maturation, and (B) description of the generation of electric fields in wounds from the combination of Na+ and Cl− ions. Source (Own elaboration).

1.1.1 Endogenous skin field and Conductivity

The skin, in addition to being an essential physical and sensory barrier, exhibits inherent bioelectrical activity that plays a fundamental role in various physiological processes, including wound healing[37]. This activity originates in the epidermis,

where the asymmetric distribution of ions across the epithelium generates a transepithelial potential (TEP) (**Figure 1.1B**)[38]. Under normal conditions, this electrical gradient is maintained by the functioning of ion pumps and transport channels, reaching estimated values between 10 and 60 mV in intact epithelial tissues[39]. When an injury occurs, the TEP is locally interrupted, generating an electrical "short circuit" in the affected area. This loss of polarity causes an abrupt drop in electrical potential, resulting in a directional current flowing from healthy areas toward the wound site[40]. This novel electrical gradient acts as a bioelectrical signal that guides the migration of key cells in tissue repair, such as keratinocytes, fibroblasts, and macrophages, thus promoting tissue regeneration[41].

Knowledge of this bioelectrical signaling has driven the development of biomimetic materials capable of modulating or amplifying the endogenous electric field during healing[42]. In this context, conductive hydrogels have garnered increasing interest, as they not only maintain a moist environment conducive to healing but also allow the conduction of electrical currents[43]. This property facilitates galvanotaxis—cell migration induced by electric fields—and contributes to faster and more efficient tissue repair[44]. These materials represent a new generation of functional biomaterials, capable of channeling endogenous electrical signals to the site of injury, thereby enhancing cell reorganization and accelerating the various events of the healing process[45]. Their integration into advanced dressings opens new perspectives for the effective treatment of acute and chronic wounds.

1.2 Hydrogels

Hydrogels have emerged as an advanced alternative to traditional dressings, far surpassing bandages, gauze, foams, or films, due to their three-dimensional structure, high affinity for water, and compatibility with biological tissues[46].

These hydrophilic polymeric structures are capable of absorbing large volumes of exudate, maintaining a moist environment ideal for tissue regeneration, and facilitating cell migration and proliferation, thus promoting faster and more efficient healing[47,48]. One of their key advantages lies in their ability to biodegrade in a controlled manner, preventing further damage to the surrounding tissue during dressing changes[49,50]. This ability is closely related to the presence of hydrophilic functional groups such as -NH_2, -COOH, -OH, -$CONH_2$, -CONH, and -SO_3H, which facilitate both water retention and the formation of porous polymer networks[51,52]. Unlike other materials, hydrogels possess a porous morphology that mimics the extracellular matrix (ECM), creating a favorable environment for cell growth, adhesion, and migration[53–55]. Furthermore, their porosity facilitates gas and nutrient exchange, and their flexibility makes them ideal for areas with constant movement[56].

1.2.1 Classification of Hydrogels

The versatility of hydrogels allows for their classification based on multiple criteria, as shown in **Table 1.1**. Hydrogels developed from natural polymers—mainly polysaccharides and proteins—exhibit a three-dimensional architecture that mimics the microenvironment of the extracellular matrix, conferring excellent biocompatibility[57,58]. Among the most commonly used natural polymers in hydrogel formulation are cellulose[59,60], chitosan[61,62], alginate[20,63], and collagen[64]. These materials maintain biochemical properties compatible with the host tissue[65]; however, they have certain limitations, such as low mechanical strength, difficulty in controlling drug release, poor reproducibility, and, in some cases, potential immunogenic responses. Therefore, they are frequently combined with synthetic polymers to enhance their structural and functional properties[66,67].

Table 1.1: Classification of Hydrogels.

Classification	Categories	Reference
Origin	• Natural • Synthetic • Hybrid	[68]
Composition	• Homopolymers • Copolymers • Multipolymers • Interpenetrating networks	[69]
Crosslinking	• Physical • Chemical • Hybrid	[68,70]
Stimuli-responsive	• Thermosensitive • pH-sensitive • Photosensitive • Enzyme-sensitive	[69,71,72]
Structure	• Amorphous • Semicrystalline	[68]
Degradation	• Biodegradable • Bioabsorbable • Bioerodible • Controlled degradation	[70]
Ionic charge	• Non-ionic • Ionic • Zwitterionic • Amphoteric	[71,72]

In contrast, synthetic hydrogels offer greater versatility in the design of mechanical, physicochemical, and degradation properties[73]. These are obtained through the polymerization of monomers, which provides greater uniformity in their composition and behavior. Among the most commonly used synthetic polymers are polyethylene glycol (PEG)[74,75], poly(vinyl alcohol) (PVA)[76,77], polycaprolactone (PCL)[78,79], poly(vinylpyrrolidone) (PVP)[80,81], and poly(lactic acid) (PLA)[82,83]. Hydrogels have also been developed from advanced synthetic biopolymers, such as self-assembling peptides[84] and DNA-based structures[85–87], which provide specific functionalities such as responding to external stimuli or the targeted release of therapeutic agents.

Based on the type of forces that bind their polymer chains, hydrogels are classified as physical, chemical, and hybrid (a combination of both)[88]. Physical hydrogels are stabilized by non-covalent interactions such as hydrogen bonds, ionic forces, Van der Waals interactions, or hydrophobic forces[89]. These weak bonds give them reversible properties in response to external stimuli, such as changes in temperature or pH, making them thermo- and stimulus-responsive[90,91]. However, their mechanical stability and strength in physiological environments may be limited[92]. In contrast, chemical (or permanent) hydrogels are formed by networks of covalent bonds between polymer chains, which gives them greater mechanical strength, lower solubility in aqueous media, and a non-reversible response to stimuli[67,69]. Its crosslinking is achieved through agents such as glutaraldehyde, genipin, diglycidyl ether, or methylenebisacrylamide, and allows adjustment of key properties such as swelling, biodegradability, or resistance through chemical modification strategies[93,94].

In recent years, the design of hybrid hydrogels has gained relevance by combining physical and covalent bonds in a single structure. This integration allows for continued responsiveness to environmental stimuli—such as pH, ionic

strength, temperature, or electric fields—along with greater structural stability[95,96]. Furthermore, the combination of natural and synthetic polymers allows for the convergence of the advantages of both types: biocompatibility, specific functionality, and improved mechanical properties, thus optimizing their performance in clinical applications[97]. One of the most notable advantages of hydrogels is their ability to be functionalized with bioactive agents—such as antibacterials[98], growth factors[99,100], antioxidants[101,102], or stem cells[103,104]—which increases their therapeutic efficacy in the treatment of acute, chronic, and infected wounds. Furthermore, so-called smart hydrogels, capable of responding to stimuli such as pH, temperature, or electric fields, enable the development of advanced controlled drug delivery systems, promoting targeted and personalized tissue regeneration[105,106]. Among these innovations, conductive hydrogels, which incorporate materials such as graphene, metal oxides, or doped polymers, have shown promising results in complex wounds[107,108]. These materials reproduce and amplify the endogenous bioelectrical signals of the injured tissue, promoting cell migration (galvanotaxis) and accelerating healing[109].

1.2.2 Hydrogels for wound healing

In recent years, hydrogels have garnered increasing interest in the field of biomedicine, particularly in wound healing, due to their high biocompatibility, water retention capacity, and adjustable mechanical properties[97,110]. A material is considered biocompatible when it can coexist with biological tissues without inducing an adverse response or compromising cell viability[111,112]. These characteristics have allowed hydrogels to be widely used as matrices for encapsulating cells, promoting key functions such as adhesion, migration, fibroblast proliferation, and extracellular matrix synthesis—essential elements in the dermal regeneration process[5,113]. In addition to serving as structural

support, hydrogels stand out as effective vehicles for the controlled release of bioactive agents, such as antibacterials, antioxidants, growth factors, or drugs, released in response to physical or chemical stimuli[2,114]. This capability gives them a central role in the development of smart dressings with localized and sustained therapeutic action. From a functional standpoint, an ideal dressing should meet certain characteristics:

• Tissue compatibility, without causing toxicity or inflammation at the application site.

• Moisture retention capacity, facilitating a moist environment that accelerates healing and promotes cellular hydration.

• Adequate mechanical resistance, maintaining the dressing's integrity under movement and preventing the entry of pathogens.

• Biochemical properties capable of promoting cell proliferation and tissue regeneration.

An additional advantage of hydrogels over other solid biomaterials (such as nanofibers or metals) is their ability to adapt to wounds with irregular geometry, efficiently filling cavities or hard-to-reach areas[115]. This fluidity makes them especially useful in complex clinical applications. **Table 1.2** shows the commercially available hydrogels for wounds in Chile.

Table 1.2: Commercial hydrogels for wounds in Chile.

Product	Composition / Active Ingredient	Manufacturer / Distributor	Clinical Application
Cutimed® Gel	Polyacrylate, water, glycerin, Carbomer	BSN Medical (Chile)	Healing of ulcers, burns, and chronic wounds

Saf Gel	Calcium–sodium alginate, CMC	Convatec (Dipromed)	Debridement, granulation, and hydration of necrotic tissue
Nexcare™ Tegaderm®	Water, propylene glycol, guar gum, tetraborate	3M Chile	Hydration of dry / low-exudate wounds
Nexcare™ Advanced Healing®	Hydrocolloids	3M Chile	Healing of ulcers, burns, and chronic wounds
Nu Gel™	Alginate + water	3M Chile	Wound healing, autolytic debridement
Pharmagel Hydrogel Dressing	Polyurethane gel (60% water)	Pharmaplast – Ortopedia Suiza	Sterile coverage for exudative wounds
Multidex™	Absorbent hydrogel with odor control	RoyalMed	Filling of wound cavities; controls purulent exudate
Amorphous hydrogels (various)	Alginate, collagen, silver (depending on brand)	Various suppliers (e.g., MercadoLibre)	Hydration, pain relief, and management of diverse wound types
Cranberry Hydrogel	Gel with cranberry extract	RGC.cl	Supports autolytic debridement and rehydration

In summary, hydrogels represent a multifunctional platform with high therapeutic value and the potential to transform the clinical management of wounds. Their ability to mimic the physiological microenvironment, release bioactive compounds in a controlled manner, and modulate cellular responses positions them as key players in the development of smart dressings and next-generation regenerative therapies.

1.3 Chitosan

Chitosan (CS) is a natural polysaccharide derived from the partial deacetylation of chitin, present in the exoskeletons of crustaceans and the cell walls of some fungi[116]. It is composed of glucosamine and N-acetylglucosamine units linked by β-1,4-glycosidic bonds and is notable for its high reactivity, attributed to the presence of amino and hydroxyl groups in its structure (**Figure 1.2**) [117]. This chemical configuration allows for its functional modification and the development of advanced materials for biomedical applications[118]. CS has been extensively investigated for its remarkable biocompatible, biodegradable, antimicrobial, hemostatic, antioxidant, and anti-inflammatory properties, as well as its low toxicity[119,120]. Furthermore, it is a pH-sensitive cationic polymer, soluble in acidic media due to the protonation of its amine groups, making it suitable for formulations in aqueous media[121].

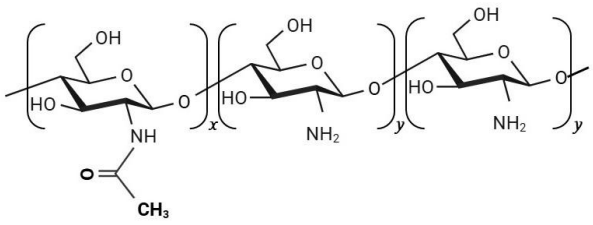

Figure 2.2. Molecular structure of chitosan. Source (Own elaboration)

In the context of wound healing, CS acts as a bioactive agent that positively influences various stages of the process [122]. It promotes cell migration and proliferation, stimulates collagen and blood vessel formation (angiogenesis), and maintains a moist environment that favors the regeneration of damaged tissue[13,14]. Furthermore, the release of N-acetylglucosamine during its degradation has been shown to accelerate healing[123]. From an immunological perspective, CS has been observed to induce fibroblasts to release interleukins involved in cell signaling and tissue repair[124]. Its ability to interact with cells is related to the presence of free amino groups, which facilitate cell adhesion[125]. The degree of deacetylation of the polymer, as well as the number of amino groups, influences key properties such as coagulation and its interaction with red blood cells[126].

Despite their advantages, CS hydrogels have mechanical limitations that have driven the incorporation of nanomaterials and biomolecules to improve their strength and functionality. This has led to the development of hybrid or functionalized systems capable of releasing growth factors, drugs, or antimicrobial agents in a controlled manner, thus optimizing their application in regenerative therapies[127,128]. Overall, CS is positioned as a versatile and highly promising biopolymer in the design of advanced dressings, thanks to its ability to promote healing, prevent infections, and be modified to enhance its therapeutic properties.

1.4 Reduced Graphene Oxide (rGO)

rGO has emerged as a nanomaterial of great interest in the field of regenerative medicine, particularly in wound healing applications[129]. Derived from graphene oxide (GO) through chemical, thermal, or electrochemical treatments, rGO has a two-dimensional structure composed of carbon sheets with defects and residual functional groups (such as –OH, –COOH, and epoxides) (**Figure 1.3**), which give it a unique combination of electrical conductivity, biocompatibility, active surface

area, and functionalization capacity[130,131]. One of the most remarkable aspects of rGO is its antimicrobial activity, which has been attributed to multiple mechanisms[132]. These include the induction of oxidative stress through the generation of reactive oxygen species (ROS) and physical damage to the bacterial membrane caused by the sharp edges of the graphene sheets[133]. This property allows for the prevention of wound bed infections, a major cause of poor healing, without requiring the use of conventional antibiotics.

In the context of wound healing, rGO has also been shown to facilitate the adhesion, proliferation, and migration of skin cells such as fibroblasts and keratinocytes, accelerating re-epithelialization and promoting the regeneration of damaged tissue[134]. Furthermore, its ability to conduct electrical signals makes it an ideal material for integration into conductive dressings or electroactive hydrogels, which can enhance galvanotaxis and stimulate the cellular response mediated by endogenous electric fields[135]. Moreover, rGO can be easily functionalized or combined with other polymeric materials (natural or synthetic), resulting in hybrid systems that improve its dispersion, reduce its cytotoxicity, and increase therapeutic efficacy[136]. For example, it has been incorporated into hydrogels, sponges, or films along with polymers such as chitosan, alginate, or collagen, generating multifunctional platforms with enhanced antimicrobial, antioxidant, and wound-healing properties[137].

Although the use of rGO in biomedical applications is still in the preclinical research phase, the results obtained in *in vitro* and *in vivo* models are promising. However, it is necessary to continue evaluating aspects related to its biodegradability, long-term toxicity, and systemic safety, especially in formulations designed for direct and prolonged contact with human tissue. In summary, reduced graphene oxide represents an innovative nanomaterial with considerable therapeutic potential in the treatment of acute and chronic wounds, thanks to its antimicrobial, electrical, and bioactive properties, and its ability to be integrated into advanced cell delivery or support systems.

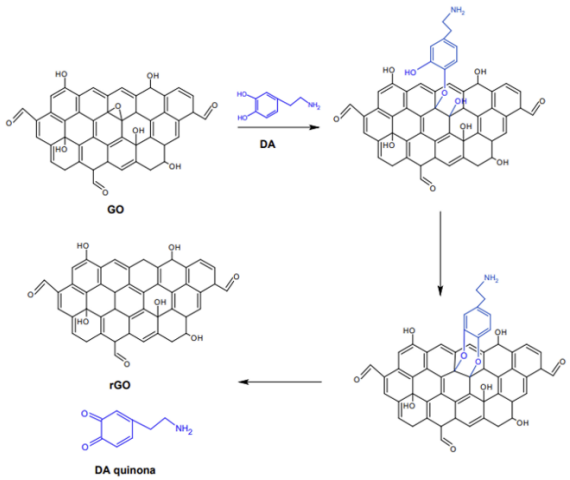

Figure 3.3. Mechanism of graphene oxide reduction by dopamine catechol groups. Source (Cheng et al., 2013).

1.4.1 Methods for reducing graphene oxide (rGO)

-Chemical Reduction

Chemical reduction is one of the strategies with the greatest potential for large-scale rGO production. This method generally consists of subjecting graphene oxide (GO) to an aqueous solution containing a chemical reducing agent, under controlled temperature and time conditions, to promote the removal of oxygenated functional groups—mainly epoxides, hydroxyls, and carbonyls—and partially restore the sp^2 conjugated domains characteristic of graphene, thus increasing the material's electrical conductivity[138,139]. Among the most commonly used reducing agents are hydrazine (one of the most widely used), lithium aluminum hydride, as well as acidic or basic reagents such as hydrochloric acid, acetic acid, and sodium hydroxide[140]. This approach offers the main advantages of high reduction efficiency, a significant improvement in electrical conductivity, and good reproducibility at the laboratory scale, provided that parameters such as reaction time, temperature, and the reducing agent: GO ratio

are properly controlled[141]. However, chemical reduction has significant limitations, especially from a biomedical perspective. Many of the reducing agents used are highly toxic, volatile, or hazardous, making them difficult to handle and posing environmental and biosafety risks[142]. Furthermore, excessive reduction can promote the aggregation of rGO sheets and decrease their dispersibility in aqueous media due to the loss of polar groups, negatively impacting their integration into hydrophilic polymer matrices[143]. Additionally, this method can introduce structural defects or leave chemical and ionic residues if washing and purification processes are not thorough[144].

For these reasons, although chemical reduction is physically and electrically efficient, it is unattractive for the development of biomaterials intended for clinical applications, where biocompatibility, colloidal stability, and safety are critical factors.

-Thermal Reduction

Thermal reduction is one of the most widely used methods for obtaining rGO. In this approach, reduction and exfoliation of the material occur simultaneously, which is why the precursor used is usually graphite oxide instead of previously exfoliated GO[145]. The process mainly consists of heating the material to high temperatures, either in an ambient atmosphere or under an inert atmosphere, which causes the thermal decomposition of the oxygenated functional groups present in the graphite oxide structure[146]. During heating, the epoxide, hydroxyl, and carbonyl groups decompose, releasing gases such as CO, CO_2, and H_2O[147]. The rapid expansion of these gases generates high pressure between the graphitic layers, which overcomes the Van der Waals forces responsible for their cohesion, leading to the exfoliation of the material and the formation of rGO sheets[148]. At the structural level, this mechanism leads to progressive deoxygenation and partial restoration of conjugated sp^2 domains, resulting in a significant increase in the material's electrical conductivity[149].

Among the main advantages of thermal reduction is the fact that it does not require the use of additional chemical reagents, thus reducing waste generation and simplifying the process from a chemical standpoint[150]. Furthermore, when high temperatures are employed, this method can produce rGOs with relatively high conductivities, making it attractive for applications in electronics, energy storage, and structural composite materials[142]. However, thermal reduction has significant limitations, such as the fact that the use of high temperatures can induce a high density of structural defects, including vacancies, carbon lattice breaks, and topological disorder, which can compromise the mechanical properties and structural integrity of the material[151]. In addition, this method often generates rGOs with low surface functionality and reduced dispersibility in aqueous media due to the extensive removal of oxygenated groups. From a biomedical perspective, another critical drawback is that thermal reduction is incompatible with “soft” synthesis routes, as it cannot be applied once the GO has been incorporated into polymer matrices, hydrogels, or systems containing heat-sensitive biomolecules[152].

For these reasons, although thermal reduction is highly effective for applications in fields such as energy and structural nanocomposites, it is unattractive for the development of biomaterials intended for wound healing, where a balance between electrical conductivity, surface functionality, colloidal stability, and biocompatibility is required.

-Electrochemical Reduction

The electrochemical reduction of graphene oxide is based on the direct electron transfer induced by an applied electrical potential, which promotes the partial removal of oxygenated groups from GO. This process can be carried out on GO films deposited on electrodes or in suspensions, depending on the electrochemical configuration used[153]. The mechanism mainly involves the reduction of epoxide, hydroxyl, and carbonyl groups, with the consequent partial

restoration of sp² domains responsible for electrical conductivity[154]. Among its main advantages is that it avoids the use of toxic reducing agents, since the electron acts as a reactant, making this method a cleaner alternative from a chemical point of view[155]. Furthermore, it allows relatively precise control of the degree of reduction by adjusting parameters such as the applied potential, the reduction time, and the nature of the electrolyte, which is attractive in terms of reproducibility and fine-tuning of electronic properties. Electrochemical reduction can also preserve residual functional groups useful for subsequent surface functionalization processes. However, this method has significant limitations for its application in three-dimensional biomaterials. In practice, electrochemical reduction is best suited for obtaining thin films, coatings, or devices based on well-defined electrode geometries[139,156]. Scaling it up to large volumes of powder or complex polymer systems, such as hydrogels, is technically challenging and inefficient[157]. Furthermore, the final result is highly dependent on the electrolyte composition, the configuration of the electrochemical system, and the homogeneity of the electric field, which can introduce variability if the process is not rigorously standardized[138,139].

For these reasons, although electrochemical reduction is attractive for applications in sensors, flexible electronics, or conductive coatings, it is poorly suited for the reproducible production of rGO intended for bulk biomaterials and hydrogels for wound healing, where homogeneous, scalable reduction compatible with polymer matrices and biological environments is required.

-Green Reduction

The green reduction of GO is based on the use of benign reducing agents, generally of natural or biocompatible origin, capable of donating electrons and/or protons to partially eliminate the oxygenated groups present in GO[158]. This mechanism promotes the preferential reduction of epoxide, hydroxyl, and, to a lesser extent, carbonyl groups, allowing the partial restoration of sp² domains

without completely eliminating the surface functionality of the material[159]. Among its main advantages is the low toxicity of the process, which represents a critical advantage for biomedical applications and, in particular, for the development of implantable biomaterials or those in direct contact with tissues[160]. Unlike aggressive chemical methods, green reduction usually preserves a significant fraction of oxygenated functional groups, which improves the dispersibility of rGO in aqueous media and favors its interaction with hydrophilic polymer matrices, cells, and biomolecules[161]. As a result, this approach offers a suitable balance between electrical conductivity and surface functionality, especially relevant for hydrogels and scaffolds intended for wound healing[42]. Among the most frequently reported green reducing agents are ascorbic acid, plant extracts, and dopamine, which have proven effective in obtaining rGO with moderate electrical properties and high biocompatibility. However, this method also has limitations[162,163]. In general, the degree of reduction achieved is usually lower than that obtained using strong chemical reducing agents or heat treatments, resulting in lower conductivities. Furthermore, when natural extracts are used, batch-to-batch variability can exist due to differences in chemical composition, pH, or ionic strength, requiring rigorous process standardization to ensure reproducibility[164].

Despite these limitations, green reduction is considered one of the most attractive strategies for biomedical applications, as it allows for obtaining rGO with balanced functional properties, adequate colloidal stability, and a lower cytotoxic risk. For these reasons, green reduction is particularly well-suited for the manufacture of conductive hydrogels and wound-healing biomaterials, where biocompatibility, reproducibility, and preservation of chemical functionalities are as important as electrical conductivity.

The synthesized GO was reduced using dopamine (DA) as a reducing agent, following a methodology based on the protocol described by Xu et al.

(2010)[163], with experimental adjustments to ensure process efficiency and the production of a biocompatible material (**Figure 1.3**).

1.5. Pluronic F-127

Pluronic F-127 (also known as poloxamer 407) (PF) is a non-ionic triblock copolymer composed of polyethylene and polypropylene oxide units (PEO–PPO–PEO) (**Figure 1.4**), which has gained significant interest in the biomedical field due to its biocompatibility, thermoreversible gelation capacity, and versatility for incorporating therapeutic agents[165]. These properties have positioned it as an ideal candidate for the design of controlled-release systems and smart dressings applied in wound healing[12]. One of the main advantages of PF is its temperature-sensitive behavior: it is a liquid solution at room temperature but forms a semi-solid gel at body temperature (~37°C)[166]. This characteristic facilitates its topical application to open wounds, allowing the material to perfectly adapt to the morphology of the lesion and create a protective barrier without the need for surgical intervention[167]. Once gelled, PF maintains a moist environment, reduces fluid loss, and protects against external contamination, thus promoting tissue regeneration[168].

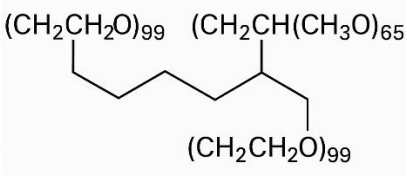

Figure 4.4. Molecular structure of Pluronic F-127. Source (Own elaboration).

Additionally, this copolymer enables the incorporation of various bioactive compounds, such as antibiotics, anti-inflammatory agents, antioxidants, growth

factors, or nanoparticles, serving as an effective matrix for the sustained and localized release of these agents[1]. Drug-loaded PF-based formulations have been shown to significantly enhance wound healing by reducing inflammation, preventing infections, and stimulating cell proliferation and angiogenesis [169]. *In vivo* studies have demonstrated that PF hydrogels promote re-epithelialization and granulation tissue formation in animal models of skin wounds, showing better results than conventional treatments[170]. Furthermore, thanks to its low immunogenic profile and minimal toxicity, this copolymer has been approved by the FDA for biomedical applications, supporting its potential for translation to clinical uses in humans[171].

1.6 Formation of the Composite Hydrogel and Mechanisms of Molecular Interaction

From a molecular perspective, it is proposed that hydrogel formation is mediated by non-covalent physical interactions between the three main components. In the presence of GO, DA self-polymerizes, forming a polydopamine (PDA) layer, which simultaneously acts as a reducing and stabilizing agent for rGO[172,173]. This process involves the transfer of electrons from the catechol groups of DA to the oxygenated (C=O) groups of GO, promoting their reduction[163]. Under slightly basic conditions, the catechol groups of PDA are oxidized to quinones, which can bond with the amino groups of CS via Michael addition or Schiff base formation reactions. Simultaneously, PF self-assembles into micelles through hydrophobic interactions. In this assembly, the central PPO block interacts with the hydrophobic regions of rGO, while the hydrophilic ends of PEO stabilize the network through interactions with CS, favoring the formation of a three-dimensional cross-linked structure. This physically assembled network, schematically represented in **Figure 1.5**, exhibits thermosensitive behavior, gelling at physiological temperature (~37°C), making it a functionally suitable

matrix for wound healing applications. This approach is consistent with previous reports of CS/PF-based thermosensitive hydrogels, whose gelation occurs in the 20–40°C range[174,175]. The sol-gel transition phenomenon is due to the progressive formation of PF micelles in aqueous solution as the temperature increases, transitioning from a liquid to a gel state as physiological conditions are reached[174].

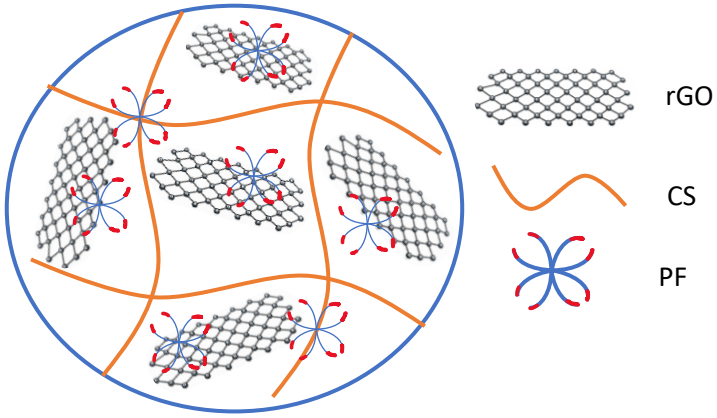

Figure 5.5. Representative diagram of the possible arrangement of PF, CS, and rGO in the formation of the designed hydrogels. Source (Own elaboration).

Thesis Plan

The main findings of this study will be presented in the following chapters in a format similar to that of a scientific journal, since most of these results have been published or submitted to Journals. This thesis is structured as follows:

Capítulo 2. Chapter 2 addresses the four specific objectives**.**

This chapter presents the synthesis and experimental design used to optimize the CS-rGO-PF formulation, based on a central composite design (CCD) and the application of response surface methodology (RSM). This approach enabled the identification of optimal rGO and PF ratios to maximize key functional properties, including electrical conductivity, mechanical behavior, swelling capacity, and biocompatibility, of the developed system. Furthermore, this chapter includes the results related to the absorption kinetics of the previously synthesized hydrogels against simulated human fluids. The optimal hydrogel was validated in an *in vivo* model. Its ability to promote wound healing was compared to a commercial dressing, Nexcare®. The results were published in the journal Chemistry Select, under the title: Optimization and validation of chitosan-reduced graphene oxide-pluronic F-127 hydrogel synthesis for potential wound dressing.

Capítulo 3. Chapter 3 addresses specific objectives 3 and 4.

This chapter describes the incorporation of tannins (TA) into the optimal hydrogel obtained in Chapter 2, with the aim of enhancing its antioxidant and antibacterial properties. The synthesis procedures for the CS-rGO-TA hydrogels and the characterization of their physicochemical properties are detailed. Furthermore, their healing capacity was evaluated through *in vitro* and *in vivo* assays, comparing hydrogels with and without TA. The therapeutic potential of the material was analyzed in a murine model of full-thickness wounds, monitoring wound closure and performing histological studies (H&E, Mallory, and Masson's trichrome stains). In addition, molecular analysis was performed using RT-qPCR and Western blot to evaluate inflammatory modulation and tissue regeneration,

along with skin irritation tests in guinea pigs to confirm its biocompatibility. The results were submitted to the journal Biomaterials Science, under the title: Bioinspired Synergistic Chitosan-Graphene-Tannin Hydrogel Orchestrates Inflammation Resolution and Accelerates Skin Tissue Repair.

Chapter 2

Optimization and validation of chitosan-reduced graphene oxide-pluronic F-127 hydrogel synthesis for potential wound dressing.

Isleidy Ruíz, Luisbel González, Aracelly Quiroz, Claudio Aguayo, Jorge Toledo, Katherina Fernández, ChemistrySelect, 10, 2025, e02598.

2.1 Abstract

The present study developed a novel conductive wound dressing based on chitosan (CS), reduced graphene oxide (rGO), and Pluronic F-127 (PF). Using 2^2 + star factorial design, the effect of rGO and PF concentrations on conductivity, swelling capacity, mechanical properties, and cell migration was evaluated. The factors that significantly influenced the variables were identified through analysis of variance. The result indicated that increased rGO concentration improved conductivity, while PF significantly affected swelling capacity. Including rGO also impacted tensile strength, elastomeric modulus, and cell migration. The properties of the dressings were characterized using SEM, FTIR, XRD, TGA, wettability test, antibacterial capacity, and cell viability. Statistical optimization revealed that the optimal concentrations (CS-rGO-PF_{10}) provided outstanding conductive properties (2.30 mS/cm), high fluid absorption (577.42%), mechanical properties (tensile strength 22.14 MPa and elastic modulus 169.97 MPa), and promoted cell migration (100% closing rate after 48 hours). Furthermore, it showed excellent antibacterial capabilities against E. coli and S. aureus. In vivo tests using a porcine model, the dressing accelerated healing and improved tissue regeneration, as evidenced by enhanced re-epithelialization and vascularization. In conclusion, the CS-rGO-PF_{10} conductive hydrogel represents a promising option for wound treatment.

2.2 Introduction

The skin is a multifunctional sensory organ and the first barrier of the human body, causing damage to its structure and function when faced with a wound[21–24]. These injuries trigger a physiological healing process, which takes place in four interrelated phases[3,4]. A key element in this process is the skin's endogenous electric field, which is generated in the epidermis, where the high electrical resistance of the dead cell layer can accelerate wound healing by promoting cell migration and tissue reorganization[176]. In this context, conductive hydrogel dressings have emerged as a promising solution[64,177,178]. Hydrogels are three-dimensional (3D) polymeric networks capable of absorbing fluid and maintaining greater humidity without degrading, which promotes healing[11,179]. In addition, they are biodegradable and biocompatible, making them an ideal option as a temporary insole during wound healing[48]. Various components, such as antibacterial and antimicrobial agents, drugs, and other supplemental biomolecules, can also be incorporated, improving their effectiveness in promoting wound healing[21]. Conductive hydrogels promote the flow of current from the edges to the center of the lesion, creating a favorable environment for healing and improving various stages of the process[180].

Chitosan (CS) is a natural polymer used in biomedical applications, derived from the partial deacetylation of chitin[116]. Among the advantageous biological qualities of CS are its biodegradability, biocompatibility, antibacterial properties, non-toxicity, and excellent swelling capacity[13,14]. In addition, it can adhere to the mucosa and has anti-cancer, pro-inflammatory, and coagulation-promoting activity[181]. Research has shown that CS contributes to hemostasis and occlusion by absorbing proteins and adhering to platelets, accelerating the healing process[124]. A study by B. S. Rajinikanth et al. (2024) highlights that CS not only acts as a wound healing agent but can also be modified to release growth

factors and enhance tissue regeneration, supporting its use in regenerative therapies[182]. Furthermore, research by P. Feng et al. (2021) shows that CS synergizes with other biomaterials to enhance immune response[183]. Pluronic F127 (PF), also known as poloxamer 407 [165], is a thermosensitive synthetic copolymer formed by the triblock of poly(ethylene oxide) -poly(propylene oxide)-poly(ethylene oxide) (PEO-PPO-PEO)[175]. This material allows the *in situ* formation of various biomaterials without potentially toxic agents. These biomaterials are mainly used in the administration of drugs[166]. The appeal of PF can be attributed to its non-toxicity, bioadhesives, stability, and ability to transform into gels at low concentrations at physiological temperatures[12]. Recent studies confirm that PF in CS increases the composite formulation's mechanical strength and viscosity[184].

Graphene oxide (GO) is a compound formed by a carbon layer with hydroxyl and epoxide groups around it[130]. Studies have shown that GO has mechanical, antibacterial, and biocompatible properties; however, its electrical conductivity is low[11]. When GO is reduced, its conductivity increases, since the carbon-oxygen bonds of GO are eliminated, to return sp^2 hybridization to the compound, obtaining mechanical, optoelectronic, or conductive properties like graphene[185]. Different reducing agents for GO have been reported in the literature, such as acids, metals, bacteria, and plant extracts[186–188]. Dopamine (DA) is a hormone belonging to the family of catecholamines and phenylethylamines. Research has shown that using DA to reduce GO is a gentle, economical, and friendly method[189]. In slightly alkaline aqueous conditions (pH 8.5) it can self-chain polymerize, becoming polydopamine (PDA), which allows the simultaneous functionalization of graphene without the need to use dangerous reducing agents[172,173]. Recent research indicates that the use of reduced graphene oxide (rGO) promotes cell adhesion and proliferation, as well as accelerates the closure and healing of antibacterial wounds[112,190]. The research by N. Nowroozi et al. (2021) developed a CS/rGO nanocomposite

incorporating curcumin for application in wound healing. These dressings present interconnected porous structures characterized by high porosity and hydrophilic properties, which favor cell adhesion and proliferation. The results obtained regarding cell viability and morphology confirm the suitability of these dressings for the healing process[191]. On the other hand, N. Elhami et al. (2024) developed a CS/rGO-based nanocomposite that significantly improves wound healing[192]. Likewise, C. Fu et al. (2021) presented an arginine/CS/rGO nanocomposite loaded with antimicrobial peptides. The results of their research indicate that this dressing not only accelerates wound closure but also significantly reduces inflammation, improves angiogenesis, and speeds up the re-epithelialization process. These findings highlight the potential of conductive dressings in regenerative medicine, offering innovative approaches to wound treatment.

For that reason, this research presents an innovative approach to the design of wound healing dressings, combining CS-rGO-PF. Through a rigorous experimental design, the concentrations of these components were optimized, achieving not only improved conductive and mechanical properties of the dressing but also enhanced biocompatibility and absorption capacity. This research offers a comprehensive and effective solution that addresses various aspects of the healing process, marking a significant advance in the treatment of wounds. The main objective of this study was to develop a new dressing based on CS enhanced with rGO and PF inclusion, to improve its effectiveness through optimization of the concentrations of these components using a 2^2 + star experimental design. The purpose was to obtain a dressing with enhanced conductive properties, absorption capacity, mechanical resistance, and biocompatibility to promote wound healing. The synergistic combination of these three compounds (CS-rGO-PF) and the properties mentioned earlier should allow the creation of a porous, conductive, and hydrophilic dressing that promotes the absorption of exudate and cell migration, thereby contributing to the wound healing process. Additionally, the improved biocompatibility of the CS-rGO-PF

dressings is expected to facilitate cell adhesion and proliferation, accelerating wound healing. The enhanced mechanical properties of the dressing also make it suitable for use on irregular skin surfaces, ensuring optimal contact and coverage. The development of this innovative CS-rGO-PF dressing should have great potential to improve wound care treatment by providing a multifunctional and effective solution to promote wound healing.

2.3 Materials and Methods

2.3.1 Materials

Graphite powder (Flakes, 325 mesh) was purchased from Asbury Online (Asbury Carbons, New Jersey, USA). Chitosan (CS) ($C_{12}H_{24}N_{2O9}$) medium molecular weight (50 -200 kDa, with a Brookfield viscosity of 200–800 cP and deacetylation ≥ 75%)(CAS Number 9012-76-4) and Pluronic F 127 (PF) (PEO97-PPO69-PEO97) (CAS Number 9003-11-06) were purchased from Sigma Aldrich chemicals (Chile, South America). Phosphoric acid (H_3PO_4), sulfuric acid (H_2SO_4), potassium permanganate powder ($KMnO_4$), hydrogen peroxide (H_2O_2, 30%), hydrochloric acid (HCl), ethanol (C_2H_5OH), tris ($(HOCH_2)_3$ CNH_2), dopamine hydrochloride (DA-HCl, minimum 98%), sodium hydroxide (NaOH), silver nitrate ($AgNO_3$), Dulbecco's modified Eagles medium (DMEM), dimethyl sulfoxide (DMSO), 3-(4,5-dimethylthiazol-2-yl)-2,5- diphenyltetrazolium bromide (MTT) reagent, phosphate-buffered saline (PBS), fetal bovine serum (FBS) were purchased from Sigma-Aldrich Company, (St. Louis, MO, USA). All reagents and solvents were of analytical grade and were used without further purification. Milli-Q® water was used throughout the study.

2.3.2 Preparation of CS-rGO-PF hydrogels

The dressings were synthesized using the Schmolka cold method[174]. First, a solution of rGO with 0.5% w/v in Milli-Q® water was obtained and subjected to 2 hours to facilitate its dispersion in the CS matrix. Subsequently, CS (1.5 g) was

dissolved in 1% HCL solution. Then, the rGO and CS solution were mixed until a homogeneous mixture was obtained and cooled to a temperature of 4°C. Once the mixture had cooled, the PF previously dissolved in PBS was added (1% w/v). The mixture was then sonicated for 30 minutes to remove possible air bubbles. Finally, the mixture was placed in a Petri dish and placed in an oven (Huanghua Faithful Instrument Co. Ltd., Huanghua, China) at a maximum temperature of 37°C to promote material gelation. The concentration of CS was kept constant in all materials (3% w/v), and the concentration of rGO and PF was varied according to **Table 2.1**. The concentrations were selected according to previous studies in the field[12,175,193–198].

2.3.3 Optimization Design through a Composite Central Design (CCD) and Response Surface Methodology (RSM)

CCD-RSM was used to optimize the formulation variables of the hydrogels. The experimental design was a central composite experimental design 2^2 + star, considering two factors (concentrations of rGO (X_1) and concentrations of PF (X_2)) and five different coded levels (-α, -1, 0, +1, +α). The dependent variables were: conductivity (Y_1), swelling (Y_2), tensile strength (Y_3), elastic modulus (Y_4) and cell migration (Y_5). Antibacterial capacity and cytotoxicity tests were not considered as independent variables in the design analysis, since all synthesized hydrogels showed similar values (>80%). The software Statgraphics Centurion XVII® was used for data analysis. Ten runs were generated with 2 replicates each and were randomly performed to avoid any source of experimental error. The coded and real levels and the composition of each formulation are shown in **Table 2.1**. A mathematical model based on linear and interaction terms was built (**Equation 2.1**) with the data adjustment:

$$Y = b_0 + b_1X_1 + \ b_2X_2 + b_3X_1X_2 \quad (2.1)$$

Where Y is the system response, b_0 is a constant term (intercept), b_1 and b_2 are the coefficients for the linear terms X_1 and X_2, respectively; b_3 is the coefficient for the interaction term X_1*X_2; X_1 and X_2 are the independent variables of the 2^2 statistical designs.

This mathematical model represents the relationship between the independent variables X_1 and X_2, incorporating the individual effects of each and their mutual interaction. The coefficients b_1 and b_2 can be estimated from the data obtained in the statistical design, allowing the value of the response variable Y to be predicted based on the values of X_1 and X_2. ANOVA was applied to estimate the significance ($p < 0.05$) of the model and individual response parameters. In the analysis, the independent variables were found to be statistically significant when they exceeded the blue dotted vertical bar (located at $\alpha = 0.05$). The effects of the factors on the response measurements were analyzed using surface response plots and formulation optimization (maximization) using the desirability approach and Pearson correlation plot. **Table 2.1** shows the responses observed for all formulations prepared according to CCD.

Table 2.1. Composition and nomenclature of the hydrogel and variables used in CCD .

DoE	**Levels**					**rGO**	**PF**	**Hydrogel**
Independent variables	-1.41	-1	0	1	1.41	-1.41	0	$CS\text{-}PF_{15}$
X_1: rGO (v/v%)	0	0.25	0.5	0.75	1	-1	-1	$CS\text{-}rGO_{0.25}\text{-}PF_{10}$
X_2: PF (v/v%)	0	10	15	20	25	1	-1	$CS\text{-}rGO_{0.75}\text{-}PF_{10}$
Response variables	**Goal**					-1	1	$CS\text{-}rGO_{0.25}\text{-}PF_{20}$
Y_1: Conductivity (mS/cm)	Maximized					1	1	$CS\text{-}rGO_{0.75}\text{-}PF_{20}$
Y_2: Swelling (%)	Maximized					1.41	0	$CS\text{-}rGO\text{-}PF_{15}$
Y_3: Tensile Strength (MPa)	Maximized					0	-1.41	$CS\text{-}rGO_{0.50}$
Y_4: Elastic Module (MPa)	Maximized					0	1.41	$CS\text{-}rGO_{0.50}\text{-}PF_{25}$
Y_5: Cellular migration (%)	Maximized					0	0	$CS\text{-}rGO_{0.50}\text{-}PF_{15}$

2.3.4 Characterization of CS-rGO-PF Hydrogels

2.3.4.1 Physicochemical Characterization of Hydrogels

The morphological and physicochemical properties of CS-rGO-PF hydrogels were studied using scanning electron microscopy (SEM), attenuated total reflection Fourier transform infrared spectroscopy (ATR-FTIR), X-ray diffraction (XRD), thermogravimetric analysis (TGA), and determination of surface wettability. **Appendix A.1** of this thesis includes detailed information on these characterization techniques.

2.3.4.2 Hydrogels Conductivity

The hydrogels were cut (1 cm^2) in triplicate, and the sample resistance values were measured with an LF meter 4192A (Keysight, California, USA). The resistivity could be calculated using the resistance by the following formula: $\rho = RS/L$, where R is the resistance of the sample, and S and L represent the cross-sectional area and length of the sample, respectively.[199] Thus, the conductivity (σ) was calculated through $\sigma = 1/\rho$.

2.3.4.3 Swelling Test

The hydrogels were cut (1 cm^2) and immersed in a solution simulating human fluids [200], at room temperature (25 °C) for time intervals from 5 minutes to 90 minutes. After each immersion, the excess solution was removed using filter paper and the weight of the hydrogels was immediately recorded. The simulated human fluid was prepared following the methodology proposed by Kukubo et al.(1990).[200]

The swelling ratio (SR) was calculated using **Equation 2.2**:

$$\mathrm{SR}(\%) = \frac{\mathrm{W_{wet} - W_{dry}}}{\mathrm{W_{dry}}} \cdot 100 \quad (2.2)$$

where W_{dry} is the dry sample weight, and W_{wet} is the wet sample weight (after contact with the liquid medium). Additionally, the diffusion of hydrogels was studied using different kinetic models proposed in the literature (**Appendix A.1**).

2.3.4.4 Mechanical Assay

The mechanical properties of the hydrogel's composites were measured using a Universal Testing Machine (Shimadzu EZ-XS, Japan) equipped with a 20 N load cell at a temperature of 20 °C and relative humidity of 50%. All samples were cut following the shape template of 10 mm width, 25 mm length, and 0.18 mm thickness. The samples were held between two clamps and pulled by the top clamp at 0.1 mm/s. The elongation and breaking force were measured when the material was taken apart. The tensile strength and elastic modulus were calculated using **Equations 2.3 and 2.4**:

$$\text{Tensile strength}(\mathrm{N}/m^2) = \frac{\text{Breaking Force (N)}}{\text{Cross} - \text{sectional area of sample } (mm^2)} \quad (2.3)$$

$$\text{Elastic modulus (kPa)} = \text{Slope } x \ \frac{\text{Length (mm)}}{\text{Cross} - \text{sectional area of sample } (mm^2)} \quad (2.4)$$

2.3.4.5 *In Vitro* Wound Healing Assay (Scratch Test)

An *in vitro* wound healing assay was performed according to previously described experimental procedures [201], with slight modifications. Briefly, human dermal fibroblast cells (50,000 cells/well) were seeded into a 24-well plate and incubated at 37 °C for 48 h in a humidified atmosphere with 5% CO_2. Subsequently, a vertical scratch was manually created in the middle of the human dermal fibroblast monolayer, using a 200 µL sterile pipette tip. Then, each material was fixed on

CellCrown 24 inserts (Corning Incorporated, PA, USA) and placed on the 24-well plate without touching the surface. The wound closure rate and the cell migration were monitored over time (48 h) using an IncuCyte light microscope (Sartorius S3, USA). Finally, the images were analyzed using ImageJ software. The wound closure rates were calculated according to **Equation 2.5**:

$$\text{Rate of wound closure}(\%) = \frac{(A_0 - A_t)}{A_0} * 100 \quad (2.5)$$

where A_0 is the initial wound area and A_t is the wound area after each time interval.

2.3.4.6 Antibacterial activity

The antibacterial activity of the hydrogels was evaluated in vitro using *Escherichia coli* (*E. coli*, ATCC 27195) and *Staphylococcus aureus* (*S. aureus*, ATCC 25923) strain models; 200 µL of the hydrogels were inoculated with a bacterial suspension of 10 µL at a concentration of 10^6 CFU/mL in 48-well plates and incubated at 37°C for 3 hours. Sterile PBS (1 mL) was added to the plate to resuspend the surviving bacteria. Agar plates were coated with 20 µL of the bacterial resuspension to evaluate antibacterial activity. These plates were then incubated at 37°C for 16 hours. A bacterial suspension of 10 µL at 10^6 CFU/mL in sterilized PBS (1mL) served as the control group. After incubation, colony-forming units were counted visually. The antibacterial activity of the hydrogels was expressed as a percentage of bacterial death (**Equation 2.6**).

$$\text{Kill}\ (\%) = \frac{(N_{control} - N_{hydrogel})}{N_{control}} * 100 \quad (2.6)$$

where $N_{control}$ was the colony-forming units of control and $N_{hydrogel}$ was the survivor count on hydrogels. The experiments were carried out in triplicate.

2.3.4.7 Hydrogel Cytotoxicity

These experiments were conducted using a cell density of 10^4 cells/ mL. First, 1 mL of DMEM medium was added to 10 mg of material and to individual materials (rGO, PF, and CS) to promote full contact. After 24 h of incubation at 37°C, the supernatant was recovered and mixed with 5% (v/v) fetal bovine serum (FBS), 1% (v/v) antibiotics (100 units/mL of penicillin and 100 units/ mL of streptomycin). The supernatant from each sample was added to the cells and incubated for 48 h at 37°C under humidified air with 5% (v/v) CO_2. At the end of the incubations, the supernatants were removed, and the cells were washed with PBS, pH 7.4. Then, 100 µL of fresh DMEM medium was added to the cells, and 5 mg/mL MTT solution was added for the determination of cell viability. The plates were incubated for 4 h at 37 °C with CO_2, then 25 µL of the medium was removed and 50 µL of dimethyl sulfoxide (DMSO) was added to the wells. After 10 min, the supernatant was removed by aspiration, and the formazan crystals were dissolved in DMSO (100 µL per well), followed by shaking for 5 min. The absorbance was determined using a microplate reader (Biotek Synergy 2, Agilent, CA, USA) at a wavelength of 540 nm. The cell viability (%), relative to control cells, was calculated from **Equation 2.7**:

$$\text{Kill}\ (\%) = \frac{\text{A}_{\text{test}}}{\text{A}_{\text{control}}} * 100 \qquad (2.7)$$

where A_{test} is the absorbance value of the wells (with the material) and A_{control} is the absorbance value of the control wells (without the material). DMEM medium was used as a positive control.

2.3.4.8 In Vivo Wound Healing Assay

The wound healing study was conducted on eight male Yorkshire pigs (Sus scrofa), with an average age of two months and an average body weight of 20–25 kg. Biopsies were taken from the wound margins on days 0, 4, and 21 using

an 8 mm diameter punch (Kruuse, India). All animal studies are carried out in accordance with the EU Directive 2010/63/EU for animal experiments. The Bioethics and Biosafety Committee (Faculty of Biological Sciences, University of Concepción) also approved each and every animal experiment (Approved Number: CEBB 865-2021 dated May 2021). The details of *in vivo* characterizations are described in **Appendix A.1**.

2.3.4.9 Histological Analysis

Sections of 5 µm thick paraffin-embedded samples were obtained and stained with hematoxylin and eosin (H&E) to analyze the progression of the wound healing process. The degree of reepithelialization was assessed using the scoring system proposed by Greenhalgh et al. The dermal-epidermal tissue also showed ulceration, pustules, hyperplasia, and hyperkeratosis. A thorough examination was conducted on the subcutaneous tissue to evaluate several factors. A comprehensive analysis was performed to assess various parameters, including hemorrhage, inflammation, granulation/fibrosis, and congestion/neovascularization. Histological analysis was performed blindly by an independent observer. The scale used is detailed in **Table A.3**, available in **Appendix A**.

2.4 Results and Discussion

2.4.1 Morphological Characterization

By SEM, the hydrogel´s microstructure was studied. (**Figure 2.1)** The morphological surface of the hydrogels is characterized by a smooth surface with defined edges and amorphous structures that may be due to the presence of PF in the case of CS-PF_{15} (**Figure 2.1A**), as a result of electrostatic interactions between CS and PF [175,202]. In the case of CS-$rGO_{0.5}$ (**Figure 2.1H**), it presents a surface with wrinkles and sheets, due to the presence of rGO in the

material[203,204]. The other materials present rough surfaces with sheets and defined, amorphous structures caused by the different interactions between the raw materials. A rough surface in hydrogels could increase cell adhesion and proliferation, desirable properties for biomedical applications[205].

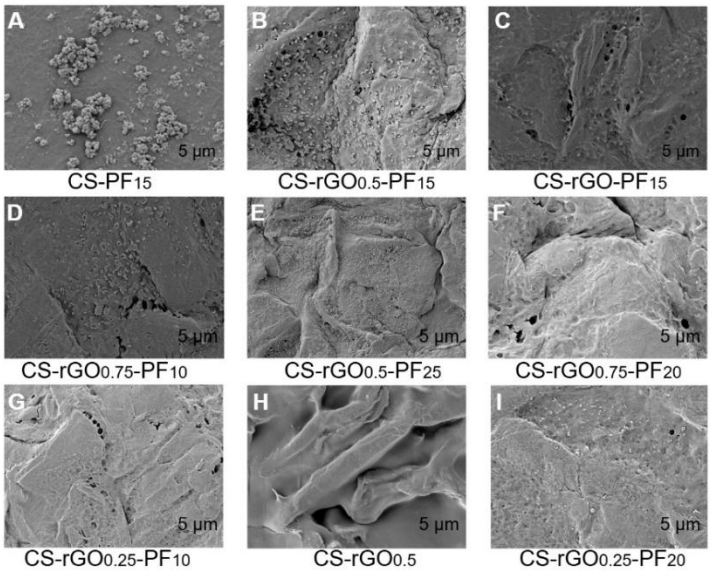

Figure 2.6. SEM images of the hydrogels synthesized by statistical experimental design.

2.4.2 Physicochemical Characterization

The chemical structure of raw materials and materials was analyzed by FTIR (**Figure 2.2A**). The raw CS shows its typical peaks related to OH, primary amine groups[206], stretching vibration of C═O of amide I, and C-O-C stretching and N-H bending of amide II[207]. Graphene reduction and functionalization of rGO by DA amino groups were evidenced by bands at 1220 and 1050 cm^{-1}, respectively[208–210]. PF spectrum displays distinct peaks at 2890 cm^{-1} (CH_2 stretching) and 1402 cm^{-1} (CH groups), along with other peaks attributed to the stretching vibrations of C-O-C and C-O groups[211,212]. The spectra of the hydrogels synthesized using a statistical experimental design are shown in

Appendix A of this thesis (**Figure A.1**), showing bands like those shown by CS-rGO-PF_{15} (**Figure 2.2A**), displaying the characteristic bands of CS (1554 cm^{-1}) and PF (1402 and 1110 cm^{-1}).

XRD analysis was performed to analyze the amorphous or crystalline structure of the components and synthesized hydrogels (**Figure 2.2B**). The CS shows two diffraction peaks corresponding to their crystalline structure types I and II (10 and 20 Å)[213]. The successful reduction of GO by DA is evidenced by the reduction of the interplanar distance to 3.95 Å, which can be attributed to the π- π stacking interactions of the aromatic rings of the PDA and/or rGO coating, Van der Waals forces, and hydrogen bonds[214,215]. PF is a semicrystalline polymer whose crystalline layers of PEO and PPO form amorphous layers. The sharp and intense peaks of PF at 2θ = 17.3° and 24.1° indicate its high stability and crystallinity[216]. The formulated materials (**Figure A.2**) presented a combination of multiple crystalline and amorphous peaks in their diffractograms with lower intensities, possibly due to the interaction of the functional groups present in the polymers, such as the carboxyl and amino groups in CS, which can form hydrogen bonds or electrostatic interactions with rGO and PF[217].

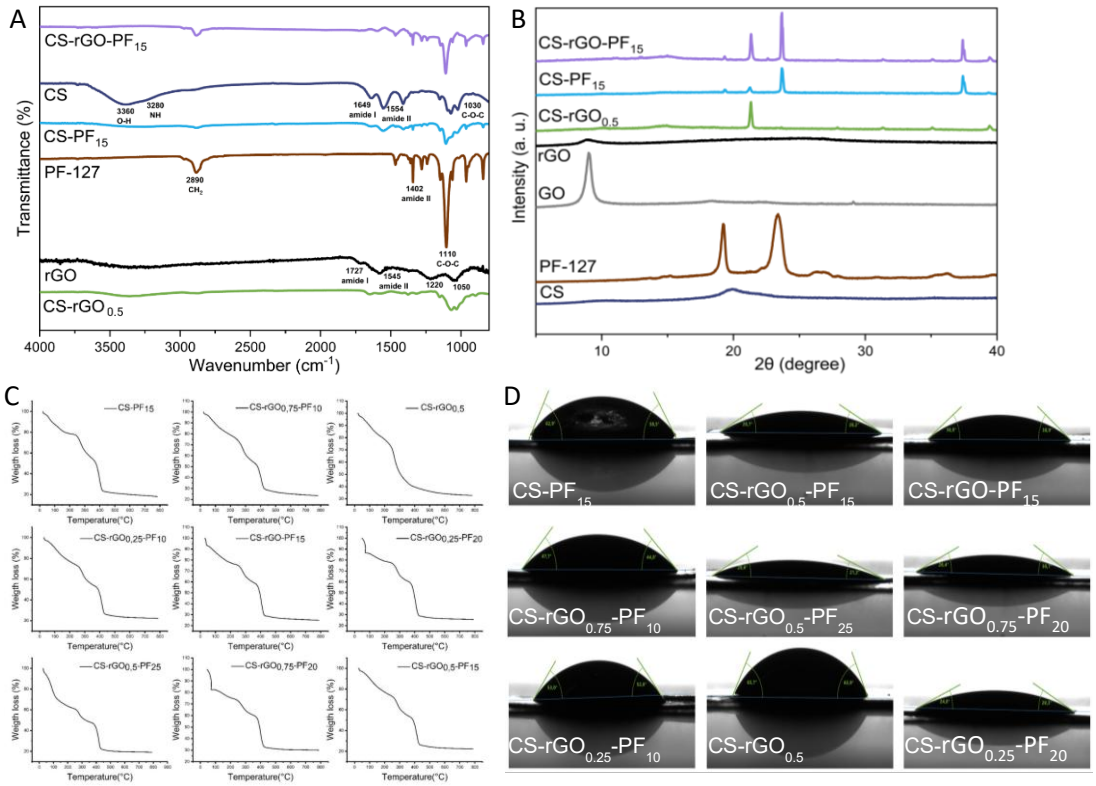

Figure 2.2. (A) FT-IR spectra of the raw materials and synthesized hydrogels; (B) XRD of raw materials and synthesized hydrogels; (C) TGA of synthesized hydrogels and (D) Images of contact angle measurements of the synthesized hydrogels.

TGA analysis (**Figure 2.2C**) shows the relationship between temperature and weight loss related to the thermal qualities of hydrogels. For CS, Dehydration, depolymerization, and decomposition occur at 250-380°C[218]. PF showed degradation of its central structure, in the temperature range of 300-400°C, that is, the elimination of functional groups[219,220]. The hydrogels showed weight losses in a stepwise manner (**Figure 2.2C**). In the first degradation phase, a loss of mostly less than 10% by weight was observed (50° to 100°C), related to moisture loss from the hydrogel matrix. In the second and third phases, a weight

loss of less than 50% (100° to 300°C) was observed, indicating the degradation of amide bonds. In the last degradation phase, around 20% weight loss occurred, indicating the degradation of the long chains of CS and PF.

The surface wettability of the hydrogels was evaluated by water contact angle measurements (WCA) (**Table A.2 and Figure 2.2D**). The incorporation of rGO into the CS matrix resulted in a decrease in water contact angles, indicating an increase in hydrophilicity. This phenomenon can be attributed to interactions between the hydrophilic functional groups present in rGO and catechol groups of CS, as well as the presence of PDA in the coating of rGO obtained through the reduction of GO with DA[210,221]. The increase of PF in the matrix leads to higher surface density, which in turn reduces pore size on the hydrogel surface, hindering water droplet penetration and resulting in a higher contact angle[222]. The dressing synthesized in this study exhibited hydrophilic surfaces (10°<WCA<90°)[223], which directly impacts biological performance and the ability of cells to adhere to the material surface. The results obtained agree with reports from other researchers, who have suggested that materials maintaining their hydrophilic properties promote cell proliferation and growth[222,224,225]. These findings indicate that CS-rGO-PF hydrogels have potential use in wound healing.

2.4.3 Analysis of experimental design

The analysis of the independent variables (rGO and PF concentrations) in the experimental design (**Figure 2.3**) revealed the importance of each parameter and their interactions through the Pareto diagram (**Figure A.3**), the estimated response surface diagram, and the Pearson correlation diagram (**Figure 2.5**). Since the study's objective was to evaluate the interaction effects of the two variables and determine their optimal composition, the focus was on interpreting the magnitude of the linear effect coefficient of the parameters. The magnitude of

each expected regression coefficient was quantified to evaluate its effect on the responses to propose the models.

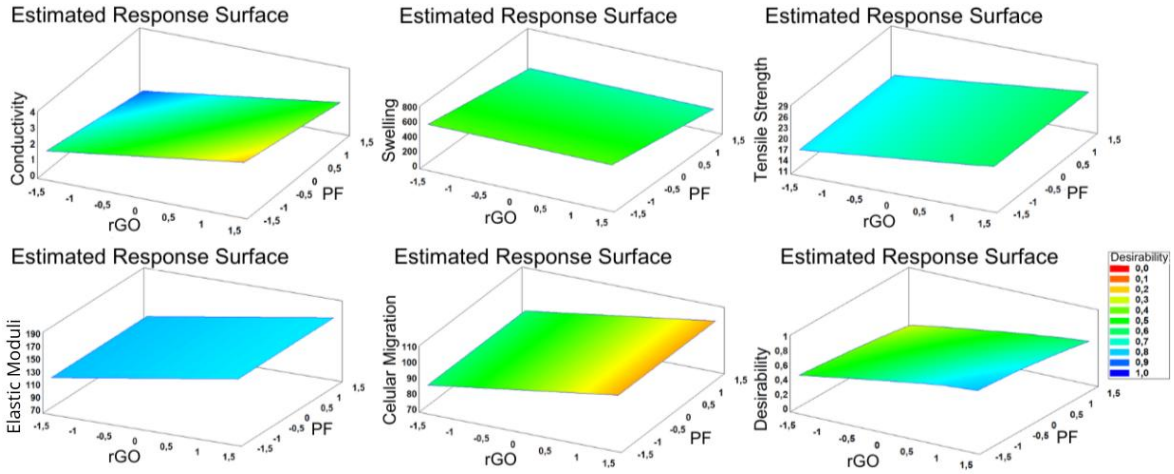

Figure 2.3. Estimated response surface plots: conductivity (Y_1); swelling (Y_2); tensile strength (Y_3); elastic moduli (Y_4), and cell migration (Y_5).

Conductivity: **Figure 2.3** presents the estimated surface diagram, which clearly illustrates how conductivity is affected by the variation of these two variables (rGO and PF). An increase in rGO concentration is observed to be correlated with an increase in conductivity, evidenced by the positive slope in the X-axis direction. In contrast, the negative slope along the Y-axis reflects that an increase in the PF proportion results in a decrease in this property. This analysis not only offers an intuitive visualization of the interaction between rGO and PF but also allows the identification of optimal regions in the variable space, where the combination of rGO and PF amounts maximizes this property. The results of the analysis of variance (ANOVA), presented in **Table 2.2** and complemented by **Equation 2.8**, highlight the differential importance of these variables. PF was found to be the most critical variable for Y1, since an increase in its proportion hurts conductivity. Specifically, it is estimated that for each additional unit of PF, the conductivity decreases by 0.389445 units, keeping the amount of rGO constant. The

coefficient of determination (R^2) was 95.31%, indicating that the regression coefficient model can predict the optimal value with a significant level of accuracy and fits the data well when applied.

Conductivity (Y_1) = 1.79367 + 0.56316* rGO - 0.389445*PF (2.8)

The conductive properties of the materials were measured using the 4-point method. Dressings for wounds with conductivity similar to human skin ($1 \cdot 10^{-4}$ mS/cm to 2.6 mS/cm) can stimulate wound healing, as the skin is composed of epidermis, dermis, and subcutaneous tissues, which are sensitive to electrical signals[226–228]. Hydrogels showed different conductivities (**Figure 2.4A**) ranging from 0.001 mS/cm (CS-PF_{15}) to 2.75 mS/cm (CS-rGO-PF_{15}), indicating that rGO positively contributed to the conductivity of the hydrogels. The gradual increase in the conductivity of the materials can be associated with the free charges in the hydrogel network and the presence of rGO. It is known that rGO acts as a conductive material that can modulate the immune function of macrophages and promote wound healing[229]. Jing et al. (2017) developed an electroactive composite compound of CS/GO/DA for tissue engineering using different concentrations of rGO (0, 0.25, 0.5, 0.75, 1)[230]. The results obtained showed conductivity values like those reported in the present study. The CS/rGO hydrogel developed by Liang et al. (2020) for chronically infected wounds also reported similar conductivity values to those found in this research[231]. Therefore, the conductivity of human skin holds great potential for bioelectrical signaling and wound healing, making our hydrogel a promising candidate for conductive dressings for skin wounds.

Swelling: This response variable is crucial in the study of hydrogels used as dressings. Analysis of the response surface diagram (**Figure 2.3**) allowed the interaction between PF and swelling of the hydrogels to be visualized. This diagram provides valuable information on how swelling levels vary depending on different PF combinations. The interpretation of the results and **Equation 2.9**

suggests that the reduction in PF levels leads to a significant increase in swelling capacity, which could have practical implications for effective dressing design. The coefficient was 98.15%, indicating that the regression coefficient R^2 model can predict the optimal value with a high degree of accuracy, and the model fits the data well when applied. **Table 2.2** presents the statistical results supporting this claim, demonstrating the consistency of the model under different experimental conditions.

$$\text{Swelling } (Y_2) = 437.101 - 92.5013*PF \quad (2.9)$$

The swelling behavior of hydrogels is presented in **Figure 2.4B**. While rGO content in the hydrogels increased, the ability of the hydrogels to absorb simulated human fluid decreased. This is because the phyllic pendant groups of rGO (OH and COOH) form hydrogen bonds with water molecules and other molecules[232]. With the rGO increase in the hydrogel, the number of amide bonds between the carbonyl groups of rGO and the amino group of CS also increases. This enhancement affects the interaction between rGO hydrophilic groups and water molecules, hindering the expansion of the network and resulting in a decrease in the swelling capacity of the hydrogel[233]. The presence of high rGO content acts as a filler material, creating steric hindrances that interfere with water molecules[234]. The low swelling can be attributed to the presence and interaction of PF, which, according to previous studies, limits this phenomenon. This is due to the formation of an interpolymeric complex between the polymer and the monomer, which restricts swelling by hydrophobic association of the PPO segments in aqueous medium. This interaction modifies the electrostatic charge density and the availability of carboxyl groups in the rGO and CS chains, leading to a more compact and dense structure. As a result, both the number and size of aqueous channels are decreased, limiting fluid absorption and hindering swelling[220,235]. The fitting of the simulated fluid absorption to kinetics models (**Table A.2**). The *n* values obtained ranged from 0.45 to 0.84, suggesting a non-

Fickian (anomalous) diffusion process involving a combination of diffusion-controlled absorption and relaxation of the polymer chains[236]. The R^2 values for the first-order model in the hydrogels were closer to one, indicating that absorption fits a first-order pattern.

Mechanical properties: In tensile strength (Y_3) and elastic modulus (Y_4) (**Figure 2.3**), the response surface plot analysis reveals a linear and increasing relationship between these two variables as a function of the amount of rGO. This finding implies an increase in tensile strength and elastic modulus for the material. The mathematical models described by **Equations 2.10 and 2.11** suggest that, for each additional unit of rGO incorporated, the tensile strength increases by 1.80261 units, while the elastic modulus increases by 15.7546 units. This pattern reveals a significant positive correlation between the rGO concentration and the mechanical properties of the studied material. Although the mathematical models obtained indicate that the effect of rGO on tensile strength and elastic modulus is a linear relationship, the experimental results reveal that it is not strictly linear, but rather dependent on the interaction with the PF concentration. Although statistical analysis shows an overall positive coefficient for rGO, experimental results show that the initial incorporation of rGO into CS/PF formulations can reduce mechanical properties.

$$\text{Tensile strength } (Y_3) = 19.562 + 1.80261^{*} \text{ rGO} \quad (2.10)$$

$$\text{Elastic modulus } (Y_4) = 144.683 + 15.7546^{*} \text{ rGO} \quad (2.11)$$

The mechanical behavior of the synthesized materials was investigated through tensile tests (**Figure 2.4C and 2.4D)**. The rGO incorporation into the CS matrix enhanced the mechanical properties of the materials. CS-PF_{15}, CS-$rGO_{0.5}$ shows higher values of the tensile strength and elastic modulus, due to the ability of rGO to generate hydrogen bonds, electrostatic interactions, and π-π stacking with the CS matrix[237]. When comparing the results of the tensile test on hydrogels with equal percentages of PF, higher values are observed with an increase in rGO

concentrations. Higher values of tensile strength (**Figure 2.4C**) and elastic modulus (**Figure 2.4D**) were observed in the hydrogels with increasing rGO concentrations. This may be because, during the stretching process, the rigid CS network breaks first to dissipate the majority of the energy, while the flexible PF network can effectively dissipate and transfer tension in the system, as well as the organization of the rGO sheets due to π-π interactions, forming a compact network with the CS[238,239]. Studies conducted by Salimiyan et al. (2023) [205] and Kosowska et al. (2019)[237] on CS-rGO hydrogels with biomedical applications, report an increase in the mechanical properties of the hydrogels with an increase in rGO concentration. This may be because the oxygen-containing functional groups on the surface of the filler form hydrogen bonds with the -NH_2 groups in the CS, which generate numerous cross-linking points in the hydrogel network; as a result, the mechanical strength is improved.

Cell migration: Obtaining conductive hydrogels that promote cell migration is essential for tissue repair, as they facilitate the movement of cells toward injured areas and provide an enabling environment for cell proliferation. The response surface diagram (**Figure 2.3**) reveals a clear upward trend along the axis corresponding to rGO. This finding suggests that an increase in the rGO concentration is associated with significant improvement in cell migration. The visualization of these results made it possible to demonstrate how different rGO concentrations impact the migratory behavior of cells. In this sense, the statistical analysis (ANOVA **Table 2.2**) has confirmed that an increase in rGO concentration generates positive and statistically significant effects on this property (Y_5). The coefficient R^2 was 96.45%, indicating that the regression model adequately fits the data obtained and allows obtaining the optimal value with high accuracy. The mathematical model (**Equation 2.12**) showed that for each additional unit of rGO, an approximate increase of 5.90112 units in this property is anticipated. This result shows a direct and positive relationship between the concentration of rGO and cell migration.

Cellular migration (Y_5) = 94.295 + 5.90112* rGO (2.12)

Cell migration capacity and wound healing rate were evaluated in HDF (**Figure 2.4E and 2.4F**). Hydrogels synthesized with rGO showed a higher cell migration over time compared to the negative control (2% SFB) and CS-PF_{15}, suggesting that the inclusion and increase of rGO concentration in the materials promote cell migration by providing a pathway for electrical signal transmission between wound cells, thus regulating their behavior and promoting wound healing (**Figure 2.4E**). Regarding wound healing rate, it was observed that wells with hydrogels containing rGO showed a closure rate approximately 15% higher than wells containing CS-PF_{15} and the negative control after 12 hours (**Figure 2.4F**). At 48 hours, increased cell migration with larger closure areas was observed, with materials containing higher concentrations of rGO showing complete wound closure. Several studies have explored the potential of CS, rGO, and PF hydrogels to promote cell migration. Scanga et al. (2010) proposed the use of CS in neural tissue engineering, demonstrating its promotion of survival, migration, and differentiation of neural stem cells and adult-derived neural progenitor cells[240]. Similarly, Kwon et al. (2012) developed a CS hydrogel in the presence of valproic acid that acted as a suitable biocompatible substrate for attachment and proliferation of muscle-derived stem cells[241]. Guo et al. (2024) found that CS conduits filled with simvastatin/PF hydrogel significantly improved migration and regeneration of peripheral nerve tissues[124]. Wang et al. (2017) developed rGO-based conductive hydrogels to promote cell adhesion and growth[242]. Liang et al. (2021) developed a compound based on carbon nanotubes coated with antibacterial, conductive, and antioxidant CS, DA, and gelatin to promote the regeneration of infected skin, with results showing effective therapeutic effects in treating infected full-thickness wounds[48]. Sayyar et al. (2015) studied cell migration in L929 cells using CS/reduced GO hydrogels with lactic acid. The results obtained showed good proliferation, adhesion, and viability, suggesting

they are excellent candidates for biodegradable materials in cellular tissue engineering structures[243].

Table 2.2. Analysis of variance (ANOVA) of the experimental design variables.

Source	Sum of Squares	Mean Square	*p*	Standard Error	F value	R^2	R^2(adj)
Conductivity (Y_1)							
X1: rGO	7.61157	7.61157	0.0000	0.440084	39.30	95.3123	94.4571
X2: PF	3.64002	3.64002	0.0000				
Error	0.0007	0.00023333					
Total	17.2589						
Swelling (Y_2)							
X2: PF	205355	205355	0.0233	0.14113	13.87	98.1587	97.3651
Error	1.5414	0.0958					
Total	1.124E4						
Tensile strength (Y_3)							
X1: rGO	77.9851	77.9851	0.0347	0.3933	32.24	96.5183	95.3574
Error	4.08411	0.1570					
Total	518.898						
Elastic Moduli (Y_4)							
X1: rGO	5956.97	5956.97	0.0197	0.3101	45.93	97.4139	96.1011
Error	2.5052	0.9635					
Total	31088.4						

Celular migration (Y_5)							
X1: rGO	835.755	835.755	0.0000	0.5874	33.26	96.4587	95.3254
Error	1.8810	0.3388					
Total	1730.0						

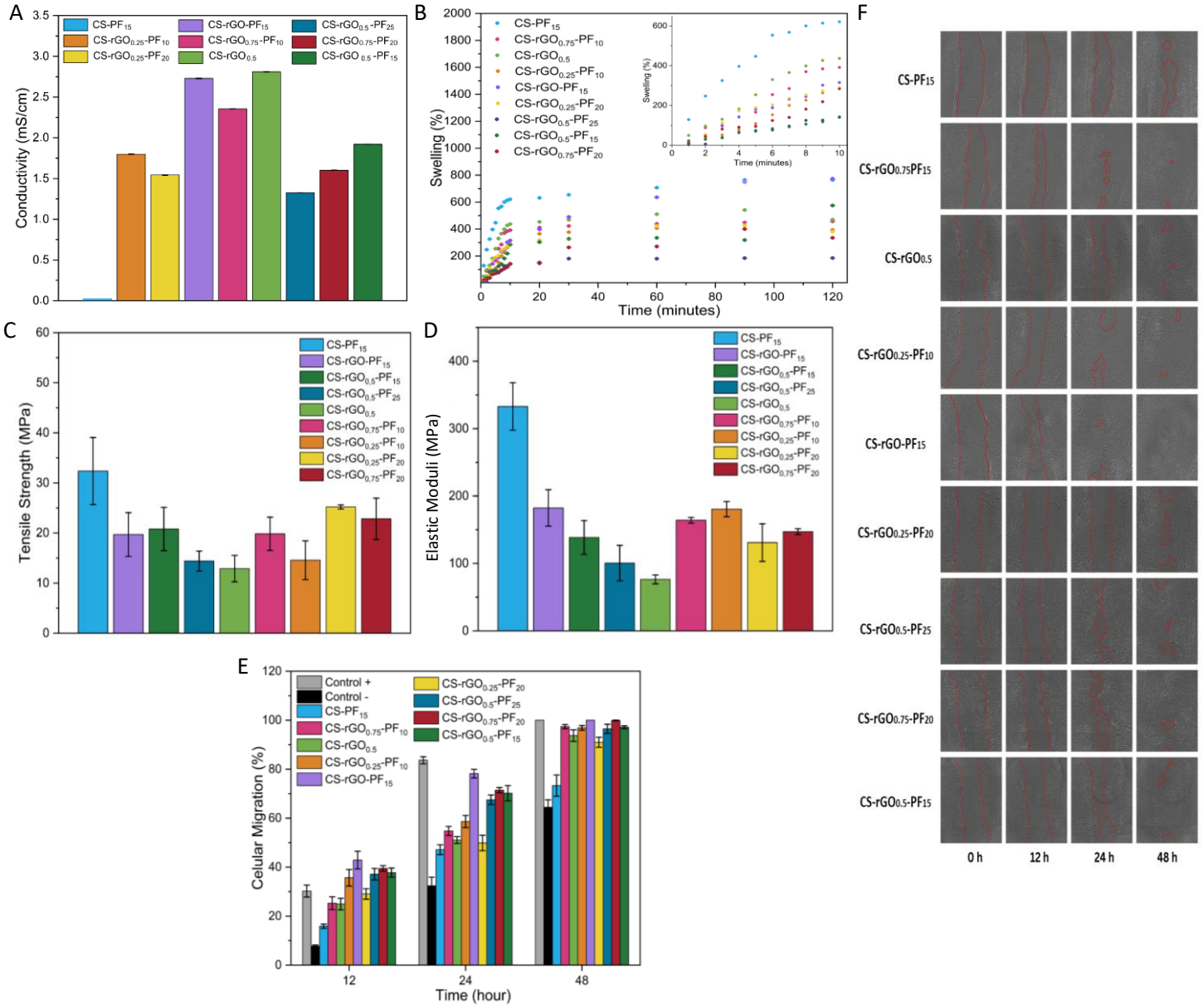

Figure 2.4. (A) Conductivity; (B) Swelling of the hydrogels; (C) Tensile strength; (D) Elastic Moduli; (E) In vitro wound healing over time for hydrogels synthesized; (F) Images of wound closure in time 0, 12, 24, and 48 hours for hydrogels synthesized.

2.4.4 Antibacterial activity

The antibacterial properties of the hydrogels were evaluated *in vitro* using two model strains, *E. coli* and *S. aureus* (**Figure 2.5A**). It has been reported that CS possesses antibacterial qualities due to its polycationic nature, which interacts with the negative charges present in the membranes of bacteria, causing their deterioration[244,245]. On the other hand, rGO has also been previously attributed to antibacterial properties for both Gram-positive and Gram-negative bacteria, associated with the generation of oxidative stress and the rupture of cell membranes due to sharp two-dimensional rGO sheets, resulting in the lysis of bacteria[246–249]. The increase in the rGO proportion in the hydrogels favored their antibacterial capacity, while the inclusion of PF did not appear to notably improve this characteristic. Additionally, it was observed that the synthesized hydrogels showed over 90% inhibition of bacterial growth after 2 hours of material incubation, with the *S. aureus* strain being more sensitive to the tested materials than *E. coli*. Hydrogels based on CS/rGO have shown promising antibacterial activity[224,250–253]. Hydrogels based on CS/PF with antibacterial properties have also been developed, although the effect is not attributed to PF[175,254]. Morsi et al.(2023) investigated the antibacterial activity of a cellulose acetate-rGO-PF composite material at different rGO concentrations. The results showed excellent antibacterial activity, even at the lowest concentration (0.005%)[255]. This research suggests that hydrogels can offer highly effective antibacterial properties and be suitable for biomedical applications.

2.4.5 Cell Viability

The cell viability of the hydrogels was studied by MTT using human dermal fibroblast cells; the results are shown in **Figure 2.5B**. It was observed that all synthesized materials showed cell viability values above 80%, indicating they are

not toxic to the cells; some materials even showed cell viability values higher than the positive control. Qu et al.(2018), evaluated the effectiveness of various compositions of a CS/PF hydrogel loaded with turmeric for wound healing dressings. The *in vitro* cell culture study revealed that the hydrogels were not toxic to L929 cell lines[256]. Another study reported good cytocompatibility results in the same cell line when using CS/PF/Glutaraldehyde hydrogels for tissue engineering applications[257]. Additionally, it has been reported that materials based on rGO/poly(2-ethyl-2oxazoline) evaluated in HDF remained highly viable (cell viability > 75%), even when incubated with a high dose of nanomaterial (100 µg/ mL) for 48 hours[258]. The hydrogels synthesized by Kosowska et al.(2020), based on CS/rGO and poly(ethylene glycol), did not show cytotoxic effects on hUC-MSC cells.[259] Sunneetha et al. (2023) developed carboxymethyl CS/rGO/PDA for wound healing applications. In this study, all hydrogels maintained cell viability (100%) after the 72-hour incubation period with fibroblasts[221]. It is important to note that *in vitro* microplate assays can broadly predict material-culture interactions.

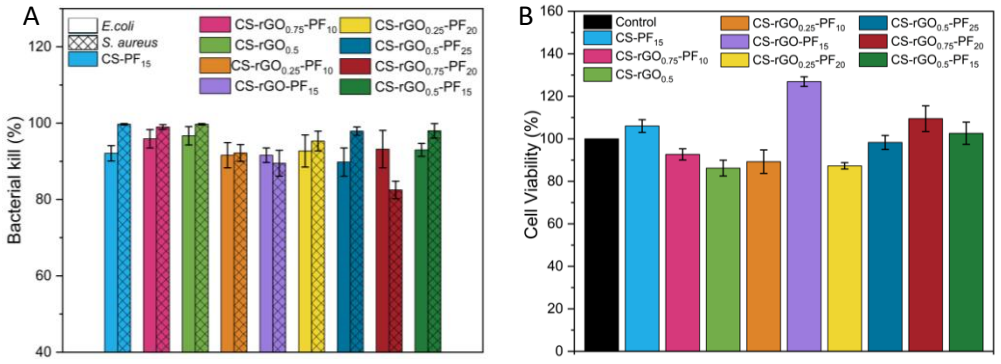

Figure 2.5. (A) Capacity of antimicrobial hydrogels synthesized and (B) Viability of fibroblast cells in humans in the presence of the hydrogels synthesized.

2.4.6 Optimization design for the hydrogel synthesis

An optimization analysis was performed to determine the combination of experimental factors that simultaneously improve the desired responses (**Table 2.3**). According to this analysis, it can be concluded that the optimal levels of concentration to synthesize a hydrogel with excellent conductive, absorption, mechanical, and biological properties are: the highest level of rGO, that is, a 1:1 ratio CS/rGO, and the lowest level of PF (10%). The Pearson diagram (**Figure A.4**) shows the relationship between two statistically significant variables. The correlation coefficient between swelling and cell migration is close to -1 (-0.70), indicating an inverse relationship between the variables. This may be attributed to the fact that, in the case of swelling, the variable with the most significant weight is PF (negatively affecting), whilst in cell migration, it is rGO (positively affecting). On the other hand, the correlation coefficient between conductivity and cell migration is close to 1 (0.75), suggesting that as one variable increases, the other also. This confirms the theory that conductive hydrogels promote the wound-healing process[260–263]. After performing the statistical analysis of the experimental design and the characterization of the hydrogels, it is concluded that the material that best meets the properties required for use as a wound dressing is the CS-rGO-PF_{10} material. This hydrogel was synthesized, and tests were carried out to evaluate the variables (Y_1, Y_2, Y_3, Y_4, and Y_5), to compare the results with the optimal values provided by the statistical software. The obtained results are consistently aligned with those generated by the software (**Table 2.3**), allowing us to affirm that the hydrogel composition that optimizes the desired properties is indeed CS-rGO-PF_{10}.

Table 2.3. Multiple Response Optimization: Combination of experimental factors, desired Outcomes, and actual values.

Response	High desirability	Low desirability	Optimal value	Goal	Actual values
Y_1	0.01	2.81	2.32	Maximized	2.30
Y_2	160.61	864.43	575.85	Maximized	577.42
Y_3	11.42	28.09	22.26	Maximized	22.14
Y_4	77.6	181.42	168.31	Maximized	169.97
Y_5	70.7	100.0	100.0	Maximized	100.0

2.4.7 Analysis of the *in vivo* assay

The hydrogel synthesized under the optimum rGO and PF concentrations was evaluated in an *in vivo* porcine model to validate its efficacy in tissue regeneration, as well as the body's immune response and its integration with the surrounding tissue. This study sought to determine not only the hydrogel's ability to promote tissue healing and regeneration but also its biocompatibility and the way it interacts with the body's cells and structures. Detailed observations were made during the regeneration process, evaluating factors such as inflammation, vascularization, and new tissue formation.

Figure 2.6A illustrates the progression of wound healing and the closure rates for different treatments over a while. By the fourth day following the injury, the negative control exhibits an absence of any repair indicators, with a significant amount of bleeding obscuring the wound. Conversely, treatment with CS-rGO-PF_{10} produces the formation of fibrinoid tissue (scab) over the wound by the fourth day—a development that does not appear in the untreated wound until the twenty-first day. These results correspond to the wound closure rates shown in **Figure 2.6B**, where CS-rGO-PF_{10} exhibits the highest rate at 25%, in contrast to the

untreated wound, which has a rate of 5%. At the 16-day mark, the best-performing material (CS-rGO-PF_{10}) shows a wound area closure rate similar to that of the commercial dressing used as a positive control, with both achieving over 80% closure. In stark contrast, the untreated wound (negative control) and the wound treated solely with CS hydrogel exhibit significantly less healing, with closure rates of 50% and 63%, respectively. By the 21st day, wounds treated with both the optimal material and the positive control reach complete closure (100%), whereas the CS hydrogel and negative control remain under 80%. These results suggest that the optimal material is as effective as traditional treatments and may provide additional benefits by speeding up the healing process. The superior performance can be credited to attributes such as enhanced cell proliferation and tissue formation, as documented in prior studies[264,265]. Moreover, the inclusion of rGO in the composite material likely boosts its antibacterial and anti-inflammatory capabilities, which further enhance its effectiveness in wound healing[266].

A histomorphometric analysis was carried out using H&E staining (**Figure 2.6C and Table A.3**) to gain a comprehensive understanding of the hydrogel behavior in a biological environment. The results indicate that treatment with CS-rGO-PF_{10} significantly improves tissue regeneration compared to CS alone and the untreated wound, showing a similar effect to the positive control. This material favors the formation of skin appendages, evidencing complete repair on day 21, which, according to the literature, should be seen from day 14 onwards.[267] In contrast, hyperkeratosis and acanthosis in the untreated wound reflect poor epithelial maturation, which improves with the treatments[268].

In **Figure 2.6C**, it can be observed that on day 4, re-epithelialization (red arrows) was more evident in the CS-rGO-PF_{10} sample, with a score of 2, indicating partial coverage of the wound, observing up to the basal and spinous stratum in one-third of the sample. In comparison, the wound treated with CS-based hydrogel alone showed re-epithelialization covering only 1/5 of the sample surface, presenting a less developed cell layer. On the other hand, the untreated wound

did not show signs of re-epithelialization (score 0), while the positive control obtained a score of 2, similar to CS-rGO-PF_{10}, reflecting partial coverage, although without notable differences between both treatments. This suggests that the CS-rGO-PF_{10} material has promising potential to stimulate epithelium formation compared to CS hydrogel alone or in untreated wounds. In terms of neovascularization, the CS-rGO-PF_{10} material showed outstanding results, reaching a score of 3, indicating the formation of more than 10 vessels per high magnification field (40X). In contrast, the untreated wound, as well as the CS treatments and the positive control, all scored 2, with a presence of between 6 and 10 vessels per visual field. Regarding granulation tissue (green arrows, **Figure 2.6C**), CS-rGO-PF_{10} also led with a score of 3, reflecting an abundant amount of this tissue essential for regeneration. Meanwhile, both the CS sample and the positive control scored 2 (moderate amount), while the untreated wound scored 1, indicating a low amount of granulation tissue. Regarding inflammatory cell infiltration, a greater inflammatory response was observed in the CS sample, with a score of 3, indicating an abundance of inflammatory cells. Both CS-rGO-PF_{10} and the positive control showed a score of 2, suggesting a moderate inflammatory response. On the other hand, the untreated sample also presented a score of 2, highlighting that the inflammatory responses were not significantly different between the treatments and the control at this analysis time. These results suggest that CS-rGO-PF_{10} achieves an adequate balance in the inflammatory response, necessary for efficient healing. On day 21, the CS-rGO-PF_{10} sample showed the best results in tissue regeneration, evidencing complete epithelial differentiation with well-defined dermal papillae and epidermal ridges, in addition to a notable vascularization close to the epithelial basement membrane. Well-organized connective tissue was observed, with clear differences between the papillary dermis and the reticular dermis, and the presence of developing hair follicles (yellow arrow, **Figure 2.6C**), without signs of hyperkeratosis or acanthosis (black arrows, **Figure 2.6C**). In comparison, the untreated wound presented

marked acanthosis and loose connective tissue. The CS sample showed mild acanthosis and absence of skin appendages, while the positive control showed epithelial maturation, although without epidermal ridges and with less organized connective tissue, accompanied by greater inflammatory than fibroblastic infiltrate. These findings are of great relevance for the development of more effective treatment strategies in tissue regeneration, highlighting the potential of the CS-rGO-PF_{10} hydrogel as a promising biomaterial for clinical applications in wound healing.

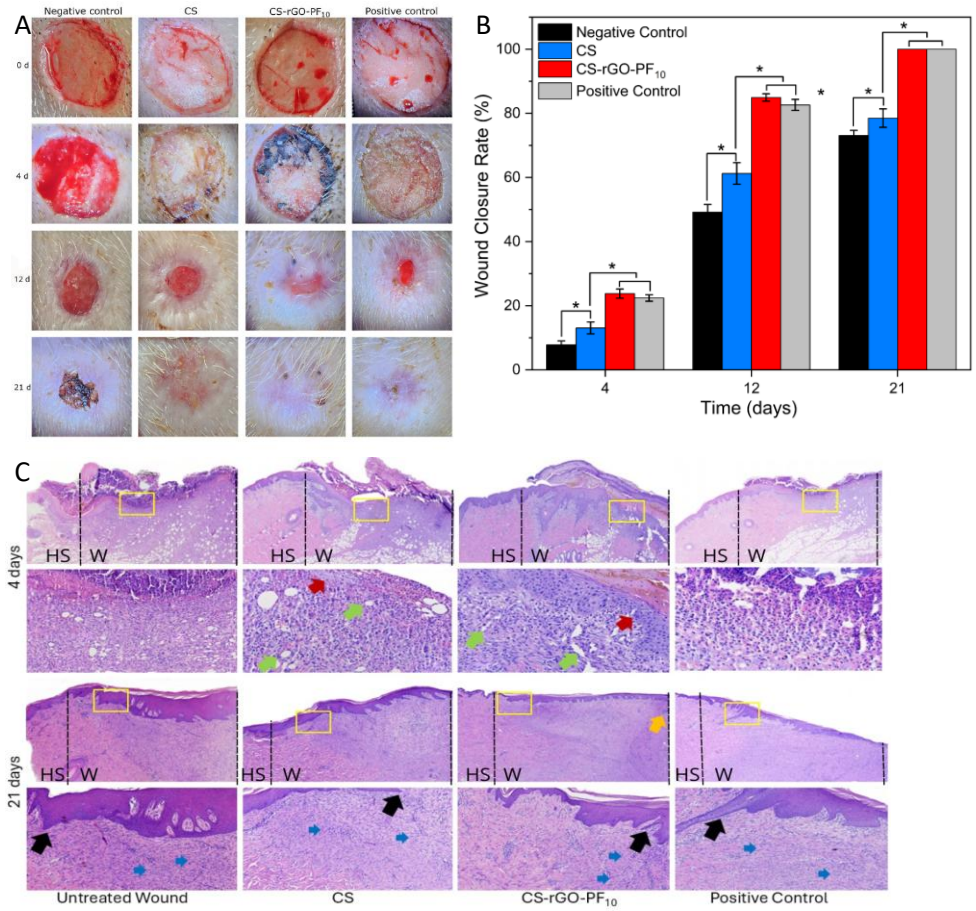

Figure 2.5. (A) Healing potential of the CS-rGO-PF_{10} in wound closure. Sample images illustrating the progression of wound healing for the synthesized hydrogels after treatment on days 0, 4, 12, and 21; (B) The percentage of wound closure

was assessed using Image J, utilizing digital analysis calibration. Results are presented as mean ± SD, derived from three independent experiments (*$p \leq 0.05$), and (C) Histological examination of the wounds was conducted using Hematoxylin and eosin (H&E) staining at a magnification of 2X, with a digital zoom to 40X from the highlighted yellow box.

Note: Between the black dotted lines, the wound is observed to the right and the adjacent healthy skin to the left. In the upper panel, day 4 post-wound. In the lower panel, day 21 post-wound. Red arrow: Re-epithelialization. Green arrow: Granulation tissue. Yellow arrow: Skin appendages (hair follicle). Black arrow: Acanthosis. Blue arrow: Fibroblasts.

2.5. Partial Conclusions

- Wound dressings were developed from a CS-rGO-PF hydrogel using a full factorial experimental design (2^2 + star). Optimization of the experimental design identified CS-rGO-PF10 as the optimal dressing.
- Morphological and physicochemical characterization demonstrated that the hydrogels exhibit excellent structural stability, with a hydrophilic surface and absorption kinetics governed by diffusion and polymer chain relaxation.
- The developed hydrogels showed conductivity comparable to that of human skin, indicating great potential for applications in bioelectrical signaling and wound healing.
- In vitro tests revealed that the hydrogels promote cell migration and increase the rate of wound closure, suggesting their ability to facilitate cell communication and regulation throughout the healing process. Furthermore, they demonstrated remarkable antimicrobial activity against E. coli and S. aureus, while maintaining cell viability above 80%.
- After 21 days of treatment, the CS-RGO-PF10 hydrogel achieved complete wound closure—a result comparable to the positive control—while the hydrogel composed solely of CS and the negative control showed significantly less progress. Beyond accelerating closure, CS-RGO-PF10 promoted high-

quality tissue regeneration, evidenced by the formation of skin appendages and adequate vascularization. Histomorphometric analysis confirmed that this material efficiently stimulates re-epithelialization, neovascularization, and the generation of abundant granulation tissue, producing structurally robust tissue accompanied by a moderate inflammatory response—key conditions for optimal healing. Taken together, these findings solidify the CS-RGO-PF10 hydrogel as a highly promising biomaterial for advanced wound treatment applications.

Chapter 3

Bioinspired Synergistic Chitosan-Graphene-Tannin Hydrogel Orchestrates Inflammation Resolution and Accelerates Skin Tissue Repair.

Isleidy Ruíz, Luisbel González, Julia Eduarda Schneider Gregória, Cintia Sena Bueno, Maria Esméria Corezola do Amaral, Guilherme Ferreira Caetano, Katherina Fernández, submitted to the journal Biomaterials Science.

3.1 Abstract

Wound healing remains a major clinical challenge due to the complex metabolic disturbances present within the wound microenvironment. In this study, we report the development and comprehensive validation of a novel multifunctional hydrogel composed of chitosan (CS), reduced graphene oxide (rGO), and tannins (TA) (CS-rGO-TA), specifically engineered as an advanced wound dressing. The hydrogel was thoroughly characterized using SEM to examine its porous microstructure, FTIR to analyze component interactions, the DPPH assay to assess antioxidant capacity, and total phenols to evaluate the release kinetics of TA. Antibacterial activity was tested in vitro against *Escherichia coli* and *Staphylococcus aureus* using standard colony-forming unit assays. Biocompatibility and regenerative potential were assessed through cell viability and migration assays using human dermal fibroblasts. *In vivo* evaluation included a skin irritability model in guinea pigs and a full-thickness excisional wound model in rats, divided into four treatment groups. Wound closure progression was monitored over time, and histological analysis was performed using hematoxylin and eosin (H&E), Mallory, and Masson's Trichrome staining to assess tissue morphology and collagen deposition. The CS-rGO-TA_3 hydrogel demonstrated

controlled and sustained TA release, strong antioxidant and antibacterial properties, and excellent biocompatibility, with no signs of irritation or adverse effects. Its application significantly accelerated wound closure and promoted organized deposition of collagen (types I and III). Molecular analysis revealed early resolution of inflammation, enhanced angiogenesis, and polarization of macrophages toward a reparative M2 phenotype, as evidenced by modulation of markers such as MPO, CD68, ARG1, and interleukins IL-6, IL-10, IL-1β, and IL-1rn. Collectively, these findings highlight the CS-rGO-TA_3 hydrogel as a safe and effective therapeutic platform with strong potential for tissue regeneration and clinical wound management.

3.2 Introduction

Wound healing treatment has evolved significantly over the years, prompting the search for innovative and effective treatment modalities[269]. Among the numerous advancements in this field, wound dressings have gained considerable attention for their ability to facilitate the healing process and minimize complications. Hydrogel dressings have emerged as a promising solution for wound healing due to their ability to provide a moist environment that facilitates the healing process[6,7]. This property helps absorb wound exudate and allows for shape adaptation, which is beneficial for wounds in areas of constant movement, offering significant advantages over traditional dry dressings, which often lack functionality and can cause pain upon adhering to the wound[34,35,178]. Hydrogels can also be modified to incorporate active compounds such as growth factors and antibacterial compounds, which enhances their effectiveness in wound healing[8,9]. Furthermore, they can be designed to be self-adhesive, antioxidant, and self-healing, which prolongs their lifespan and improves wound protection[270,271].

Chitosan (CS) is an alkaline polysaccharide obtained from the partial deacetylation of chitin present in some crustaceans[272]. CS is a biopolymer

distinguished by its antimicrobial[273], biodegradable[274], and non-toxic[275] properties, in addition to possessing excellent biocompatibility [118], mucoadhesive properties [123], limited immunological reactions [125], and characteristics that favor absorption [276]. Thanks to its remarkable biological properties, such as promoting blood coagulation, promoting fibroblast proliferation, and collagen formation, CS contributes to improving the wound healing process[122]. Despite their benefits, CS hydrogels often face challenges related to their mechanical properties, so the incorporation of nanomaterials and biomolecules is a promising strategy to improve or generate new functions in these hydrogels. Reduced graphene oxide (rGO) offers a multifaceted approach for the synthesis of new hydrogels[129]. Hydrogels containing rGO possess good mechanical [64], conductive properties [277] and antibacterial activity [132], combined with their ability to promote angiogenesis, cell proliferation, and migration in the wound healing process[10]. The hydrogel composed of CS/RGO and an electrolyzed polycaprolactone and cellulose acetate membrane designed by Graça et al. (2022) demonstrated the ability to provide a moist environment, prevent exudate accumulation, and allow gas exchange, as well as act as a barrier against bacterial penetration and show cell viability greater than 90% against human dermal fibroblast cells[278]. modern hydrogels are designed with antibacterial and antioxidant properties, which are crucial for preventing infection and promoting faster healing[279]. Recent research highlights the potential of incorporating natural biopolymers, such as tannins (TA), into these dressings to enhance their therapeutic properties[280].

The TA, a polyphenolic family, exhibits a variety of properties that significantly contribute to its use in wound dressings. Primarily known for their astringent qualities, TAs facilitate tissue regeneration by precipitating proteins, which improves the healing process and reduces inflammation[17]. Furthermore, their antioxidant properties play a crucial role in mitigating oxidative stress, a detrimental factor in wound healing[281]. The incorporation of TAs into wound

dressings has been shown to improve the overall efficacy of the dressing, offering not only protection against pathogens but also promoting moisture retention, which is essential in moist wound healing environments[18,19]. Zhou et al. (2023) developed a carboxymethyl chitosan hydrogel enriched with TA, which demonstrated antioxidant, antibacterial, and hemostatic properties, significantly improving skin tissue repair[16]. In a more recent approach, Carrasco et al. (2024) incorporated rGO and TA into an alginate-based hydrogel, achieving significant improvements in mechanical strength, tissue adhesion, and cell viability, with no observed cytotoxic effects[20].

Building upon these findings, this study presents the development and validation of a novel multifunctional hydrogel composed of tannin-loaded chitosan-reduced graphene oxide (CS-rGO-TA), specifically designed to address the multifaceted biological challenges associated with impaired wound healing. By integrating the biocompatibility and fluid absorption capacity of CS, the mechanical reinforcement and angiogenic potential of rGO, and the potent antibacterial, antioxidant, and anti-inflammatory properties of TA, this hydrogel provides a synergistic platform that addresses key pathological barriers in both chronic and acute wounds. A major novelty of this work lies in the rational design that enables not only structural support and protection but also active immunomodulation, particularly through the sustained release of TAs, which promotes a macrophage phenotypic switch from pro-inflammatory M1 to reparative M2 states. This is supported by both molecular and histological evidence, a mechanistic insight rarely emphasized in prior hydrogel research. Additionally, the combination of these three components results in enhanced antibacterial efficacy, collagen organization, and vascularization; achievements not observed in hydrogels containing only one or two of these materials. The comprehensive *in vitro* and *in vivo* validation, including Western blot, RT-qPCR, and immunohistochemistry, further substantiates the therapeutic superiority of CS-rGO-TA over conventional formulations. Altogether, this hydrogel represents a significant advancement in the development of

bioengineered wound dressing, offering a multifunctional, immunoresponsive, and tissue-regenerative alternative with broad potential for clinical translation.

3.3 Materials and Methods

3.3.1 Materials

Graphite powder (flakes, 325 mesh) was purchased from Asbury Online (Asbury Carbons, NJ, USA). Low molecular weight chitosan (CS) with a Brookfield viscosity of 200–800 cP (CAS number 9012-76-4) and Pluronic F 127 (PF) (PEO_{97}-PPO_{69}-PEO_{97}) (CAS number 9003-11-06) were purchased from Sigma Aldrich Chemicals (Chile, South America). Phosphoric acid (H_3PO_4), sulfuric acid (H_2SO_4), potassium permanganate powder ($KMnO_4$), hydrogen peroxide (H_2O_2, 30%), hydrochloric acid (HCl), ethanol (C_2H_5OH), tris ($(HOCH_2)_3CNH_2$), dopamine hydrochloride (DA-HCl, minimum 98%), sodium hydroxide (NaOH), silver nitrate ($AgNO_3$), Dulbecco's modified Eagle's medium (DMEM), dimethyl sulfoxide (DMSO), 3-(4,5-dimethylthiazol-2-yl)-2,5-diphenyltetrazolium bromide reagent (MTT), phosphate-buffered saline (PBS), and fetal bovine serum (FBS) were purchased from Sigma-Aldrich Company (St. Louis, MO, USA). All reagents and solvents were of analytical grade and used without further purification. Milli-Q® water was used throughout the study.

3.3.2 Synthesis of Hydrogels CS-rGO-TA

First, a 0.5% w/v rGO solution was prepared in Milli-Q® water and subjected to 2 hours of cooling to facilitate its dispersion in the CS matrix. CS (1.5 g) was then dissolved in a 1% HCl solution. The rGO and CS solutions were then mixed (1:1 v/v) until a homogeneous mixture was obtained and cooled to 4°C. In parallel, Pluronic F-127 (PF) was dissolved in PBS (1% w/v) and loaded with different concentrations of TA (1%, 3%, 5% w/v) by vigorous stirring for 1 hour. These solutions were added to the pre-cooled CS-rGO solution. The mixture was then

sonicated for 30 minutes to remove any air bubbles. Finally, the mixture was placed in a Petri dish and placed in an oven (Huanghua Faithful Instrument Co. Ltd., Huanghua, China) at a maximum temperature of 37°C to promote gelation. The resulting composite hydrogels were named CS-rGO-TA_1, CS-rGO-TA_3, and CS-rGO-TA_5. The rGO used was synthesized in the same way as detailed in the introduction of this thesis (**Chapter 1**). The TA extraction methodology is detailed in **Appendix B.1** of this thesis.

3.3.3 Characterization of Hydrogels CS-rGO-TA

3.3.3.1 Physicochemical Characterization of Hydrogels

The morphological and physicochemical properties of CS-rGO-TA hydrogels were studied using scanning electron microscopy (SEM) and attenuated total reflection Fourier transform infrared spectroscopy (ATR-FTIR). **Appendix A.1** of this thesis includes detailed information on these characterization techniques.

3.3.3.2 Drug release capacity

Samples of the previously synthesized hydrogels (0.5 cm^2) were taken and weighed to determine their mass (mH). They were then placed in 50 mL of PBS and stirred at 37 °C, pH 7.4, at a speed of 60 rpm. At specific time intervals, 100 µL of the soaking solution was collected, and the TA absorbance at 765 nm was measured by UV-Vis spectrophotometry (Techcomp, UV2300, China). The TA concentration was determined from the standard curve, and the mass of TA released from the hydrogel (m_H) was indirectly calculated. The release rate of the CS-rGO-TA hydrogels was calculated according to **Equation 3.1**. The samples were analyzed in triplicate.

$$\text{Release rate}\ (\%) = \ m_H/m_a \ \times 100 \qquad (3.1)$$

3.3.3.3 Antioxidant capacity

Antioxidant activity was measured by an in vitro DPPH. The antioxidant capacity of the hydrogels was evaluated by their ability to scavenge DPPH free radicals. First, a 0.1 mM DPPH solution in ethanol was prepared as a working solution. Next, 20 mg of hydrogel was dissolved in 2 ml of this DPPH working solution and incubated for 1 h in the dark. After incubation, the supernatant was collected, and the absorbance at 517 nm was measured using a UV-Vis spectrophotometer (Techcomp, UV2300, China). The DPPH free radical scavenging activity was calculated by **Equation 3.2**:

$$\text{Scavenging activity}\ (\%) = \mathrm{A_{blank}} - \mathrm{A_{sample}}/\mathrm{A_{blank}} \times 100 \qquad (3.2)$$

Where A_{blank} and A_{sample} are the absorbance values of the DPPH working solution and the sample, respectively. Each sample was analyzed in triplicate. All experiments were conducted at room temperature, atmospheric pressure, and 85% humidity.

3.3.3.4 Hydrogel biocompatibility

The cytotoxicity of the hydrogels was determined using the 3-(4,5-dimethylthiazol-2-yl)-2,5-diphenyltetrazolium (MTT) bromide assay, and cell migration was assessed using a scraping assay. Human dermal fibroblasts were used to evaluate the in vitro cytotoxicity and cell migration of all synthesized materials. The same methodology described in **Chapter 2** was followed for both assays.

3.3.3.5 *In vitro* antibacterial activity

The antibacterial activity of the hydrogels was evaluated in vitro using model strains of *Escherichia coli* (*E. coli*, ATCC 27195) and *Staphylococcus aureus* (*S.*

aureus, ATCC 25923). The same methodology described in **Chapter 2** was followed.

3.3.3.6 Animal Experiments

Each experiment was conducted following the Experimental Standards and Biodiversity Rights (NIH Publication 80-23, revised in 1996, and Arouca Law-11, 794, 2008), approved by CEUA/UNIARARAS (026/2017), and the principles of biosafety and bioethics, with the approval of the Bioethics and Biosafety Committee of the University of Concepción (Approval Number: CEBB 865-2021, May 2021).

3.3.3.6.1 Irritability Assessment

The irritation potential of the hydrogels was evaluated in five guinea pigs (Cavia porcellus, 300–500 g body weight). The procedure began with the administration of anesthesia using ketamine (40–50 mg per kilogram) and xylazine (4–5 mg per kilogram). The dorsal surface of each animal was shaved for 24 h, and two pieces of the material were placed on the shaved skin. The hydrogels were then covered with a transparent dressing (3M Tegaderm™, USA) for a total of 12, 24, 48, and 120 h, after which the dressing was removed and dermal reactions, including erythema, eschar, and edema, were scored according to established guidelines (**Table B.1**). A group of three untreated animals served as controls. After 5 days, the animals were euthanized by CO_2 inhalation in a euthanasia chamber, followed by cervical dislocation.

3.3.3.6.2 Evaluation of the healing potential of hydrogel in the rat dorsal skin wound model.

Wound healing was studied in 36 male Wister rats (mean weight 190–210 g), divided into 4 groups and 3 experimental times (2, 7, and 14 days). The wound healing rate (WHR) of the different groups was assessed by clinical and photographic evaluation of the wounds, and the evolution of the injured areas was recorded using ImageJ software. Finally, all wound biopsies were collected for subsequent histological analysis. Details of the *in vivo* characterizations are described in **Appendix B.2**.

3.3.3.6.3 Histological Analysis

The excised wound tissues were fixed in 10% (v/v) formalin solution, dehydrated through a graded alcohol series (50–100% (v/v)), cleared in xylene, and embedded in paraffin. Serial 4.0 µm-thick sections were cut using a microtome and stained with hematoxylin and eosin (H&E) (assessment of inflammatory infiltrate). The slides were then stained with Mallory and Masson's Trichrome staining (collagen formation evaluation) and examined under a light microscope using Leica Application Suite version 3.2.0 software. For each wound skin sample from each animal, six sections were taken and examined (400x magnification). Collagen formation was quantified using the "Color Deconvolution" plugin in ImageJ software, where the three colors of the trichrome stain were deconvolved. Only the percentage of the total blue area (collagen) in the image was determined. The results were expressed as the average collagen distribution per treatment.

3.3.3.6.4 Histological Analysis

The excised wound tissues were fixed in 10% (v/v) formalin solution, dehydrated through a graded alcohol series (50–100% (v/v)), cleared in xylene, and embedded in paraffin. Serial 4.0 µm-thick sections were cut using a microtome and stained with hematoxylin and eosin (H&E) (assessment of inflammatory infiltrate). The slides were then stained with Mallory and Masson's Trichrome

staining (collagen formation evaluation) and examined under a light microscope using Leica Application Suite version 3.2.0 software. For each wound skin sample from each animal, six sections were taken and examined (400x magnification). Collagen formation was quantified using the "Color Deconvolution" plugin in ImageJ software, where the three colors of the trichrome stain were deconvolved. Only the percentage of the total blue area (collagen) in the image was determined. The results were expressed as the average collagen distribution per treatment.

3.3.3.6.5 Molecular analysis by Western Blot

The quantified proteins (50 µg of total protein) were electrophoresed on a 12% polyacrylamide gel (SDS-PAGE) using the BioRad minigel apparatus with electrophoresis buffer. Transfer of the separated proteins from the gel to a nitrocellulose membrane was performed electrically using a Bio-Rad® device for approximately 1.5 hours at 120V, with the membrane kept on ice. The primary antibodies used are described in **Table B.2**. Optical density was read using ImageJ® software. The results were normalized by comparing the expression with GAPDH. Details of the test procedure are described in **Appendix B.1**.

3.3.3.6.6 RNA Extraction and RT-qPCR

Total RNA from samples collected at 30 days postoperatively was macerated in liquid nitrogen and isolated using TRIzol™ reagent (Invitrogen, Waltham, MA, USA) for RNA isolation, following the manufacturer's instructions. According to the manufacturer's instructions, RNA was converted to cDNA from 1.5 µg of total RNA using the High-Capacity Kit (Thermo Fisher Scientific, Waltham, MA, USA). The TaqMan assays used are described in **Table B.2** and were purchased from Applied Biosystems. Reactions were performed in triplicate with TaqMan Gene Expression Master Mix (Applied Biosystems, Waltham, MA, USA). The entire qPCR procedure was performed according to the previously described

protocol[282]. GAPDH was used as a control for data normalization and validated using BestKeeper software. The PCL group was used as a calibrator, and the results were calculated using the $2^{-\Delta\Delta Ct}$ method.

3.3.4 Statistical Analysis

Students' t-test was used to compare each experimental group with the control group. Different letters indicate statistically significant differences between groups ($p < 0.05$, one-way ANOVA with Tukey's post hoc test). Graphs and statistical analyses were performed using Statgraphics Centurion® XVII software.

3.4 Results and Discussion

3.4.1 Physicochemical Characterization

The surface morphology of the hydrogels was observed by SEM (**Figure 3.1A**). All hydrogels exhibited rough surfaces characterized by well-defined lamellae and amorphous structures, attributable to the varied interactions between the constituent raw materials. Notably, increasing TA content led to denser surface morphology, which is likely due to a higher crosslinking density resulting from enhanced hydrogen bonding and hydrophobic interactions involving the PF.

FTIR analysis was performed to investigate the chemical composition and successful integration of the hydrogel components. The FTIR spectrum of pure CS displayed its characteristic absorption bands, including broad peaks corresponding to hydroxyl (–OH) groups, primary amines, the C=O stretching of amide I, and the C–O–C stretching and N–H bending vibrations of amide II (**Figure 3.1B**)[207,283,284]. The effective reduction of graphene oxide (GO) and subsequent functionalization of rGO with dopamine (DA) amino groups were confirmed by the appearance of distinct absorption bands at 1220 cm^{-1} and 1050 cm^{-1}, respectively[208–210]. The spectrum of TA revealed prominent bands

attributed to both aromatic and non-aromatic hydroxyl groups, C=O stretching vibrations, and C–O stretching modes in aromatic and aliphatic structures[177]. The PF spectrum exhibited characteristic peaks corresponding to CH_2 and CH stretching vibrations, along with distinct signals attributed to C–O–C and C–O bond stretching[211,212]. In the synthesized hydrogels (**Figure 3.1C**), the characteristic bands of CS and rGO were retained, and the intensity of TA-related peaks increased progressively with higher TA concentrations. These spectral features confirm the successful incorporation of TA into the hydrogel matrix and the preservation of essential functional groups from each component, supporting the structural integrity and multifunctional nature of the final formulation.

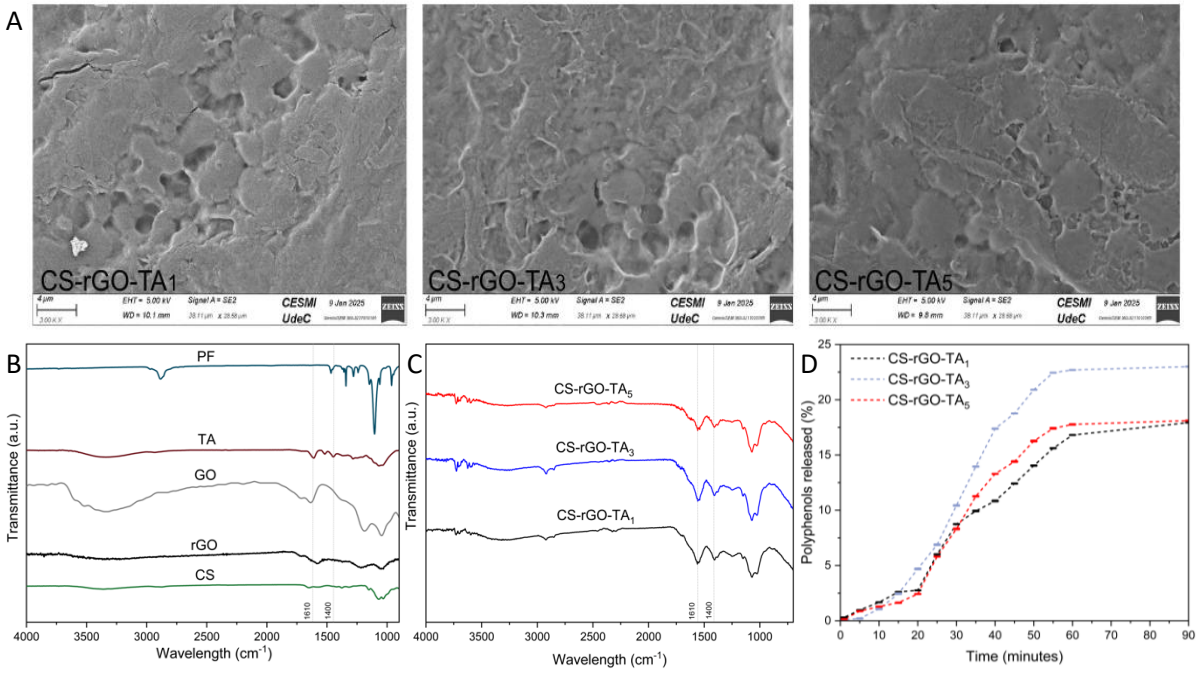

Figure 3.1. (A) SEM images of the hydrogels synthesized; FTIR spectra of (B) the raw materials and (C) the synthesized hydrogel; (D) Release profiles of polyphenols over time.

In the previous chapter, the synthesis of the hydrogel was optimized, and its physicochemical characterization was carried out, yielding representative values of conductivity (2.30 mS/cm), swelling capacity (577.42%), tensile strength (22.14

MPa), and elastic modulus (169.97 MPa). These parameters confirmed the formation of a polymeric network with mechanical and transport properties suitable for biomedical applications, particularly in the fields of tissue engineering and wound healing. Such properties are essential to ensure both the structural stability of the material and its ability to maintain a moist and bioactive microenvironment in direct contact with the injured tissue. Building on this foundation, the present work advances toward the *in vivo* validation of the hydrogel's therapeutic potential, specifically analyzing its effect on the wound healing process. The study focuses on assessing how the incorporation of tannins into the formulation modulates the tissue response, given that these phenolic compounds are well recognized for their anti-inflammatory, antioxidant, and antimicrobial properties.

3.4.2 TA Release Assays

TA release from the hydrogels was evaluated in PBS (pH 7.4), as shown in **Figure 3.1D**. The release profiles demonstrated a sustained and prolonged release over time, indicative of controlled release kinetics. Among the formulations tested, the CS-rGO-TA_3 hydrogel exhibited the highest cumulative release, reaching approximately 23% within the first hour. This controlled release behavior is likely attributed to the stronger interactions between polyfunctional components and TA, as well as the denser network structure of the composite hydrogel, which regulates diffusion. In terms of antioxidant performance, the CS-rGO hydrogel alone exhibited minimal free radical scavenging activity (3%). In contrast, the TA-loaded hydrogels showed a substantial enhancement in antioxidant capacity, with CS-rGO-TA_3 achieving the highest activity at 19%. This effect aligns with the well-established antioxidant capacity of tannic acid, a natural polyphenol known for its ability to neutralize free radicals produced during the wound-healing process effectively[279]. The sustained release of TA from the

hydrogel matrix likely helps mitigate oxidative stress-induced cellular damage, thereby supporting and accelerating tissue repair[285].

3.4.3 Antibacterial Activity

The ability to inhibit microbial growth is a crucial feature of effective wound dressings. In this study, the bactericidal activity of the hydrogels was assessed against two representative pathogens: *Escherichia coli* (a Gram-negative bacterium) and *Staphylococcus aureus* (a Gram-positive bacterium). All hydrogel formulations demonstrated over 90% bacterial reduction for both strains, with the CS-rGO-TA_3 hydrogel showing a slight yet consistent improvement in antimicrobial efficacy (**Figure 3.2A and 3.2B**). This pronounced bactericidal effect is attributed to the synergistic interplay among the hydrogel's three components. CS exerts its well-documented antimicrobial action through electrostatic interactions between its positively charged amino groups and the negatively charged bacterial membranes, resulting in membrane destabilization and ultimately leading to cell death[286]. For its part, rGO enhances this effect through both physical disruption—via its sharp edges—and the induction of oxidative stress by generating reactive oxygen species[287]. The addition of TA further amplifies the antimicrobial response by forming complexes with bacterial proteins, interfering with key metabolic pathways, and contributing to the modulation of the local inflammatory environment[288,289]. Although the incremental increase in bacterial death observed with CS-rGO-TA_3 was not statistically significant, it suggests a potential additive effect of TA. These findings align with those reported by Li et al. (2023), who demonstrated enhanced antibacterial efficacy in CS-based hydrogels loaded with TA compared to those without the polyphenol[290].

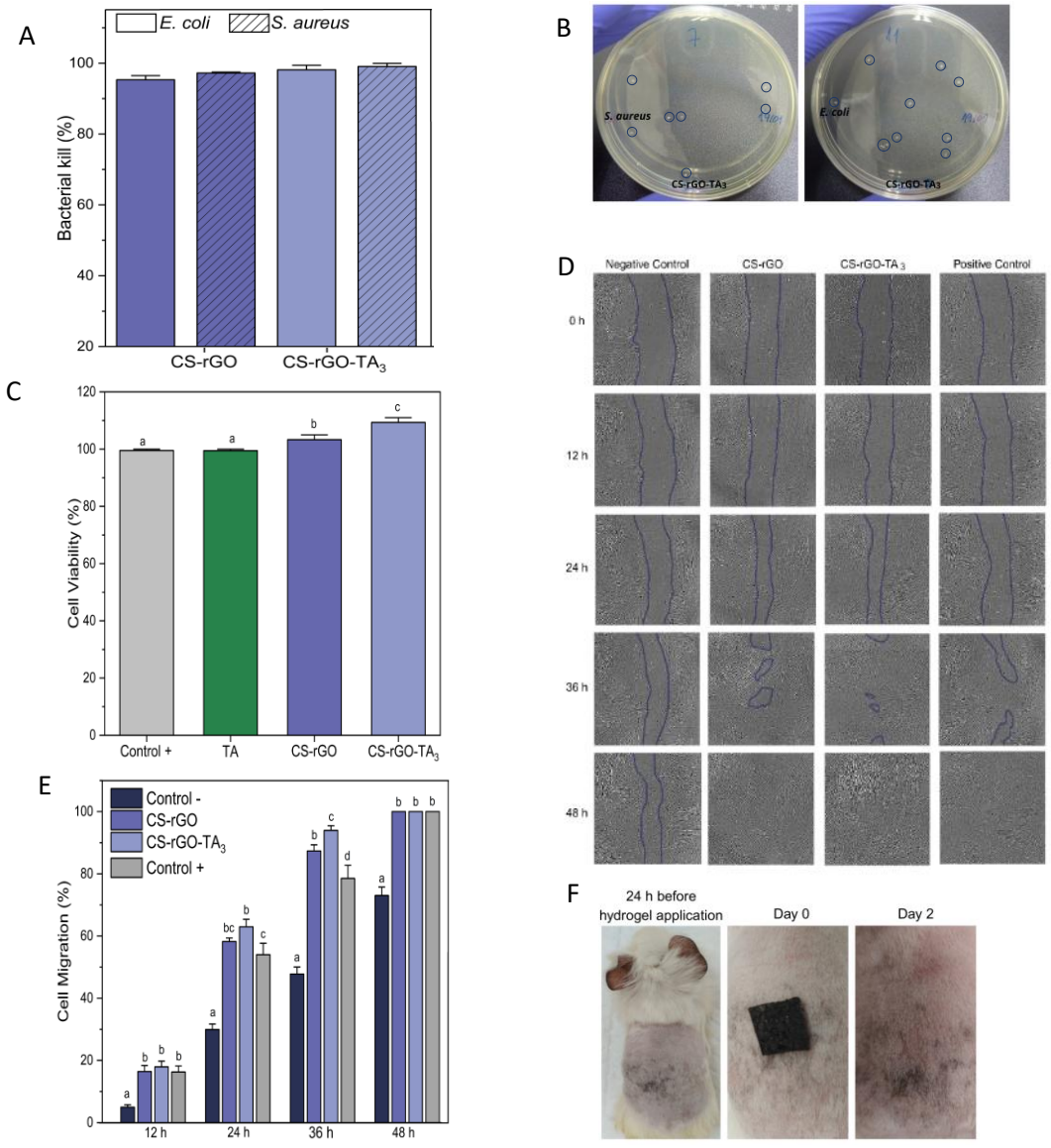

Figure 3.2. (A) *In vitro* antibacterial activities of synthesized hydrogels: *S. aureus* and *E. coli* killing ratio; (B) Photographs of *S. aureus* and *E. coli* colonies on agar plates. *In vitro* characterization of human dermal fibroblast cells in the presence of synthesized hydrogels: (C) Cell viability, (D) Images of wound closure at 0, 12, 24, 36, and 48 hours, and (E) Wound closure rate over time. (F) Images of the dermal irritability assay in guinea pigs.

Results were expressed as mean ± standard error of the mean (significance levels were set at $p < 0.05$, and differences were considered significant when the groups compared displayed different letters)

3.4.4 Cell Viability and Migration Assays

Biocompatibility is a critical factor in the design of wound dressings, as it directly influences cellular responses and tissue regeneration. To evaluate the biocompatibility of the TA-enhanced hydrogel (CS-rGO-TA_3), *in vitro* cytotoxicity assays were performed using human dermal fibroblasts (HDFs). The results showed that HDF viability exceeded 100% after 24 hours of incubation (**Figure 3.2C**), indicating not only the absence of cytotoxic effects but also a stimulatory influence on cell proliferation. Interestingly, the incorporation of TA significantly improved cell viability, suggesting that the CS-rGO-TA_3 hydrogel creates a favorable environment for fibroblast activity and wound repair. Fibroblasts play a central role in wound healing by producing collagen fibers and extracellular matrix components, thereby supporting granulation tissue formation and structural tissue remodeling[291]. To assess the hydrogel's effect on fibroblast migration, a scratch assay was conducted (**Figure 3.2D and 3.2E**). During the first 12 hours post-injury, wounds treated with the hydrogels exhibited closure rates comparable to those of the positive control and significantly greater than those observed in the untreated negative control (**Figure 3.2E**). At 24 and 36 hours, cell migration was notably enhanced in the CS-rGO group, with the TA-loaded formulation (CS-rGO-TA_3) further accelerating closure. Specifically, the CS-rGO-TA_3 hydrogel achieved over 60% closure in 24 hours and exceeded 90% by 36 hours. By 48 hours, complete closure was observed in both hydrogel-treated groups and the positive control, while the negative control remained at approximately 70%. These findings highlight the hydrogel's excellent cytocompatibility and pro-migratory properties, both of which are essential for effective wound healing. Moreover, the results are consistent with previous studies, such as that by Sun et al. (2024), in which a

chitosan/polyethylene oxide hydrogel loaded with TA promoted over 80% cell viability after 72 hours and significantly enhanced fibroblast migration, leading to improved wound closure outcomes in *in vitro* models[292].

3.4.5 Irritation Potential

Materials intended for wound healing must demonstrate both biocompatibility and safety to prevent adverse reactions in dermal tissues. Sensitive skin models, such as guinea pigs, offer valuable insight into the dermatological safety of hydrogel formulations before potential clinical application. In this study, the skin irritation potential of the CS-rGO-TA_3 hydrogel was evaluated (**Figure 3.2F**). The results showed that CS-rGO-TA_3 did not induce any signs of irritation, with no visible changes observed upon removal of the hydrogel, resulting in an irritation index of 0.0 (**Table B.1**). Furthermore, all animals maintained normal feeding and drinking behavior, exhibited unimpaired motor function, and showed no abnormal signs such as lethargy, restlessness, pruritus, or irritability. As no clinical symptoms were detected throughout the observation period, histopathological skin sampling was deemed unnecessary. These findings collectively support the excellent biocompatibility and dermatological safety of the CS-rGO-TA_3 hydrogel.

3.4.6 *In vivo* Healing Assays

Building upon our earlier *in vitro* findings that highlighted the potent antimicrobial properties and excellent biocompatibility of the CS-rGO-TA_3 hydrogel, we proceeded to evaluate its therapeutic efficacy in a rat model of full-thickness excisional wounds. All treatment groups exhibited significantly enhanced wound contraction compared to the untreated control, achieving over 20% wound closure as early as day 2 post-injury (**Figure 3.3A and 3.3B**). This early response suggests a rapid onset of bioactivity, likely facilitated by the hydrogel's capacity to maintain a moist environment, control microbial load, and modulate the local

inflammatory milieu. Among the groups, CS-rGO-TA_3-treated wounds displayed the greatest reduction in wound area and the fastest rate of closure, outperforming both the untreated control and hydrogels lacking TA (**Figure 3.3A and 3.3B**). This superior performance is likely attributable to the combined effects of the hydrogel's physicochemical properties: effective exudate absorption, sustained hydration of the wound bed, and intimate contact with tissue surfaces, which together enhance antibacterial efficacy and attenuate inflammation. By day 7, wound closure rates had increased significantly across all treated groups. Specifically, the CS-rGO-TA_3 group achieved 65.15 ± 2.87% closure, compared to 60.06 ± 2.42% in the CS-rGO group, 55.94 ± 1.76% in the CS group, and 51.47 ± 2.87% in the untreated control (**Figure 3.3A**). By day 14, wounds treated with the TA-loaded hydrogel were nearly fully re-epithelialized, accompanied by visible hair regrowth around the wound edges—a sign of dermal restoration. Quantitative analysis confirmed statistically significant differences between groups, with CS-rGO-TA_3-treated wounds reaching 98.77 ± 0.69% closure, compared to 77.58 ± 1.21% in the untreated group (**Figure 3.3B**). The enhanced healing observed in the CS-rGO-TA_3 group can be largely attributed to the astringent and bioactive properties of tannic acid, which support faster wound contraction and re-epithelialization[293]. These findings align with and extend previous reports. For example, Elhami et al. (2024) demonstrated that chitosan/rGO-based nanocomposites significantly enhance tissue repair by offering both structural support and effective antimicrobial protection[294]. In a related study, Sun et al. (2024) reported that chitosan-based dressings enriched with polyphenolic compounds promote hemostasis, stimulate angiogenesis, and exert antioxidant activity, collectively contributing to improved wound healing, particularly in complex or chronic wound environments such as diabetic ulcers[292].

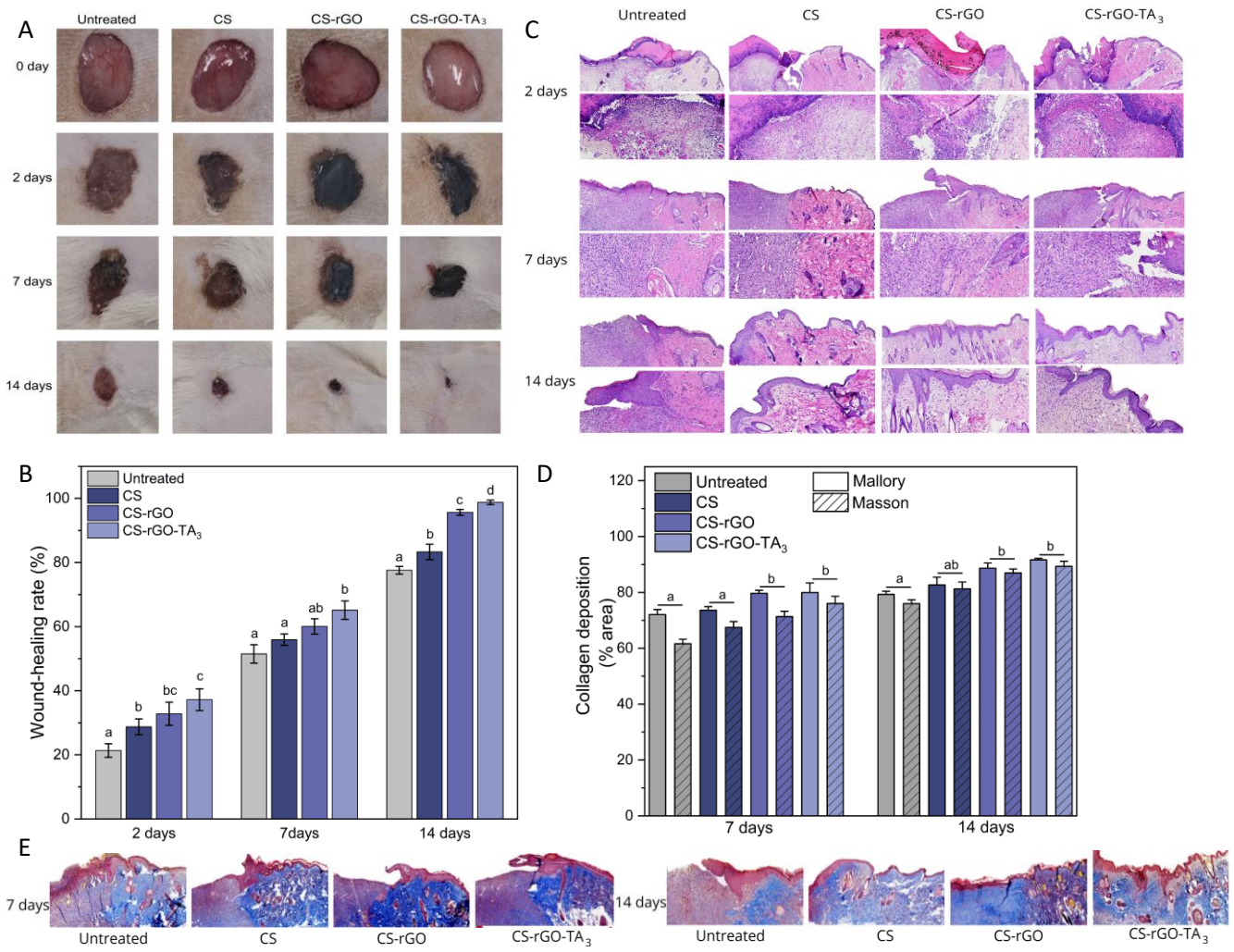

Figure 3.3. Characterization of the synthesized materials in an *in vivo* model (rats): (A) Images of wound evolution over time, (B) Wound closure rate, (C) Qualitative histological evaluation of the experimental groups using hematoxylin and eosin (H&E) staining at 600× and 100× magnification. (D) Quantification of collagen deposition using Mallory staining and Masson's trichrome staining at 7 and 14 days. (E) Images of Masson's trichrome staining at 600× magnification at 7 and 14 days.

Results were expressed as mean ± standard error of the mean (significance levels were set at $p < 0.05$, and differences were considered significant when the groups compared displayed different letters).

To gain deeper insight into tissue-level healing, histopathological analyses were conducted to evaluate the progression of wound regeneration following treatment. Hematoxylin and eosin (H&E) staining revealed progressive re-epithelialization across all treated groups, with the CS-rGO-TA_3 hydrogel displaying the most robust and organized epidermal regeneration (**Figure 3.3C**). Wound contraction was evident beneath the newly formed epidermis, and by day 7, the presence of inflammatory infiltrates—including neutrophils, lymphocytes, and macrophages—confirmed active engagement of the inflammatory phase. These histological findings were consistent with molecular data from gene expression analysis, reinforcing the observed biological activity. Between days 7 and 14 post-injury, tissue sections from the treated groups demonstrated ongoing re-epithelialization, abundant granulation tissue formation, emerging hair follicles, and clear signs of neovascularization. A gradual reduction in inflammatory cell infiltration was observed over time, with the CS-rGO-TA_3 group displaying the lowest inflammatory scores by day 14, indicating a more rapid resolution of inflammation and an accelerated transition toward the proliferative phase of healing. Interestingly, the TA-treated group also showed a thinner, more compact epidermis at later stages, consistent with advanced tissue remodeling. This may be attributed to tannic acid's capacity to precipitate lipid-protein complexes and promote the formation of a flexible, protective scab that supports tissue stabilization and reduces further irritation[295].

3.4.7 Collagen Deposition Assay

Collagen deposition is critical for wound strength and dermal remodeling[296]. Quantitative analysis of collagen content, performed using Mallory and Masson's Trichrome staining alongside image analysis via ImageJ software (**Figure 3.3D and 3.3E**), demonstrated a significant increase in collagen deposition in all treated

groups compared to the untreated control. Notably, the CS-rGO-TA_3 hydrogel induced the highest levels of collagen accumulation at both 7- and 14-day post-injury. These effects were especially evident in the CS-rGO and CS-rGO-TA_3 groups, with the TA-enriched hydrogel showing the most substantial collagen density by day 14. These findings highlight the hydrogel's capacity to enhance extracellular matrix remodeling and restore tissue integrity. The observed increase in collagen content is likely influenced by the anti-inflammatory activity of tannic acid, which reduces oxidative and inflammatory damage while promoting a regenerative microenvironment[297,298]. In this context, the dual role of collagen types becomes relevant: type I collagen, the most abundant in mature skin, provides tensile strength and structural integrity, while type III collagen plays a regulatory role during early repair, facilitating matrix organization, cellular migration, and scar minimization[299]. Protein expression assays (**Figure 3.4A and 3.4B**) revealed a predominance of type III collagen in the early stages of healing, followed by a progressive shift toward type I collagen as remodeling advanced, reflecting the physiological dynamics of wound maturation[300]. Correspondingly, mRNA expression analysis confirmed the upregulation of both type I and III collagen transcripts during the proliferative phase, with the CS-rGO-TA_3 group exhibiting significantly higher expression levels than the untreated group (**Figure 3.4A and 3.4B**). These effects may be further enhanced by the astringent nature of TA, which is believed to facilitate collagen fiber crosslinking, thereby improving the mechanical strength and structural organization of the extracellular matrix[301].

3.4.8 Molecular Analysis by Western Blot and RT-qPCR

The expression of interleukins following tissue injury plays a central role in regulating inflammation, orchestrating healing responses, and influencing scar formation[302]. Interleukin-10 (IL-10), a key anti-inflammatory cytokine, plays a

crucial role in regulating the inflammatory phase of wound healing by limiting excessive immune activation and promoting tissue homeostasis. It suppresses excessive neutrophil and macrophage activation and downregulates the expression of proinflammatory cytokines such as interleukin-6 (IL-6)[303,304]. In addition, IL-10 contributes to tissue repair by facilitating the recruitment of endothelial progenitor cells and promoting re-epithelialization, thereby supporting vascular regeneration and epidermal restoration[305]. As shown in **Figures 3.4C and 3.4D**, both gene and protein expression levels of IL-6 were elevated during the early inflammatory phase (day 2), whereas IL-10 expression remained relatively low. This pattern is consistent with the physiological response to acute injury. However, as healing progressed into the proliferative phase (days 7 to 14), a reversal in expression trends was observed. Importantly, treatment with CS-rGO-TA_3 resulted in a pronounced reduction in IL-6 expression and a concomitant increase in IL-10 levels at both the transcriptional and protein levels, indicating effective modulation of the inflammatory response. These findings suggest that the TA-loaded hydrogel more effectively attenuated the inflammatory response, promoting an earlier transition toward tissue regeneration—an effect supported by existing literature on the anti-inflammatory properties of TA. Efficient resolution of inflammation is a prerequisite for the onset of the proliferative phase, during which granulation tissue forms and fibroblasts synthesize extracellular matrix components such as collagen. Collagen serves as a scaffold for cellular organization, enabling angiogenesis and epithelial coverage[306]. The gene and protein expression of type I collagen further supports this regenerative progression, with the CS-rGO-TA_3 hydrogel promoting significantly higher expression levels compared to other groups. These data highlight the critical link between controlled inflammation and enhanced matrix deposition.

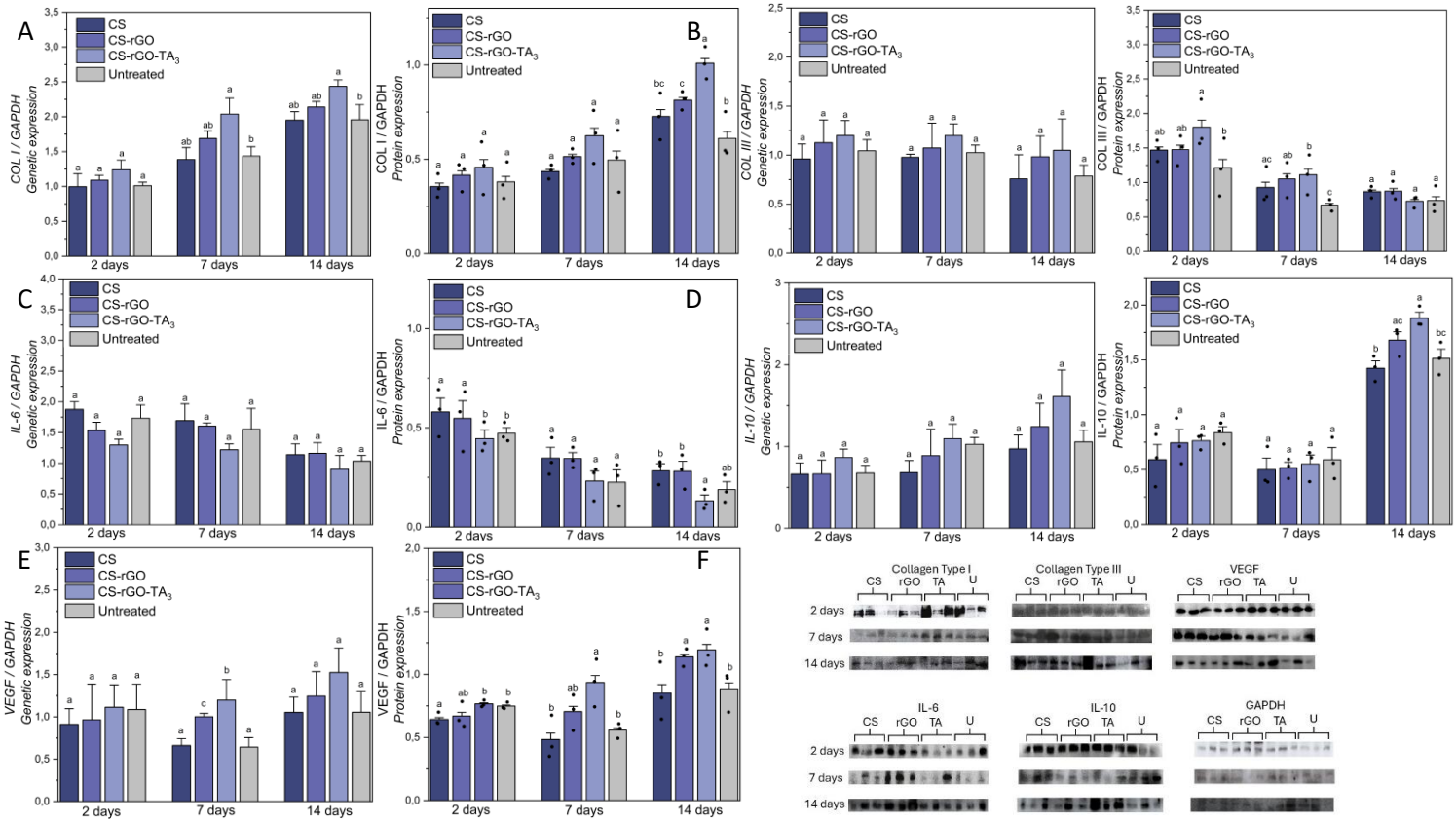

Figure 3.4. Relative Gene and Protein expression at 2, 7, and 14 days: (A) COL I, (B) COL III, (C) IL-6, (D) IL-10, and (E) VEGF. (F) Protein expression bands by Western blot analysis.

Results were expressed as mean ± standard error of the mean (significance levels were set at $p < 0.05$, and differences were considered significant when the groups compared displayed different letters).

Vascular endothelial growth factor (VEGF), a key regulator of angiogenesis, plays a pivotal role in wound healing by supporting vascular remodeling, re-epithelialization, and collagen synthesis[307]. As shown in **Figure 3.4E**, VEGF expression was upregulated across all treatment groups during the regenerative phase, with the highest levels observed in the TA-loaded hydrogel group ($p < 0.05$). This enhanced VEGF activity likely contributed to improved tissue perfusion

and oxygenation, thereby alleviating metabolic stress within the wound microenvironment[308–310]. Collectively, these results underscore the diverse biological functions of tannins in modulating key phases of wound healing, from inflammation control to tissue regeneration. Beyond their well-established antioxidant and anti-inflammatory properties, TA have also been shown to stimulate fibroblast and keratinocyte proliferation, promote neovascularization, and facilitate wound contraction—critical processes that work synergistically to accelerate tissue regeneration and support functional skin repair[311]. The combined effect of these mechanisms, as demonstrated by the CS-rGO-TA_3 hydrogel, suggests its strong therapeutic potential in accelerating wound healing and improving overall tissue repair quality.

Myeloperoxidase (MPO) is a key enzyme produced by activated neutrophils, playing a central role in microbial clearance through the generation of reactive oxygen species (ROS)[312]. At day 2 post-injury, all hydrogel-treated groups exhibited elevated MPO gene expression relative to the untreated control, although these differences did not reach statistical significance. As healing progressed, however, a significant reduction in MPO expression was observed in the CS-rGO-TA_3 group by day 14, compared to both the CS and untreated groups (**Figure 3.5A**). Although MPO levels were also lower than those in the CS-rGO group, this difference was not statistically significant. These findings align with the enhanced wound closure and elevated type I collagen expression observed in the CS-rGO-TA_3 group, reinforcing its role in promoting effective tissue regeneration. Elevated MPO levels are often associated with prolonged inflammation and impaired healing, as excessive ROS production can damage surrounding tissues and delay the transition to the proliferative phase. The observed reduction in MPO expression at later time points suggests successful resolution of the inflammatory phase, likely following initial microbial control. This interpretation aligns with previous *in vivo* and *ex vivo* studies, which demonstrated that MPO can inhibit neutrophil adhesion and migration, and that the accumulation of hydrogen

peroxide (H_2O_2), along with MPO released by infiltrating neutrophils, exacerbates oxidative stress and epithelial injury[313].

Arginase 1 (ARG1), on the other hand, is a hallmark of reparative (M2) macrophage polarization and plays a crucial role in orchestrating wound healing. It modulates the inflammatory response, facilitates cell migration, supports restoration of the skin barrier, and contributes to tissue remodeling[314,315]. At day 2 post-wounding, ARG1 mRNA expression was upregulated in all treated groups compared to the control, with CS-rGO-TA_3 showing significantly higher levels (**Figure 3.5B**). This trend persisted at days 7 and 14, where Arg1 expression remained elevated in all treatment groups, with the CS-rGO-TA_3 hydrogel consistently inducing the highest expression. These findings suggest a sustained pro-repair immune response in the CS-rGO-TA_3 group, supporting faster resolution of inflammation and enhanced tissue regeneration. This is further supported by previous reports highlighting the role of ARG1 in promoting collagen synthesis through the conversion of L-arginine into ornithine, a key precursor in collagen biosynthesis[316]. These results corroborate our findings on enhanced collagen expression in treated groups. The elevated ARG1 levels observed in our study correlate well with the enhanced collagen deposition documented in histological and molecular analyses, further underscoring the regenerative capacity of the CS-rGO-TA_3 hydrogel.

A prolonged or dysregulated inflammatory response is a recognized barrier to effective wound healing, underscoring the critical role of tightly regulated proinflammatory cytokine activity in orchestrating successful tissue repair.[317] Among these, the interleukin-1 receptor antagonist (IL-1rn) plays a pivotal role in modulating the local inflammatory environment by suppressing IL-6 and IL-1β expression while promoting IL-10 production[318]. In our study, IL-1rn expression levels at days 2 and 7 post-injury showed no significant differences between the treated and control groups, suggesting that early anti-inflammatory signaling remained comparable across conditions during the initial phases of wound

healing. However, at day 2, the untreated group exhibited markedly higher IL-1β expression compared to all treated groups, indicating a delayed resolution of inflammation, even in an acute wound model. By day 14, the CS-rGO-TA_3-treated group showed the highest IL-1rn expression and the lowest IL-1β levels across all groups (**Figure 3.5D and 3.5E**), suggesting more efficient control of the inflammatory response. This observation is supported by prior studies indicating that IL-1 inhibition can attenuate proinflammatory cytokine production (e.g., IL-1β, IL-6), reduce myofibroblast activity, and enhance anti-inflammatory cytokine release (e.g., IL-10), as well as endothelial cell recruitment, M2 macrophage polarization, and granulation tissue formation—creating a transiently less inflammatory environment conducive to tissue repair[319,320].

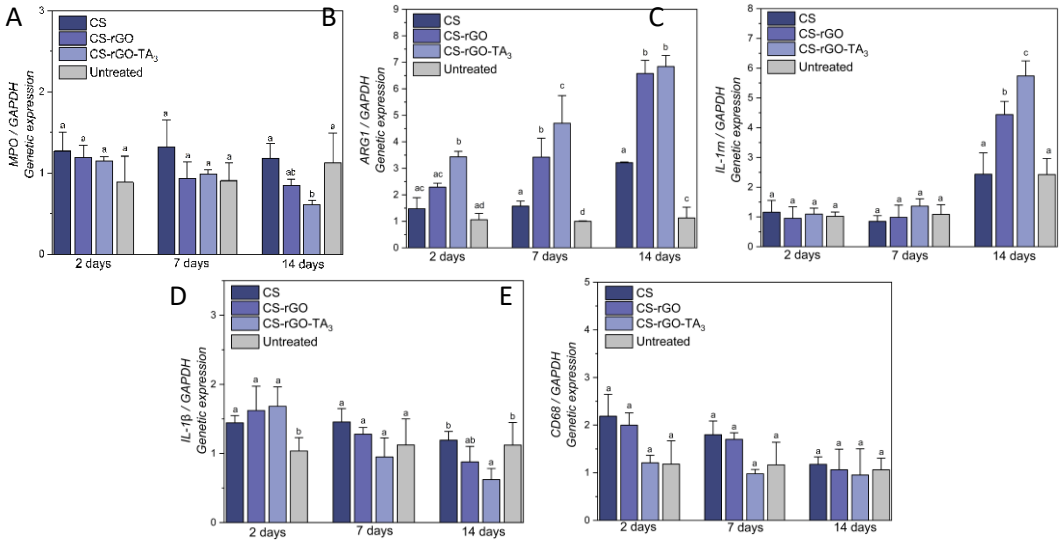

Figure 3.5. Relative gene expressions at 2, 7, and 14 days: (A) MPO, (B) ARG1, (C) IL-1rn, (D) IL-1β, and (E) CD68.

Results were expressed as mean ± standard error of the mean (significance levels were set at $p < 0.05$, and differences were considered significant when the groups compared displayed different letters).

At 2 days post-injury, the CD68 expression marker of macrophage infiltration was significantly elevated in the CS and CS-rGO groups compared to the CS-rGO-TA_3 and untreated groups, indicating a more intense early inflammatory response (**Figure 3.5E**). This pattern is characteristic of the early inflammatory phase, during which macrophage recruitment plays a pivotal role in clearing cellular debris and defending against potential pathogens. By day 7, CD68 expression had declined across all groups, with the CS-rGO-TA_3 group showing the lowest levels, suggesting a more rapid resolution of macrophage-mediated inflammation. This is notable given that prolonged persistence of proinflammatory macrophages is associated with delayed healing, chronic inflammation, and fibrosis[321,322]. By day 14, CD68 expression had normalized across all groups, reflecting progression into the proliferative and remodeling phases of wound repair. This temporal pattern aligns with well-established dynamics of macrophage infiltration, where a decrease in inflammatory cell presence coincides with the onset of tissue regeneration and extracellular matrix remodeling[323]. These findings are consistent with previously reported expression patterns of both pro- and anti-inflammatory markers (IL-6, IL-1β, IL-10, IL-1rn, Arg1), as well as with the accelerated wound healing observed in the CS-rGO-TA_3 group. The sustained reduction in macrophage activity in this group aligns with known anti-inflammatory effects of polyphenolic compounds, such as tannic acid, which have been shown to promote macrophage polarization toward the M2 reparative phenotype[324,325]. This immunomodulatory shift supports the hypothesis that TA-enriched hydrogels facilitate the transition from inflammation to regeneration, thereby enhancing the wound healing process. Moreover, the improved outcomes observed in collagen deposition, neovascularization, and overall wound closure in the CS-rGO-TA_3 group are likely downstream effects of this early and effective modulation of the inflammatory response. These results are consistent with previous studies highlighting the therapeutic potential of TA

and other natural anti-inflammatory agents in promoting cutaneous repair through immune regulation and support of the proliferative phase[326].

3.5. Partial Conclusions

- Wound dressings were developed from a CS-rGO-PF hydrogel loaded with different concentrations of TA. The CS-rGO-TA_3 hydrogel showed a controlled and sustained release of TA, attributed to its dense polymer network, which also enhanced its antioxidant activity through the efficient scavenging of free radicals.
- The hydrogel exhibited excellent antibacterial activity against *E. coli* and *S. aureus*, as well as remarkable biocompatibility, evidenced by the high viability of human dermal fibroblasts and the absence of toxicity or irritation.
- In the animal model, the CS-rGO-TA_3 hydrogel effectively promoted cell migration and the organized deposition of type I and III collagen, favoring adequate tissue regeneration. Furthermore, it significantly accelerated healing, reduced inflammation, and facilitated the formation of a flexible scab, contributing to a faster and structurally more robust recovery.
- The presence of TA effectively modulated the inflammatory response, decreasing pro-inflammatory cytokines (IL-6, IL-1β) and increasing anti-inflammatory cytokines (IL-10, IL-1rn), thus promoting an early transition to the proliferative phase. Simultaneously, the hydrogel regulated macrophage activity by reducing the expression of pro-inflammatory markers (CD68, MPO) and increasing ARG1, associated with polarization toward the M2 reparative phenotype.
- Taken together, these findings position CS-rGO-TA_3 hydrogel as a safe and effective therapeutic strategy for skin repair, especially in wounds with delayed or chronic healing, by generating an optimal microenvironment that accelerates regeneration and improves the quality of the repaired tissue.

General Conclusions

In this study, chitosan-based (CS) hydrogels incorporating reduced graphene oxide (rGO) and Pluronic F-127 (PF) (CS-rGO-PF) were developed and optimized using a 2^{2+} star factorial experimental design. Characterization analyses demonstrated that the incorporation of rGO significantly improved the material's stiffness, structural stability, and electrical conductivity, while PF enhanced flexibility and thermal stability. Together, these properties created a microenvironment conducive to cell migration and proliferation, key conditions for accelerating skin wound healing. Furthermore, absorption kinetics in simulated human fluids confirmed the hydrogel's ability to retain moisture and maintain an environment favorable for tissue repair. *In vitro* assays revealed that the developed hydrogels exhibited antibacterial activity against Gram-positive and Gram-negative bacteria, high viability in human dermal fibroblasts, and marked stimulation of cell migration, confirming their biocompatibility and regenerative potential. Subsequently, hydrogels loaded with different concentrations of tannins (TA) were synthesized, and the CS-rGO-TA_3 formulation was selected for in vivo studies. In dermal irritation tests in guinea pigs, CS-rGO-TA_3 showed no signs of toxicity or irritation. In the murine model, CS-rGO-TA_3 promoted significantly faster and more organized wound healing than the controls, facilitating an early transition from the inflammatory to the proliferative phase. Histological analyses revealed increased deposition of type I and type III collagen, abundant granulation tissue, and enhanced angiogenesis compared with CS hydrogel alone and untreated wounds. At the molecular level, RT-qPCR and Western blot analyses demonstrated that CS-rGO-TA_3 effectively modulated the immune response by decreasing pro-inflammatory cytokines (IL-6, IL-1β) and increasing anti-inflammatory cytokines (IL-10, IL-1rn). Furthermore, the upregulation of Arg1 alongside reduced CD68 expression indicated macrophage polarization toward the reparative M2 phenotype, consistent with early inflammation resolution. These

molecular changes correlated with increased VEGF and collagen levels, explaining the faster and more structurally organized regeneration observed. In the porcine model, which more closely resembles human skin physiology, the CS-rGO-PF_{10} hydrogel achieved complete wound closure within 21 days, comparable to the commercial dressing Nexcare™, but with additional advantages, including improved dermal tissue organization, regeneration of hair follicles, and absence of fibrosis or hyperkeratosis. These findings confirm its clinical potential for regenerative medicine applications. Overall, the results obtained validate the proposed hypothesis, demonstrating that the developed hydrogels not only accelerate cutaneous wound healing but also modulate the inflammatory response in a balanced manner, stimulate angiogenesis, and promote structural and functional skin regeneration. Their performance—comparable to or even superior to commercial treatments—positions these hydrogels as highly promising biomaterials for the advanced management of acute and chronic wounds.

Scope of future work

This research yields interesting conclusions that support the use of these hydrogels to promote wound healing. However, further studies are needed to validate their final application. These studies involve evaluating coagulation parameters related to the alternative coagulation pathways promoted by the hydrogels. The effects of loading higher concentrations of TA into the hydrogels on their hemostatic performance in vitro and in vivo should also be investigated. Exploring new biomedical applications for these hydrogels based on their properties is also worthwhile.

Appendixes

Appendix A: Supporting Information for Chapter 2

A.1 Materials characterization techniques

Scanning electron microscopy (SEM). The micromorphology of the hydrogel compounds was evaluated using SEM analysis. SEM images were recorded with a JEOL JSM-6380LV microscope, Japanese model, at 10 kV. The hydrogels were coated with a sputtered gold coating, and their surfaces were observed at different resolutions (5 μm, 20 μm, and 50 μm).

Attenuated total reflection Fourier transform infrared spectroscopy (ATR-FTIR). ATR-FTIR was used to investigate the chemical nature of the CS-rGO-PF hydrogel interaction. Spectra were recorded on a Perkin Elmer UATR Two FTIR spectrometer. The wavenumber range analyzed was 4000 to 500 cm^{-1}, and a total of 40 cumulative scans were acquired.

X-ray diffraction (XRD). XRD was used to evaluate the degree of oxidation of GO and the crystallinity of the CS-rGO-PF hydrogels. Measurements were performed on an X-ray diffractometer (Bruke Axs, D4 Endeavour, USA) with a reference objective: Cu Kα radiation (λ = 1.541841 Å; 2.2 kW), voltage: 40 kV, and current: 20 mA. The samples were measured from 2 to 50° for 141 s in 0.02° steps.

Wettability. The contact angles of the samples were determined to assess wettability (DSA-25 goniometer droplet shape analyzer (Krüss, Germany)). Deionized water was dispensed onto the hydrogel samples using a microsyringe needle, and a photograph of the resulting droplet was taken. The software examined the droplet shape by capturing photos at 30 ms intervals. To reduce material absorption errors, the initial measurement value was used. The baseline was manually adjusted to mitigate the impact of material roughness.

In Vivo Wound Healing Assay. The wound healing assay was conducted in eight male Yorkshire pigs (Sus scrofa), with an average age of two months and an average weight of 20–25 kg. An intravenous anesthetic protocol was implemented, consisting of the administration of ketamine (20 mg/kg) and xylazine (2 mg/kg). In addition, 2% lidocaine (100 µL) was topically applied to the wound site. Subsequently, unconsciousness was induced and response to stimuli was confirmed. Ten wounds of 2.5 cm diameter and 4–5 mm depth were made in each animal using a scalpel. Wounds were treated with advanced wound healing dressings (Nexcare™, 3M, St. Paul, Minnesota, USA) as a positive control and with CS and CS-rGO-PF_{10} hydrogels. One wound was left untreated. Biopsies were obtained from wound margins on days 0, 4 and 21 using an 8 mm diameter punch (Kruuse, India). The samples were fixed in 10% buffered formalin for 24 hours, subsequently transferred to ethanol and embedded in paraffin for histological analysis. Assessment of wound healing was performed according to Sevimli-Gür et al. (2011). Histological features were assessed by the same specialist (blinded to the treatment). Histologic wound assessment scoring included: reepithelialization (0 = none; 1 = partial; 2 = complete but immature/thin; 3 = complete and mature), neovascularization (0 = none; 1 = up to 5 vessels/high power field [HMF]; 2 = 6–10 vessels/HMF; 3 = >10 vessels/HMF), amount of granulation tissue (0 = none; 1 = scant; 2 = moderate; 3 = abundant), and inflammatory cells (0 = none; 1 = scant; 2 = moderate; 3 = abundant). At the end of the experiment, pigs were euthanized with 5% thiopental solution at a dose of 10 mg/kg/h, followed by pathologic examination of the heart, pancreas, liver, and kidneys. The experiments with pigs were carried out following the principles of biosafety and bioethics and were approved by the Bioethics and Biosafety Committee of the Faculty of Biological Sciences of the University of Concepción.

Obtaining GO and rGO:

Graphene oxide (GO) was synthesized following the method of Hummers et al. (1958)[327], with some experimental adaptations to improve the efficiency and safety of the process[328]. Initially, a concentrated acid mixture was prepared by combining 30 mL of phosphoric acid (H_3PO_4) with 270 mL of sulfuric acid (H_2SO_4) in a beaker under continuous magnetic stirring. This exothermic reaction raised the temperature of the system to approximately 40°C. Once the mixture had cooled to 25°C, 2.25 g of graphite were gradually added, taking care to maintain the temperature below 30°C. Subsequently, 13.5 g of potassium permanganate ($KMnO_4$) were added, also gradually and under constant stirring. Once all the reagents were dissolved, the mixture was placed on a hot plate for 1 hour, maintaining the temperature between 35°C and 50°C. After this time, the reaction was stopped by the slow addition of 55–60 mL of 60% hydrogen peroxide (H_2O_2) in an ice bath. This step produced a visible change in the mixture, from black to green, accompanied by a sudden temperature increase to approximately 100°C. The mixture was allowed to cool to room temperature until foaming ceased, while stirring. The product was then transferred to centrifuge tubes and centrifuged at 5000 rpm for 20 minutes to separate the solid fraction from the acid solution. The supernatant was discarded, and the remaining solid was washed successively with ultrapure water (milliQ), repeating the centrifugation process twice, until a color change to brownish-yellow was observed. To remove trace metals, 100 mL of 0.1% HCl was added and the mixture was vigorously shaken before further centrifugation. This washing was repeated three times with MilliQ water. Chloride ion removal was verified by adding drops of silver nitrate ($AgNO_3$) solution to the supernatant; the absence of a white precipitate indicated adequate purification. The solid was then washed with 100 mL of absolute ethanol, shaken, and centrifuged again. Finally, graphene oxide exfoliation was carried out by sonication for 45 minutes in an ice bath, ensuring that the temperature did not exceed 37°C. The resulting product was frozen and subsequently lyophilized for storage.

The reduction process began with the preparation of 200 mL of a 10 mM Tris buffer solution. 50 mg of dopamine hydrochloride (DA·HCl) were added to this solution, stirring continuously until completely dissolved. Subsequently, 100 mg of GO were incorporated under constant mechanical stirring. The pH of the solution must be maintained at 8.5, so it was carefully adjusted by adding HCl or NaOH, as needed. Once the appropriate pH and homogeneity were achieved, the mixture was sonicated in an ice-water bath for 20 minutes to uniformly disperse the GO in the solution. The reaction was then carried out at 60°C for 24 hours under continuous mechanical stirring. During this period, a progressive color change was observed in the solution, indicating the reduction of GO and the formation of rGO. After the reaction time, the mixture was vacuum filtered using membrane paper, and the retained solid was washed with ultrapure water (MiliQ) two to three times to remove unreacted reagents. The resulting solid was redissolved in MiliQ water and subjected to dialysis for three days, with daily water changes, to ensure complete removal of impurities and soluble byproducts. After dialysis, the material was again vacuum filtered and washed with MiliQ water. Finally, the solid was dried on filter paper at room temperature. Once dry, the rGO was recovered and stored in a hermetically sealed container for subsequent characterization and application.

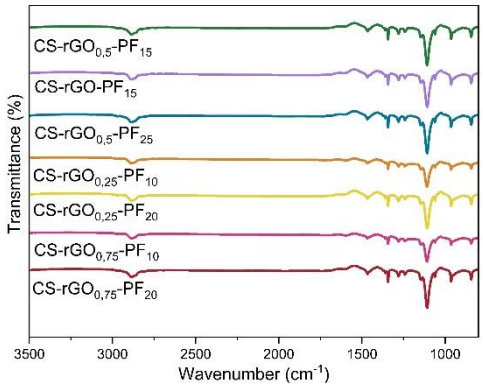

Figure A.1. FT-IR spectra of the synthesized hydrogels using statistical experimental design.

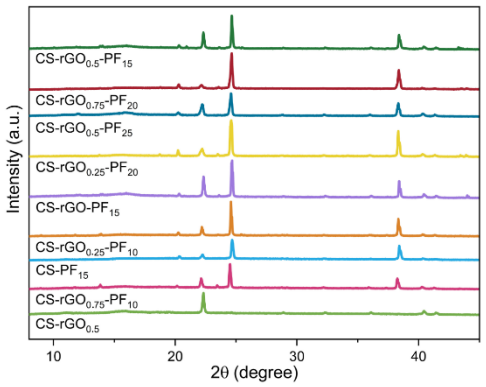

Figure A.2. XRD spectra of the synthesized hydrogels using statistical experimental design.

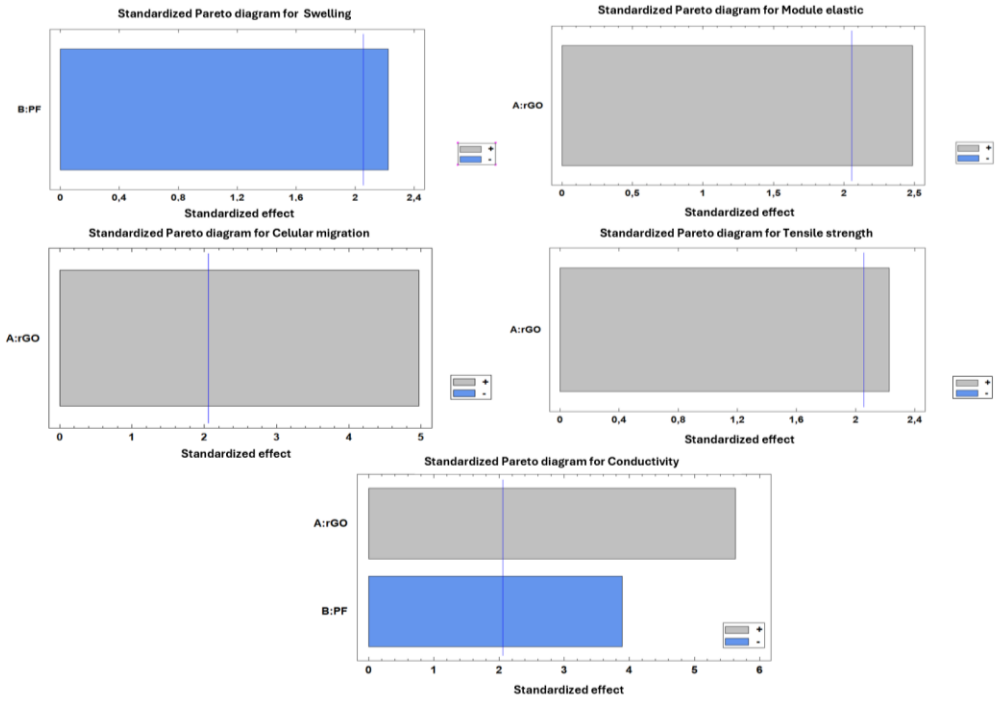

Figure A.3. Pareto diagram for conductivity (Y_1); swelling (Y_2); tensile strength (Y_3); elastic modulus (Y_4), and cell migration (Y_5).

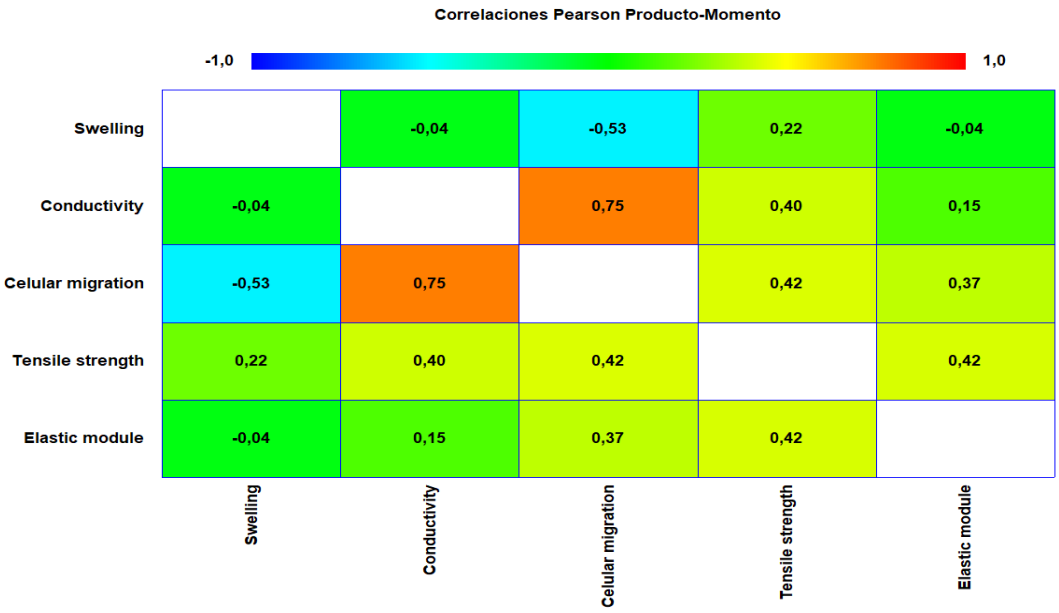

Figure A.4. Pearson Diagram.

Table A.1: Kinetic model of Swelling.

Kinetic model	**Equations** $\alpha = \frac{W_t}{W_e}$
Peppas[329,330]	$\alpha = kt^n$
Mampel[329,331]	$-\ln(1-\alpha) = kt$
Second-order equation[332,333]	$(1-\alpha)^{-1} - 1 = kt$
Mixed model[236]	$\alpha = 1 - e^{-k_1 t\left(1+\frac{2\tau^{1/2}}{t^{1/2}}\right)}$

Where W_t and W_e are the swelling of the hydrogel at time t and an equilibrium, respectively, k is the rate constant of the swelling process, and n is the diffusion coefficient. An n value of 0.45 represents Fickian diffusion, and a value of 0.45 < n< 0.89 represents anomalous (non-Fickian) diffusion [12].

Table A.2: Swelling kinetic parameters and contact angle.

Samples	*n* Fick	1st order		Peppas		Mampel		Mixed		Contact angle (degree)
		k	R^2	k	R^2	k	R^2	k	R^2	
CS-PF $_{15}$	0.45	0.061	0.920	0.189	0.973	0.142	0.947	0.480	0.962	60.2±0.05
CS-rGO $_{0.25}$ -PF $_{10}$	0.76	0.083	0.983	0.028	0.995	0.075	0.990	1,365	0.910	37.2±0.03
CS-rGO $_{0.75}$ -PF $_{10}$	0.67	0.085	0.973	0.030	0.991	0.154	0.963	0.100	0.949	26.8±0.02
CS-rGO $_{0.25}$ -PF $_{20}$	0.58	0.068	0.944	0.059	0.985	0.964	0.972	0.254	0.942	52.2±0.02
CS-rGO $_{0.75}$ -PF $_{20}$	0.68	0.050	0.942	0.030	0.991	0.913	0.950	0.235	0.928	46.7±0.02
CS-rGO-PF $_{15}$	0.68	0.040	0.969	0.018	0.992	0.095	0.985	1,685	0.992	29.0±0.02
CS-rGO $_{0.50}$	0.49	0.087	0.972	0.166	0.978	0.224	0.928	1,365	0.927	62.0±0.03
CS-rGO$_{0.50}$ -PF $_{25}$	0.75	0.084	0.973	0.026	0.995	0.783	0.941	0.495	0.992	26.7±0.003
CS-rGO$_{0.50}$ -PF $_{15}$	0.84	0.013	0.998	0.020	0.937	0.208	0.998	1,693	0.927	22.6±0.01

Table A.3: Quantitative results of *in vivo* assay.

Samples	Re-epithelialization	Neovascularization	Granulation tissue	Inflammatory cells
		Untreated		
4 days	0	2	1	2
21 days	Marked epidermal acanthosis. Loose connective tissue is seen in the papillary and reticular dermis.			
		CS		

4 days	1	2	2	3
21 days	There is mild acanthosis, no hyperkeratosis. There are no traces of skin appendages in the wound area yet.			
	CS-rGO-PF$_{10}$			
4 days	2	3	3	2
21 days	Good differentiation of the epithelium. Dermal papillae and epidermal ridges are clearly visible, with many blood vessels close to the epithelial basement membrane. Differences are seen between the loose connective tissue of the papillary dermis versus a denser and more organized/molded tissue in the reticular dermis. In addition, the generation of developing hair follicles is seen. No hyperkeratosis or acanthosis is observed.			
	Positive Control			
4 days	1	2	1	3
21 days	Complete maturation of the epithelium, but epidermal ridges or marked dermal papillae are not yet observed. Loose connective tissue is observed in the papillary and reticular dermis. There is a greater presence of inflammatory cells than fibroblasts.			

Re-epithelialization (0 = none; 1 = partial; 2 = complete but immature/thin; 3 = complete and mature). Neovascularization (0 = none; 1 = up to 5 vessels/high power field [HMF]; 2 = 6-10 vessels/HCF; 3 = >10 vessels/HCF). At this point, 3 visual fields were analyzed, and an average was obtained. Amount of granulation tissue (0 = none; 1 = scant; 2 = moderate; 3 = abundant) Inflammatory cells (0 = none; 1 = scant; 2 = moderate; 3 = abundant).

Appendix B: Supporting Information for Chapter 3

B.1 Pinus Radiata Bark Extract Production (TA)

Pinus radiata bark extracts were produced through a pilot-scale extraction process, as described by Bocalandro et al. (2012)[334]. For this purpose, a reactor volume of 4 m^3 and a vapor heating system composed of a shell and a tube heat exchanger with 6 m^2 heat transference area were used. In addition, a recirculation circuit for the extracted solution was implemented. Briefly, the Pinus radiata bark was ground with a double-knife mill to an average size lower than 20 mm. Then, the bark was dried at room temperature to a humidity of 24.5% (dry weight), and 100 kg (dry weight) of bark was soaked in an ethanol/water solution at a 1:20 ratio (w/v) for 120 min at 120 °C. Subsequently, the ethanol was evaporated in a vacuum (absolute pressure 0.05 bar) at room temperature. Thus, the water-insoluble particulate material after decanting and the water-soluble polyphenol fraction were obtained. Finally, the water-soluble polyphenols were lyophilized at room temperature, and the obtained extracts were stored in sealed amber glass containers for further analysis.

B.2 Materials characterization techniques

Western blotting. Tissue samples were placed in liquid nitrogen and macerated with a hammer in a stainless steel support. Subsequently, the lyophilized samples were homogenized in a buffer containing 1% Triton-X-100, 100 mM Tris (pH 7.4), 100 mM sodium pyrophosphate, 100 mM sodium fluoride, 10 mM EDTA, 10 mM sodium orthovanadate, 2 mM PMSF and 0.01 mg/mL of antiprotease cocktail using the Politron® equipment. The homogenate was centrifuged at 12,000 rpm at 4 °C for 20 minutes to separate the sample according to its density. Subsequently, the supernatant was aspirated and its proteins were quantified with the biuret reagent. Subsequently, the samples received Laemmli buffer added with 200 mM dithiothreitol in a 5:1 ratio. Finally, they were subjected to a

temperature of 100°C for 5 minutes. After protein quantification, 50 µg of total protein was subjected to 12% polyacrylamide gel electrophoresis (SDS-PAGE) in a BioRad Minigel apparatus with electrophoresis buffer. Initially, they were subjected to 80 V up to the gel stacking line and subsequently to 120 V up to the gel resolution line. A molecular weight marker with established molecular weight values was used in each gel. The proteins separated in the gel were transferred electrically to a nitrocellulose membrane using a BioRad® apparatus for approximately 1.5 hours at 120 V, kept on ice. To reduce nonspecific binding, the PVDF membrane was incubated in 5% BSA diluted in basal solution at room temperature for 1 hour. After blocking, the membrane was washed three times with basal solution and incubated with specific antibodies diluted in 3% BSA blocking solution, and kept at 4°C overnight with gentle shaking. The primary antibodies used are described in Table S2 (1:5000). The following day, they were washed with basal solution and incubated with secondary antibody for approximately one hour. Approximately 2 ml of chemiluminescence solution in a 1:1 dilution of the reagents from the Thermo Fisher® commercial kit was then added for approximately two minutes. Light emission was detected and captured using the SysGen® photodocumentation system. Optical density was read using ImageJ® software. The results were normalized by comparing the expression with GAPDH.

B.3 Surgical Procedure and Groups

The animals were anesthetized by intraperitoneal injection of a 2.5% tribromoethanol solution (100 µL/10 g; Sigma, USA). The animals' backs were shaved, and after asepsis with 70% ethanol, two full-thickness circular incisions were made in the dorsocervical region with a sterile histological punch (1.5 cm in diameter), the thickness of which encompassed all skin layers. The excised skin from each animal was preserved for subsequent histological and biochemical analysis, representing samples from the initial day (day 0) without treatment.

The groups, consisting of 9 animals each, were separated according to wound treatment: in group 1, both wounds of each animal were treated with chitosan hydrogels (circular, 2.0 cm in diameter) pre-moistened with 0.9% saline; in group 2, both wounds of each animal were treated with chitosan-reduced graphene oxide hydrogels (circular, 2.0 cm in diameter) pre-moistened with 0.9% saline; In group 3, both wounds of each animal were treated with chitosan-reduced graphene oxide-tannin hydrogels (circular, 2.0 cm in diameter) pre-moistened with 0.9% saline; in group 4, the wounds were treated only with 0.9% saline (150 µL each). The wounds of all animals in both groups were covered with gas, and the dressing was changed daily after hydration with 0.9% saline (100 µL) until the follow-up day. The hydrogels were removed only after euthanasia of the animals at 2, 7, and 14 days.

Table B.1. Skin irritation assessment: scoring scale for erythema, scaling, and edema.

Reaction	Irritation Score
Formation of erythema and eschar	
Without erythema	0
Mild erythema (barely noticeable)	1
Well-defined erythema	2
Moderate to severe erythema	3
Severe erythema (red) tending to eschar formation	4
Edema formation	
No edema	0
Mild edema (barely noticeable)	1
Well-defined edema (edges of the area well defined by magnification)	2

Moderate erythema (increase approx. 1 mm)	3
Severe edema (increase of more than 1 mm and extension beyond the area of exposure.	4
Maximum possible score for irritation	8

Table B.2. TaqMan assays used for Western blot and RT-qPCR.

TaqMan Assays	Product Codes
Gapdh *Glyceraldehyde-3-Phosphate Dehydrogenase*	*Rn01775763_g1*
Vegf *Vascular endothelial growth factor*	*Rn01511602_m1*
COL I *Collagen type I*	*Rn01463848_m1*
COL II *Collagen type III*	*Rn01437681_m1*
MPO *Myeloperoxidase*	*Rn01460205_m1*
CD68 *Glycoprotein CD68*	*Rn01495634_m1*
Arg1 *Arginase 1*	*Rn00691090_m1*
IL-6 *Interleukin 6*	*Rn01410330_m1*
IL-10 *Interleukin 10*	*Rn01495634_g1*
IL-1β *Interleukin 1β*	*Rn00580432_m1*

IL-1rn	*Rn02586400_m1*
Interleukin 1 receptor antagonist	

Table B.3. Quantitative results of *in vivo* assay.

Samples	Re-epithelialization	Neovascularization	Granulation tissue	Inflammatory cells
		Untreated		
2 days	0	2	1	2
14 days	Marked epidermal acanthosis. Loose connective tissue is seen in the papillary and reticular dermis.			
		CS		
2 days	1	2	2	3
14 days	There is mild acanthosis, no hyperkeratosis. There are no traces of skin appendages in the wound area yet.			
		CS-rGO		
2 days	1	2	1	3
14 days	Complete maturation of the epithelium, but epidermal ridges or marked dermal papillae are not yet observed. Loose connective tissue is observed in the papillary and reticular dermis. There is a greater presence of inflammatory cells than fibroblasts.			
		CS-rGO-TA$_3$		
2 days	2	3	3	2
14 days	Good differentiation of the epithelium. Dermal papillae and epidermal ridges are clearly visible, with many blood vessels close to the epithelial basement membrane. Differences are seen between the loose connective tissue of the papillary dermis versus a denser and more organized/molded tissue in the reticular dermis. In addition, the			

generation of developing hair follicles is seen. No hyperkeratosis or acanthosis is observed.

Re-epithelialization (0 = none; 1 = partial; 2 = complete but immature/thin; 3 = complete and mature). Neovascularization (0 = none; 1 = up to 5 vessels/high power field [HMF]; 2 = 6-10 vessels/HCF; 3 = >10 vessels/HCF). At this point, 3 visual fields were analyzed, and an average was obtained. Amount of granulation tissue (0 = none; 1 = scant; 2 = moderate; 3 = abundant) Inflammatory cells (0 = none; 1 = scant; 2 = moderate; 3 = abundant).

References

[1] Delgado-Pujol, E.J. *et al.* (2025). Hydrogels and Nanogels: Pioneering the Future of Advanced Drug Delivery Systems. *Pharmaceutics*. https://doi.org/10.3390/pharmaceutics17020215.

[2] Liu, B. and Chen, K. (2024). Advances in Hydrogel-Based Drug Delivery Systems. *Gels*. https://doi.org/10.3390/gels10040262.

[3] Laseca-Arranz, A. *et al.* (2021). Formulaciones para la cicatrización de heridas, presente y futuro Formulations for wound healing: present and future.

[4] Rivas, B. (2021). Sintesis de un hidrogel biocompatible con potencial aplicación en la ingeniería de tejidos.

[5] Obagi, Z. *et al.* (2019). Principles of Wound Dressings: A Review. *Surgical technology international*.

[6] Gounden, V. and Singh, M. (2024). Hydrogels and Wound Healing: Current and Future Prospects. *Gels*. https://doi.org/10.3390/gels10010043.

[7] Zhao, X. *et al.* (2017). Antibacterial anti-oxidant electroactive injectable hydrogel as self-healing wound dressing with hemostasis and adhesiveness for cutaneous wound healing. *Biomaterials*. https://doi.org/10.1016/j.biomaterials.2017.01.011.

[8] Fan, F. *et al.* (2021). Biomimetic Hydrogels to Promote Wound Healing. *Frontiers in Bioengineering and Biotechnology*. https://doi.org/10.3389/fbioe.2021.718377.

[9] Chen, H. *et al.* (2018). An injectable self-healing hydrogel with adhesive and antibacterial properties effectively promotes wound healing. *Carbohydrate polymers*. https://doi.org/10.1016/j.carbpol.2018.08.090.

[10] Jiao, D. *et al.* (2021). Bidirectional differentiation of BMSCs induced by a biomimetic procallus based on a gelatin-reduced graphene oxide reinforced hydrogel for rapid bone regeneration. *Bioactive Materials*. https://doi.org/https://doi.org/10.1016/j.bioactmat.2020.12.003.

[11] Nie, L. *et al.* (2023). Fabrication and desired properties of conductive hydrogel dressings for wound healing. *RSC Advances*. https://doi.org/10.1039/d2ra07195a.

[12] Pelegrino, M.T. *et al.* (2018). S-nitrosoglutathione-containing chitosan nanoparticles dispersed in Pluronic F-127 hydrogel: Potential uses in topical applications. *Journal of Drug Delivery Science and Technology*. https://doi.org/10.1016/J.JDDST.2017.10.016.

[13] Shang, S. *et al.* (2024). A bioactive composite hydrogel dressing that promotes healing of both acute and chronic diabetic skin wounds. *Bioactive Materials*. https://doi.org/10.1016/j.bioactmat.2023.12.026.

[14] Ding, S. *et al.* (2023). Photopolymerizable, immunomodulatory hydrogels of gelatin methacryloyl and carboxymethyl chitosan as all-in-one strategic dressing for wound healing. *International Journal of Biological Macromolecules*. https://doi.org/10.1016/j.ijbiomac.2023.127151.

[15] Ruíz, I. *et al.* (2025). Optimization and Validation of Chitosan-Reduced Graphene Oxide-Pluronic F-127 Hydrogel Synthesis for Potential Wound Dressing. *ChemistrySelect*. https://doi.org/10.1002/slct.202502598.

[16] Zhou, X. *et al.* (2023). Carboxymethyl Chitosan/Tannic Acid Hydrogel with Antibacterial, Hemostasis, and Antioxidant Properties Promoting Skin Wound

angiogenesis. *Carbohydrate Polymers*. https://doi.org/https://doi.org/10.1016/j.carbpol.2024.122147.

[63] Mohammed Kassim. Al-Hussainawy *et al.* (2024). New Synthesis Method of Biopolymer Composites Based on Alginate, Carrageenan and ZnONPS for Wound Healing Applications. *Iraqi Journal of Pharmaceutical Sciences*. https://doi.org/10.31351/vol33iss4pp195-207.

[64] González, L. *et al.* (2024). Innovative Approach to Accelerate Wound Healing: Synthesis and Validation of Enzymatically Cross-Linked COL–rGO Biocomposite Hydrogels. *Gels*. https://doi.org/10.3390/gels10070448.

[65] Peña, B. *et al.* (2018). Injectable Hydrogels for Cardiac Tissue Engineering. *Macromolecular Bioscience*. https://doi.org/10.1002/mabi.201800079.

[66] Khan, F. *et al.* (2022). Synthesis, classification and properties of hydrogels: their applications in drug delivery and agriculture. *Journal of Materials Chemistry B*. https://doi.org/10.1039/D1TB01345A.

[67] Gradinaru, V. *et al.*Hydrogel-Tissue Chemistry: Principles and Applications. https://doi.org/https://doi.org/10.1146/annurev-biophys-070317-032905.

[68] Bustamante-Torres, M. *et al.* (2021). Hydrogels classification according to the physical or chemical interactions and as stimuli-sensitive materials. *Gels*. https://doi.org/10.3390/gels7040182.

[69] Bashir, S. *et al.* (2020). Fundamental concepts of hydrogels: Synthesis, properties, and their applications. *Polymers*. https://doi.org/10.3390/polym12112702.

[70] Benwood, C. *et al.* (2021). Natural biomaterials and their use as bioinks for printing tissues. *Bioengineering*. https://doi.org/10.3390/bioengineering8020027.

[71] Zhang, Y. and Huang, Y. (2021). Rational Design of Smart Hydrogels for Biomedical Applications. *Frontiers in Chemistry*. https://doi.org/10.3389/fchem.2020.615665.

[72] Vasile, C. *et al.* (2020). New developments in medical applications of hybrid hydrogels containing natural polymers. *Molecules*. https://doi.org/10.3390/molecules25071539.

[73] Vijayavenkataraman, S. *et al.* (2019). Conductive collagen/polypyrrole-b-polycaprolactone hydrogel for bioprinting of neural tissue constructs. *International Journal of Bioprinting*. https://doi.org/10.18063/ijb.v5i2.1.229.

[74] Liang, Y. *et al.* (2025). A highly adhesive and melatonin-loaded PEG hydrogel prevents tumor recurrence and promotes wound healing for tumor-resection wound management of liposarcoma. *Materials Today Bio*. https://doi.org/https://doi.org/10.1016/j.mtbio.2025.101842.

[75] Li, Y. *et al.* (2025). A 3R (remove-remodel-repair)-integrated self-assembled Chlorella-gelatin-PEG hydrogel for diabetic wound healing. *Materials Today Bio*. https://doi.org/https://doi.org/10.1016/j.mtbio.2025.101935.

[76] Gu, L. *et al.* (2025). AIE-active PVA/berberine antibacterial hydrogel for wound healing, visual monitoring pH and dehydration. *Biomaterials*. https://doi.org/https://doi.org/10.1016/j.biomaterials.2025.123432.

[77] Abbasi, Y.F. *et al.* (2025). High molecular weight laminarin/AgNPs-impregnated PVA based in situ hydrogels accelerated diabetic wound healing. *Carbohydrate Polymers*. https://doi.org/https://doi.org/10.1016/j.carbpol.2025.123991.

[119] Bagher, Z. *et al.* (2020). Wound healing with alginate/chitosan hydrogel containing hesperidin in rat model. *Journal of Drug Delivery Science and Technology*. https://doi.org/10.1016/J.JDDST.2019.101379.

[120] Zidan, T.A. *et al.* (2020). N-Aminorhodanine modified chitosan hydrogel for antibacterial and copper ions removal from aqueous solutions. *International Journal of Biological Macromolecules*. https://doi.org/10.1016/J.IJBIOMAC.2020.04.180.

[121] Chenite, A. *et al.* (2000). Novel injectable neutral solutions of chitosan form biodegradable gels in situ. *Biomaterials*. https://doi.org/10.1016/S0142-9612(00)00116-2.

[122] Li, A. *et al.* (2024). Chitosan-based injectable hydrogel with multifunction for wound healing: A critical review. *Carbohydrate polymers*. https://doi.org/10.1016/j.carbpol.2024.121952.

[123] Matica, M. *et al.* (2019). Chitosan as a Wound Dressing Starting Material: Antimicrobial Properties and Mode of Action. *International Journal of Molecular Sciences*. https://doi.org/10.3390/ijms20235889.

[124] Guo, W. *et al.* (2024). Self-adhesive and self-healing hydrogel dressings based on quaternary ammonium chitosan and host-guest interacted silk fibroin. *Colloids and Surfaces A: Physicochemical and Engineering Aspects*. https://doi.org/10.1016/j.colsurfa.2024.133145.

[125] Bai, Q. *et al.* (2023). Chitosan and hyaluronic-based hydrogels could promote the infected wound healing. *International journal of biological macromolecules*. https://doi.org/10.1016/j.ijbiomac.2023.123271.

[126] López, H. (2022). "Síntesis y aplicación de un nanocompósito de quitosano-glicidil metacrilato-colágeno tipo I y nanopartículas de oro sobre la cicatrización de heridas cutáneas."

[127] Yuan, N. *et al.* (2023). Chitosan, alginate, hyaluronic acid and other novel multifunctional hydrogel dressings for wound healing: A review. *International Journal of Biological Macromolecules*. https://doi.org/https://doi.org/10.1016/j.ijbiomac.2023.124321.

[128] Li, A. *et al.* (2024). Chitosan-based injectable hydrogel with multifunction for wound healing: A critical review. *Carbohydrate Polymers*. https://doi.org/https://doi.org/10.1016/j.carbpol.2024.121952.

[129] Bellier, N. *et al.* (2022). Recent biomedical advancements in graphene oxide- and reduced graphene oxide-based nanocomposite nanocarriers. *Biomaterials Research*. https://doi.org/10.1186/s40824-022-00313-2.

[130] Ghawanmeh, A.A. *et al.* (2019). Graphene oxide-based hydrogels as a nanocarrier for anticancer drug delivery. *Nano Research*. https://doi.org/10.1007/s12274-019-2300-4.

[131] Chiticaru, E.A. and Ionita, M. (2022). Graphene toxicity and future perspectives in healthcare and biomedicine. *FlatChem*. https://doi.org/https://doi.org/10.1016/j.flatc.2022.100417.

[132] Cebadero-Domínguez, O. *et al.* (2022). In vitro toxicity evaluation of graphene oxide and reduced graphene oxide on Caco-2 cells. *Toxicology Reports*. https://doi.org/https://doi.org/10.1016/j.toxrep.2022.05.010.

[133] Mohammed, H. *et al.* (2020). Antimicrobial Mechanisms and Effectiveness of Graphene and Graphene-Functionalized Biomaterials. A Scope Review. *Frontiers*

[178] Ruiz, I. *et al.* (2024). Inclusion of Reduced Graphene Oxide to Silk Fibroin Hydrogels Improve the Conductive, Swelling and Wound Healing Capacity. *ChemistrySelect*. https://doi.org/10.1002/slct.202402444.

[179] Safarzadeh Kozani, P. *et al.* (2022). Polysaccharide-based hydrogels: properties, advantages, challenges, and optimization methods for applications in regenerative medicine. *International Journal of Polymeric Materials and Polymeric Biomaterials*. https://doi.org/10.1080/00914037.2021.1962876.

[180] Lu, H. *et al.* (2019). Electroconductive hydrogels for biomedical applications. *Wiley Interdisciplinary Reviews: Nanomedicine and Nanobiotechnology*. https://doi.org/10.1002/wnan.1568.

[181] Fathi, A. *et al.* (2024). Thermoresponsive in situ forming and self-healing double-network hydrogels as injectable dressings for silymarin/levofloxacin delivery for treatment of third-degree burn wounds. *Carbohydrate Polymers*. https://doi.org/10.1016/j.carbpol.2024.121856.

[182] Feng, P. *et al.* (2021). Chitosan-Based Functional Materials for Skin Wound Repair: Mechanisms and Applications. *Frontiers in Bioengineering and Biotechnology*.

[183] Rajinikanth B, S. *et al.* (2024). Chitosan-Based Biomaterial in Wound Healing: A Review. *Cureus*. https://doi.org/10.7759/cureus.55193.

[184] Gegel', N.O. *et al.* (2022). Influence of Chitosan on Orientation–Micellar Ordering of the Pluronic F-127 Gel Phase in an Aqueous Medium. *Optics and Spectroscopy*. https://doi.org/10.1134/S0030400X22040051.

[185] Mattevi, C. *et al.* (2009). Evolution of electrical, chemical, and structural properties of transparent and conducting chemically derived graphene thin films. *Advanced Functional Materials*. https://doi.org/10.1002/adfm.200900166.

[186] Emmanuel Ibukun, A. *et al.* (2024). Recent developments in synthesis and characterisation of graphene oxide modified with deep eutectic solvents for dispersive and magnetic solid-phase extractions. *Microchemical Journal*. https://doi.org/10.1016/j.microc.2024.110111.

[187] Abdillah, O.B. *et al.* (2023). Recent progress on reduced graphene oxide and polypyrrole composites for high performance supercapacitors: A review. *Journal of Energy Storage*. https://doi.org/10.1016/j.est.2023.109300.

[188] AL-Salman, H.N.K. *et al.* (2023). Graphene oxide-based biosensors for detection of lung cancer: A review. *Results in Chemistry*. https://doi.org/10.1016/j.rechem.2023.101300.

[189] Xu, L.Q. *et al.* (2010). Dopamine-Induced Reduction and Functionalization of Graphene Oxide Nanosheets. *Macromolecules*. https://doi.org/10.1021/ma101526k.

[190] Liang, Y. *et al.* (2019). Adhesive Hemostatic Conducting Injectable Composite Hydrogels with Sustained Drug Release and Photothermal Antibacterial Activity to Promote Full-Thickness Skin Regeneration During Wound Healing. *Small*. https://doi.org/10.1002/smll.201900046.

[191] Nowroozi, N. *et al.* (2021). Biological and structural properties of graphene oxide/curcumin nanocomposite incorporated chitosan as a scaffold for wound healing application. *Life Sciences*. https://doi.org/https://doi.org/10.1016/j.lfs.2020.118640.

[192] Elhami, N. *et al.* (2024). Development of nanocomposites based on

[232] Ulutürk, C. and Alemdar, N. (2019). Production of reduced graphene oxide-based electrically conductive hydrogel by using modified chitosan. *Journal of Applied Polymer Science*. https://doi.org/10.1002/app.48008.

[233] Xiong, D. *et al.* (2015). Oxygen-containing Functional Groups Enhancing Electrochemical Performance of Porous Reduced Graphene Oxide Cathode in Lithium Ion Batteries. *ACS nano*. https://doi.org/https://doi.org/10.1016/j.electacta.2015.06.041.

[234] Wang, J. *et al.* (2015). Facile self-assembly of magnetite nanoparticles on three-dimensional graphene oxide–chitosan composite for lipase immobilization. *Biochemical Engineering Journal*. https://doi.org/https://doi.org/10.1016/j.bej.2014.11.013.

[235] Escalona-Rayo, C.F. *et al.* (2020). Optimization of Unidirectional Mucoadhesive Buccal Patches Based on Chitosan and Pluronic® F-127 for Metoprolol Controlled Release: In Vitro and Ex Vivo Evaluations. *Journal of Pharmaceutical Innovation*. https://doi.org/10.1007/s12247-019-09401-8.

[236] Yavari, N. and Azizian, S. (2022). Mixed diffusion and relaxation kinetics model for hydrogels swelling. *Journal of Molecular Liquids*. https://doi.org/10.1016/J.MOLLIQ.2022.119861.

[237] Kosowska, K. *et al.* (2019). Synthesis and characterization of chitosan/reduced graphene oxide hybrid composites. *Materials*. https://doi.org/10.3390/ma12132077.

[238] Rokhade, A. *et al.* (2007). Novel hydrogel microspheres of chitosan and pluronic F-127 for controlled release of 5-fluorouracil. *Journal of Microencapsulation*. https://doi.org/10.1080/02652040701281365.

[239] Song, Y. *et al.* (2024). A chitosan-based conductive double network hydrogel doped by tannic acid-reduced graphene oxide with excellent stretchability and high sensitivity for wearable strain sensors. *International Journal of Biological Macromolecules*. https://doi.org/https://doi.org/10.1016/j.ijbiomac.2023.128861.

[240] Scanga, V.I. *et al.* (2010). Biomaterials for neural-tissue engineering - Chitosan supports the survival, migration, and differentiation of adult-derived neural stem and progenitor cells. *Canadian Journal of Chemistry*. https://doi.org/10.1139/V09-171.

[241] Kwon, J.S. *et al.* (2012). Chitosan-based hydrogels to induce neuronal differentiation of rat muscle-derived stem cells. *International Journal of Biological Macromolecules*. https://doi.org/https://doi.org/10.1016/j.ijbiomac.2012.08.007.

[242] Wang, Y. *et al.* (2017). Conductive graphene oxide hydrogels reduced and bridged by l-cysteine to support cell adhesion and growth. *Journal of Materials Chemistry B*. https://doi.org/10.1039/c6tb02333a.

[243] Sayyar, S. *et al.* (2015). Processable conducting graphene/chitosan hydrogels for tissue engineering. *Journal of Materials Chemistry B*. https://doi.org/10.1039/c4tb01636j.

[244] Guo, S. *et al.* (2022). Injectable Self-Healing Adhesive Chitosan Hydrogel with Antioxidative, Antibacterial, and Hemostatic Activities for Rapid Hemostasis and Skin Wound Healing. *ACS Applied Materials & Interfaces*. https://doi.org/10.1021/acsami.2c08870.

[288] Fernández, K. *et al.* (2023). Self-Assembled CNF/rGO/Tannin Composite: Study of the Physicochemical and Wound Healing Properties. *Polymers*. https://doi.org/10.3390/polym15122752.

[289] Zuo, L. *et al.* (2023). Preparation and characterization of tannin-maltodextrin-polyvinyl alcohol hydrogel based on hydrogen bonding for wound healing. *Journal of the Mechanical Behavior of Biomedical Materials*. https://doi.org/https://doi.org/10.1016/j.jmbbm.2023.105942.

[290] Li, D. *et al.* (2024). Cellulose nanofibers embedded chitosan/tannin hydrogel with high antibacterial activity and hemostatic ability for drug-resistant bacterial infected wound healing. *Carbohydrate Polymers*. https://doi.org/10.1016/j.carbpol.2023.121687.

[291] Su, X. *et al.* (2017). Wound-healing promoting effect of total tannins from Entada phaseoloides (L.) Merr. in rats. *Burns*. https://doi.org/https://doi.org/10.1016/j.burns.2016.10.010.

[292] Sun, W. *et al.* (2024). Quaternary ammonium grafted chitosan hydrogel with enhanced antibacterial performance as tannin acid and deferoxamine carrier to promote diabetic wound healing. *Colloids and Surfaces B: Biointerfaces*. https://doi.org/https://doi.org/10.1016/j.colsurfb.2024.114160.

[293] Hernandes, L. *et al.* (2010). Wound-healing evaluation of ointment from Stryphnodendron adstringens (barbatimão) in rat skin. *Article Brazilian Journal of Pharmaceutical Sciences*.

[294] Elhami, N. *et al.* (2024). Development of nanocomposites based on chitosan/reduced graphene oxide for wound healing application. *International Journal of Biological Macromolecules*. https://doi.org/https://doi.org/10.1016/j.ijbiomac.2023.128832.

[295] Pinto, S.C.G. *et al.* (2015). Stryphnodendron adstringens: Clarifying Wound Healing in Streptozotocin-Induced Diabetic Rats. *Planta Medica*. https://doi.org/10.1055/s-0035-1546209.

[296] Li, L. *et al.* (2023). Pilose antler extract restores type I and III collagen to accelerate wound healing. *Biomedicine & Pharmacotherapy*. https://doi.org/https://doi.org/10.1016/j.biopha.2023.114510.

[297] Kumar, T. *et al.* (2015). HERBAL PLANTS WITH POTENTIAL OF WOUND HEALING ACTIVITY: A REVIEW ARTICLE. *www.wjpps.com* |. https://doi.org/10.20959/wjpps20233-24260.

[298] Vitale, S. *et al.* (2022). Phytochemistry and Biological Activity of Medicinal Plants in Wound Healing: An Overview of Current Research. *Molecules*. https://doi.org/10.3390/molecules27113566.

[299] Mathew-Steiner, S.S. *et al.* (2021). Collagen in wound healing. *Bioengineering*. https://doi.org/10.3390/bioengineering8050063.

[300] Merkel, J.R. *et al.* (1988). Type I and type III collagen content of healing wounds in fetal and adult rats. *Proceedings of the Society for Experimental Biology and Medicine. Society for Experimental Biology and Medicine (New York, N.Y.)*. https://doi.org/10.3181/00379727-187-42694.

[301] Rodrigues, D.F. *et al.* (2017). Treatment of excisional wound in rabbits with barbatiman extracts associated with autologous bone marrow mononuclear cells. *SCielo*. https://doi.org/10.1590/1678-4162-9301.

[302] Arranz-Valsero, I. *et al.* (2014). IL-6 as a corneal wound healing mediator in an

[1] Delgado-Pujol, E.J. *et al.* (2025). Hydrogels and Nanogels: Pioneering the Future of Advanced Drug Delivery Systems. *Pharmaceutics*. https://doi.org/10.3390/pharmaceutics17020215.

[2] Liu, B. and Chen, K. (2024). Advances in Hydrogel-Based Drug Delivery Systems. *Gels*. https://doi.org/10.3390/gels10040262.

[3] Laseca-Arranz, A. *et al.* (2021). Formulaciones para la cicatrización de heridas, presente y futuro Formulations for wound healing: present and future.

[4] Rivas, B. (2021). Sintesis de un hidrogel biocompatible con potencial aplicación en la ingeniería de tejidos.

[5] Obagi, Z. *et al.* (2019). Principles of Wound Dressings: A Review. *Surgical technology international*.

[6] Gounden, V. and Singh, M. (2024). Hydrogels and Wound Healing: Current and Future Prospects. *Gels*. https://doi.org/10.3390/gels10010043.

[7] Zhao, X. *et al.* (2017). Antibacterial anti-oxidant electroactive injectable hydrogel as self-healing wound dressing with hemostasis and adhesiveness for cutaneous wound healing. *Biomaterials*. https://doi.org/10.1016/j.biomaterials.2017.01.011.

[8] Fan, F. *et al.* (2021). Biomimetic Hydrogels to Promote Wound Healing. *Frontiers in Bioengineering and Biotechnology*. https://doi.org/10.3389/fbioe.2021.718377.

[9] Chen, H. *et al.* (2018). An injectable self-healing hydrogel with adhesive and antibacterial properties effectively promotes wound healing. *Carbohydrate polymers*. https://doi.org/10.1016/j.carbpol.2018.08.090.

[10] Jiao, D. *et al.* (2021). Bidirectional differentiation of BMSCs induced by a biomimetic procallus based on a gelatin-reduced graphene oxide reinforced hydrogel for rapid bone regeneration. *Bioactive Materials*. https://doi.org/https://doi.org/10.1016/j.bioactmat.2020.12.003.

[11] Nie, L. *et al.* (2023). Fabrication and desired properties of conductive hydrogel dressings for wound healing. *RSC Advances*. https://doi.org/10.1039/d2ra07195a.

[12] Pelegrino, M.T. *et al.* (2018). S-nitrosoglutathione-containing chitosan nanoparticles dispersed in Pluronic F-127 hydrogel: Potential uses in topical applications. *Journal of Drug Delivery Science and Technology*. https://doi.org/10.1016/J.JDDST.2017.10.016.

[13] Shang, S. *et al.* (2024). A bioactive composite hydrogel dressing that promotes healing of both acute and chronic diabetic skin wounds. *Bioactive Materials*. https://doi.org/10.1016/j.bioactmat.2023.12.026.

[14] Ding, S. *et al.* (2023). Photopolymerizable, immunomodulatory hydrogels of gelatin methacryloyl and carboxymethyl chitosan as all-in-one strategic dressing for wound healing. *International Journal of Biological Macromolecules*. https://doi.org/10.1016/j.ijbiomac.2023.127151.

[15] Ruíz, I. *et al.* (2025). Optimization and Validation of Chitosan-Reduced Graphene Oxide-Pluronic F-127 Hydrogel Synthesis for Potential Wound Dressing. *ChemistrySelect*. https://doi.org/10.1002/slct.202502598.

[16] Zhou, X. *et al.* (2023). Carboxymethyl Chitosan/Tannic Acid Hydrogel with Antibacterial, Hemostasis, and Antioxidant Properties Promoting Skin Wound

angiogenesis. *Carbohydrate Polymers*. https://doi.org/https://doi.org/10.1016/j.carbpol.2024.122147.

[63] Mohammed Kassim. Al-Hussainawy *et al.* (2024). New Synthesis Method of Biopolymer Composites Based on Alginate, Carrageenan and ZnONPS for Wound Healing Applications. *Iraqi Journal of Pharmaceutical Sciences*. https://doi.org/10.31351/vol33iss4pp195-207.

[64] González, L. *et al.* (2024). Innovative Approach to Accelerate Wound Healing: Synthesis and Validation of Enzymatically Cross-Linked COL–rGO Biocomposite Hydrogels. *Gels*. https://doi.org/10.3390/gels10070448.

[65] Peña, B. *et al.* (2018). Injectable Hydrogels for Cardiac Tissue Engineering. *Macromolecular Bioscience*. https://doi.org/10.1002/mabi.201800079.

[66] Khan, F. *et al.* (2022). Synthesis, classification and properties of hydrogels: their applications in drug delivery and agriculture. *Journal of Materials Chemistry B*. https://doi.org/10.1039/D1TB01345A.

[67] Gradinaru, V. *et al.*Hydrogel-Tissue Chemistry: Principles and Applications. https://doi.org/https://doi.org/10.1146/annurev-biophys-070317-032905.

[68] Bustamante-Torres, M. *et al.* (2021). Hydrogels classification according to the physical or chemical interactions and as stimuli-sensitive materials. *Gels*. https://doi.org/10.3390/gels7040182.

[69] Bashir, S. *et al.* (2020). Fundamental concepts of hydrogels: Synthesis, properties, and their applications. *Polymers*. https://doi.org/10.3390/polym12112702.

[70] Benwood, C. *et al.* (2021). Natural biomaterials and their use as bioinks for printing tissues. *Bioengineering*. https://doi.org/10.3390/bioengineering8020027.

[71] Zhang, Y. and Huang, Y. (2021). Rational Design of Smart Hydrogels for Biomedical Applications. *Frontiers in Chemistry*. https://doi.org/10.3389/fchem.2020.615665.

[72] Vasile, C. *et al.* (2020). New developments in medical applications of hybrid hydrogels containing natural polymers. *Molecules*. https://doi.org/10.3390/molecules25071539.

[73] Vijayavenkataraman, S. *et al.* (2019). Conductive collagen/polypyrrole-b-polycaprolactone hydrogel for bioprinting of neural tissue constructs. *International Journal of Bioprinting*. https://doi.org/10.18063/ijb.v5i2.1.229.

[74] Liang, Y. *et al.* (2025). A highly adhesive and melatonin-loaded PEG hydrogel prevents tumor recurrence and promotes wound healing for tumor-resection wound management of liposarcoma. *Materials Today Bio*. https://doi.org/https://doi.org/10.1016/j.mtbio.2025.101842.

[75] Li, Y. *et al.* (2025). A 3R (remove-remodel-repair)-integrated self-assembled Chlorella-gelatin-PEG hydrogel for diabetic wound healing. *Materials Today Bio*. https://doi.org/https://doi.org/10.1016/j.mtbio.2025.101935.

[76] Gu, L. *et al.* (2025). AIE-active PVA/berberine antibacterial hydrogel for wound healing, visual monitoring pH and dehydration. *Biomaterials*. https://doi.org/https://doi.org/10.1016/j.biomaterials.2025.123432.

[77] Abbasi, Y.F. *et al.* (2025). High molecular weight laminarin/AgNPs-impregnated PVA based in situ hydrogels accelerated diabetic wound healing. *Carbohydrate Polymers*. https://doi.org/https://doi.org/10.1016/j.carbpol.2025.123991.

[119] Bagher, Z. *et al.* (2020). Wound healing with alginate/chitosan hydrogel containing hesperidin in rat model. *Journal of Drug Delivery Science and Technology*. https://doi.org/10.1016/J.JDDST.2019.101379.

[120] Zidan, T.A. *et al.* (2020). N-Aminorhodanine modified chitosan hydrogel for antibacterial and copper ions removal from aqueous solutions. *International Journal of Biological Macromolecules*. https://doi.org/10.1016/J.IJBIOMAC.2020.04.180.

[121] Chenite, A. *et al.* (2000). Novel injectable neutral solutions of chitosan form biodegradable gels in situ. *Biomaterials*. https://doi.org/10.1016/S0142-9612(00)00116-2.

[122] Li, A. *et al.* (2024). Chitosan-based injectable hydrogel with multifunction for wound healing: A critical review. *Carbohydrate polymers*. https://doi.org/10.1016/j.carbpol.2024.121952.

[123] Matica, M. *et al.* (2019). Chitosan as a Wound Dressing Starting Material: Antimicrobial Properties and Mode of Action. *International Journal of Molecular Sciences*. https://doi.org/10.3390/ijms20235889.

[124] Guo, W. *et al.* (2024). Self-adhesive and self-healing hydrogel dressings based on quaternary ammonium chitosan and host-guest interacted silk fibroin. *Colloids and Surfaces A: Physicochemical and Engineering Aspects*. https://doi.org/10.1016/j.colsurfa.2024.133145.

[125] Bai, Q. *et al.* (2023). Chitosan and hyaluronic-based hydrogels could promote the infected wound healing. *International journal of biological macromolecules*. https://doi.org/10.1016/j.ijbiomac.2023.123271.

[126] López, H. (2022). "Síntesis y aplicación de un nanocompósito de quitosano-glicidil metacrilato-colágeno tipo I y nanopartículas de oro sobre la cicatrización de heridas cutáneas."

[127] Yuan, N. *et al.* (2023). Chitosan, alginate, hyaluronic acid and other novel multifunctional hydrogel dressings for wound healing: A review. *International Journal of Biological Macromolecules*. https://doi.org/https://doi.org/10.1016/j.ijbiomac.2023.124321.

[128] Li, A. *et al.* (2024). Chitosan-based injectable hydrogel with multifunction for wound healing: A critical review. *Carbohydrate Polymers*. https://doi.org/https://doi.org/10.1016/j.carbpol.2024.121952.

[129] Bellier, N. *et al.* (2022). Recent biomedical advancements in graphene oxide- and reduced graphene oxide-based nanocomposite nanocarriers. *Biomaterials Research*. https://doi.org/10.1186/s40824-022-00313-2.

[130] Ghawanmeh, A.A. *et al.* (2019). Graphene oxide-based hydrogels as a nanocarrier for anticancer drug delivery. *Nano Research*. https://doi.org/10.1007/s12274-019-2300-4.

[131] Chiticaru, E.A. and Ionita, M. (2022). Graphene toxicity and future perspectives in healthcare and biomedicine. *FlatChem*. https://doi.org/https://doi.org/10.1016/j.flatc.2022.100417.

[132] Cebadero-Domínguez, O. *et al.* (2022). In vitro toxicity evaluation of graphene oxide and reduced graphene oxide on Caco-2 cells. *Toxicology Reports*. https://doi.org/https://doi.org/10.1016/j.toxrep.2022.05.010.

[133] Mohammed, H. *et al.* (2020). Antimicrobial Mechanisms and Effectiveness of Graphene and Graphene-Functionalized Biomaterials. A Scope Review. *Frontiers*

[178] Ruiz, I. *et al.* (2024). Inclusion of Reduced Graphene Oxide to Silk Fibroin Hydrogels Improve the Conductive, Swelling and Wound Healing Capacity. *ChemistrySelect*. https://doi.org/10.1002/slct.202402444.

[179] Safarzadeh Kozani, P. *et al.* (2022). Polysaccharide-based hydrogels: properties, advantages, challenges, and optimization methods for applications in regenerative medicine. *International Journal of Polymeric Materials and Polymeric Biomaterials*. https://doi.org/10.1080/00914037.2021.1962876.

[180] Lu, H. *et al.* (2019). Electroconductive hydrogels for biomedical applications. *Wiley Interdisciplinary Reviews: Nanomedicine and Nanobiotechnology*. https://doi.org/10.1002/wnan.1568.

[181] Fathi, A. *et al.* (2024). Thermoresponsive in situ forming and self-healing double-network hydrogels as injectable dressings for silymarin/levofloxacin delivery for treatment of third-degree burn wounds. *Carbohydrate Polymers*. https://doi.org/10.1016/j.carbpol.2024.121856.

[182] Feng, P. *et al.* (2021). Chitosan-Based Functional Materials for Skin Wound Repair: Mechanisms and Applications. *Frontiers in Bioengineering and Biotechnology*.

[183] Rajinikanth B, S. *et al.* (2024). Chitosan-Based Biomaterial in Wound Healing: A Review. *Cureus*. https://doi.org/10.7759/cureus.55193.

[184] Gegel', N.O. *et al.* (2022). Influence of Chitosan on Orientation–Micellar Ordering of the Pluronic F-127 Gel Phase in an Aqueous Medium. *Optics and Spectroscopy*. https://doi.org/10.1134/S0030400X22040051.

[185] Mattevi, C. *et al.* (2009). Evolution of electrical, chemical, and structural properties of transparent and conducting chemically derived graphene thin films. *Advanced Functional Materials*. https://doi.org/10.1002/adfm.200900166.

[186] Emmanuel Ibukun, A. *et al.* (2024). Recent developments in synthesis and characterisation of graphene oxide modified with deep eutectic solvents for dispersive and magnetic solid-phase extractions. *Microchemical Journal*. https://doi.org/10.1016/j.microc.2024.110111.

[187] Abdillah, O.B. *et al.* (2023). Recent progress on reduced graphene oxide and polypyrrole composites for high performance supercapacitors: A review. *Journal of Energy Storage*. https://doi.org/10.1016/j.est.2023.109300.

[188] AL-Salman, H.N.K. *et al.* (2023). Graphene oxide-based biosensors for detection of lung cancer: A review. *Results in Chemistry*. https://doi.org/10.1016/j.rechem.2023.101300.

[189] Xu, L.Q. *et al.* (2010). Dopamine-Induced Reduction and Functionalization of Graphene Oxide Nanosheets. *Macromolecules*. https://doi.org/10.1021/ma101526k.

[190] Liang, Y. *et al.* (2019). Adhesive Hemostatic Conducting Injectable Composite Hydrogels with Sustained Drug Release and Photothermal Antibacterial Activity to Promote Full-Thickness Skin Regeneration During Wound Healing. *Small*. https://doi.org/10.1002/smll.201900046.

[191] Nowroozi, N. *et al.* (2021). Biological and structural properties of graphene oxide/curcumin nanocomposite incorporated chitosan as a scaffold for wound healing application. *Life Sciences*. https://doi.org/https://doi.org/10.1016/j.lfs.2020.118640.

[192] Elhami, N. *et al.* (2024). Development of nanocomposites based on

[232] Ulutürk, C. and Alemdar, N. (2019). Production of reduced graphene oxide-based electrically conductive hydrogel by using modified chitosan. *Journal of Applied Polymer Science*. https://doi.org/10.1002/app.48008.

[233] Xiong, D. *et al.* (2015). Oxygen-containing Functional Groups Enhancing Electrochemical Performance of Porous Reduced Graphene Oxide Cathode in Lithium Ion Batteries. *ACS nano*. https://doi.org/https://doi.org/10.1016/j.electacta.2015.06.041.

[234] Wang, J. *et al.* (2015). Facile self-assembly of magnetite nanoparticles on three-dimensional graphene oxide–chitosan composite for lipase immobilization. *Biochemical Engineering Journal*. https://doi.org/https://doi.org/10.1016/j.bej.2014.11.013.

[235] Escalona-Rayo, C.F. *et al.* (2020). Optimization of Unidirectional Mucoadhesive Buccal Patches Based on Chitosan and Pluronic® F-127 for Metoprolol Controlled Release: In Vitro and Ex Vivo Evaluations. *Journal of Pharmaceutical Innovation*. https://doi.org/10.1007/s12247-019-09401-8.

[236] Yavari, N. and Azizian, S. (2022). Mixed diffusion and relaxation kinetics model for hydrogels swelling. *Journal of Molecular Liquids*. https://doi.org/10.1016/J.MOLLIQ.2022.119861.

[237] Kosowska, K. *et al.* (2019). Synthesis and characterization of chitosan/reduced graphene oxide hybrid composites. *Materials*. https://doi.org/10.3390/ma12132077.

[238] Rokhade, A. *et al.* (2007). Novel hydrogel microspheres of chitosan and pluronic F-127 for controlled release of 5-fluorouracil. *Journal of Microencapsulation*. https://doi.org/10.1080/02652040701281365.

[239] Song, Y. *et al.* (2024). A chitosan-based conductive double network hydrogel doped by tannic acid-reduced graphene oxide with excellent stretchability and high sensitivity for wearable strain sensors. *International Journal of Biological Macromolecules*. https://doi.org/https://doi.org/10.1016/j.ijbiomac.2023.128861.

[240] Scanga, V.I. *et al.* (2010). Biomaterials for neural-tissue engineering - Chitosan supports the survival, migration, and differentiation of adult-derived neural stem and progenitor cells. *Canadian Journal of Chemistry*. https://doi.org/10.1139/V09-171.

[241] Kwon, J.S. *et al.* (2012). Chitosan-based hydrogels to induce neuronal differentiation of rat muscle-derived stem cells. *International Journal of Biological Macromolecules*. https://doi.org/https://doi.org/10.1016/j.ijbiomac.2012.08.007.

[242] Wang, Y. *et al.* (2017). Conductive graphene oxide hydrogels reduced and bridged by l-cysteine to support cell adhesion and growth. *Journal of Materials Chemistry B*. https://doi.org/10.1039/c6tb02333a.

[243] Sayyar, S. *et al.* (2015). Processable conducting graphene/chitosan hydrogels for tissue engineering. *Journal of Materials Chemistry B*. https://doi.org/10.1039/c4tb01636j.

[244] Guo, S. *et al.* (2022). Injectable Self-Healing Adhesive Chitosan Hydrogel with Antioxidative, Antibacterial, and Hemostatic Activities for Rapid Hemostasis and Skin Wound Healing. *ACS Applied Materials & Interfaces*. https://doi.org/10.1021/acsami.2c08870.

[288] Fernández, K. *et al.* (2023). Self-Assembled CNF/rGO/Tannin Composite: Study of the Physicochemical and Wound Healing Properties. *Polymers*. https://doi.org/10.3390/polym15122752.

[289] Zuo, L. *et al.* (2023). Preparation and characterization of tannin-maltodextrin-polyvinyl alcohol hydrogel based on hydrogen bonding for wound healing. *Journal of the Mechanical Behavior of Biomedical Materials*. https://doi.org/https://doi.org/10.1016/j.jmbbm.2023.105942.

[290] Li, D. *et al.* (2024). Cellulose nanofibers embedded chitosan/tannin hydrogel with high antibacterial activity and hemostatic ability for drug-resistant bacterial infected wound healing. *Carbohydrate Polymers*. https://doi.org/10.1016/j.carbpol.2023.121687.

[291] Su, X. *et al.* (2017). Wound-healing promoting effect of total tannins from Entada phaseoloides (L.) Merr. in rats. *Burns*. https://doi.org/https://doi.org/10.1016/j.burns.2016.10.010.

[292] Sun, W. *et al.* (2024). Quaternary ammonium grafted chitosan hydrogel with enhanced antibacterial performance as tannin acid and deferoxamine carrier to promote diabetic wound healing. *Colloids and Surfaces B: Biointerfaces*. https://doi.org/https://doi.org/10.1016/j.colsurfb.2024.114160.

[293] Hernandes, L. *et al.* (2010). Wound-healing evaluation of ointment from Stryphnodendron adstringens (barbatimão) in rat skin. *Article Brazilian Journal of Pharmaceutical Sciences*.

[294] Elhami, N. *et al.* (2024). Development of nanocomposites based on chitosan/reduced graphene oxide for wound healing application. *International Journal of Biological Macromolecules*. https://doi.org/https://doi.org/10.1016/j.ijbiomac.2023.128832.

[295] Pinto, S.C.G. *et al.* (2015). Stryphnodendron adstringens: Clarifying Wound Healing in Streptozotocin-Induced Diabetic Rats. *Planta Medica*. https://doi.org/10.1055/s-0035-1546209.

[296] Li, L. *et al.* (2023). Pilose antler extract restores type I and III collagen to accelerate wound healing. *Biomedicine & Pharmacotherapy*. https://doi.org/https://doi.org/10.1016/j.biopha.2023.114510.

[297] Kumar, T. *et al.* (2015). HERBAL PLANTS WITH POTENTIAL OF WOUND HEALING ACTIVITY: A REVIEW ARTICLE. *www.wjpps.com* |. https://doi.org/10.20959/wjpps20233-24260.

[298] Vitale, S. *et al.* (2022). Phytochemistry and Biological Activity of Medicinal Plants in Wound Healing: An Overview of Current Research. *Molecules*. https://doi.org/10.3390/molecules27113566.

[299] Mathew-Steiner, S.S. *et al.* (2021). Collagen in wound healing. *Bioengineering*. https://doi.org/10.3390/bioengineering8050063.

[300] Merkel, J.R. *et al.* (1988). Type I and type III collagen content of healing wounds in fetal and adult rats. *Proceedings of the Society for Experimental Biology and Medicine. Society for Experimental Biology and Medicine (New York, N.Y.)*. https://doi.org/10.3181/00379727-187-42694.

[301] Rodrigues, D.F. *et al.* (2017). Treatment of excisional wound in rabbits with barbatiman extracts associated with autologous bone marrow mononuclear cells. *SCielo*. https://doi.org/10.1590/1678-4162-9301.

[302] Arranz-Valsero, I. *et al.* (2014). IL-6 as a corneal wound healing mediator in an

[1] Delgado-Pujol, E.J. *et al.* (2025). Hydrogels and Nanogels: Pioneering the Future of Advanced Drug Delivery Systems. *Pharmaceutics*. https://doi.org/10.3390/pharmaceutics17020215.

[2] Liu, B. and Chen, K. (2024). Advances in Hydrogel-Based Drug Delivery Systems. *Gels*. https://doi.org/10.3390/gels10040262.

[3] Laseca-Arranz, A. *et al.* (2021). Formulaciones para la cicatrización de heridas, presente y futuro. Formulations for wound healing: present and future.

[4] Rivas, B. (2021). Síntesis de un hidrogel biocompatible con potencial aplicación en la ingeniería de tejidos.

[5] Obagi, Z. *et al.* (2019). Principles of Wound Dressings: A Review. *Surgical Technology International*.

[6] Gounden, V. and Singh, M. (2024). Hydrogels and Wound Healing: Current and Future Prospects. *Gels*. https://doi.org/10.3390/gels10010043.

[7] Zhao, X. *et al.* (2017). Antibacterial anti-oxidant electroactive injectable hydrogel as self-healing wound dressing with hemostasis and adhesiveness for cutaneous wound healing. *Biomaterials*. https://doi.org/10.1016/j.biomaterials.2017.01.011.

[8] Fan, F. *et al.* (2021). Biomimetic Hydrogels to Promote Wound Healing. *Frontiers in Bioengineering and Biotechnology*. https://doi.org/10.3389/fbioe.2021.718377.

[9] Chen, H. *et al.* (2018). An injectable self-healing hydrogel with adhesive and antibacterial properties effectively promotes wound healing. *Carbohydrate polymers*. https://doi.org/10.1016/j.carbpol.2018.08.090.

[10] Jiao, D. *et al.* (2021). Bidirectional differentiation of BMSCs induced by a biomimetic procallus based on a gelatin-reduced graphene oxide reinforced hydrogel for rapid bone regeneration. *Bioactive Materials*. https://doi.org/https://doi.org/10.1016/j.bioactmat.2020.12.003.

[11] Nie, L. *et al.* (2023). Fabrication and desired properties of conductive hydrogel dressings for wound healing. *RSC Advances*. https://doi.org/10.1039/d2ra07195a.

[12] Pelegrino, M.T. *et al.* (2018). S-nitrosoglutathione-containing chitosan nanoparticles dispersed in Pluronic F-127 hydrogel: Potential uses in topical applications. *Journal of Drug Delivery Science and Technology*. https://doi.org/10.1016/J.JDDST.2017.10.016.

[13] Shang, S. *et al.* (2024). A bioactive composite hydrogel dressing that promotes healing of both acute and chronic diabetic skin wounds. *Bioactive Materials*. https://doi.org/10.1016/j.bioactmat.2023.12.026.

[14] Ding, S. *et al.* (2023). Photopolymerizable, immunomodulatory hydrogels of gelatin methacryloyl and carboxymethyl chitosan as all-in-one strategic dressing for wound healing. *International Journal of Biological Macromolecules*. https://doi.org/10.1016/j.ijbiomac.2023.127151.

[15] Ruíz, I. *et al.* (2025). Optimization and Validation of Chitosan-Reduced Graphene Oxide-Pluronic F-127 Hydrogel Synthesis for Potential Wound Dressing. *ChemistrySelect*. https://doi.org/10.1002/slct.202502598.

[16] Zhou, X. *et al.* (2023). Carboxymethyl Chitosan/Tannic Acid Hydrogel with Antibacterial, Hemostasis, and Antioxidant Properties Promoting Skin Wound Repair. *ACS Biomaterials Science and Engineering*. https://doi.org/10.1021/acsbiomaterials.2c00997.

[17] Guimarães, I. *et al.* (2021). Polyphenols: A promising avenue in therapeutic solutions for wound care. *Applied Sciences (Switzerland)*. https://doi.org/10.3390/app11031230.

[18] Pintado, M. *et al. Bioproducts for Health II*.

[19] Jacques, M.C. *et al.* (2023). Polyethylene oxide biofilms incorporated into Plantago major extract as dressings for dermal lesion. *Brazilian Journal of Health Review*. https://doi.org/10.34119/bjhrv6n6-230.

[20] Carrasco, S. *et al.* (2024). Enhancing Alginate Hydrogels as Possible Wound-Healing Patches: The Synergistic Impact of Reduced Graphene Oxide and Tannins on Mechanical and Adhesive Properties. *Polymers*. https://doi.org/10.3390/polym16081081.

[21] Gounden, V. and Singh, M. (2024). Hydrogels and Wound Healing: Current and Future Prospects. *Gels*. https://doi.org/10.3390/gels10010043.

[22] Qiao, L. *et al.* (2023). Antibacterial conductive self-healing hydrogel wound dressing with dual dynamic bonds promotes infected wound healing. *Bioactive Materials*. https://doi.org/10.1016/j.bioactmat.2023.07.015.

[23] Tavakoli, S. and Klar, A.S. (2021). Bioengineered Skin Substitutes: Advances and Future Trends. *Applied Sciences*.

[24] Sharma, A. *et al.* (2021). Medicinal plants and their components for wound healing applications. *Future Journal of Pharmaceutical Sciences*. https://doi.org/10.1186/s43094-021-00202-w.

[25] Singer, A.J. (2022). Healing Mechanisms in Cutaneous Wounds: Tipping the Balance. *Tissue Engineering - Part B: Reviews*. https://doi.org/10.1089/ten.teb.2021.0114.

[26] Wilkinson, H.N. and Hardman, M.J. (2023). Wound healing: Cellular mechanisms and pathological outcomes, in *Advances in Surgical and Medical Specialties*, Taylor and Francis, pp. 341–370.

[27] Zlobina, K. *et al.* (2023). Robust classification of wound healing stages in both mice and humans for acute and burn wounds based on transcriptomic data. *BMC Bioinformatics*. https://doi.org/10.1186/s12859-023-05295-z.

[28] Lee, I. *et al.* (2018). Investigation of wound healing process guided by nano-scale topographic patterns integrated within a microfluidic system. *PLoS ONE*. https://doi.org/10.1371/journal.pone.0201418.

[29] Singer, A.J. (2022). Healing Mechanisms in Cutaneous Wounds: Tipping the Balance. *Tissue Engineering - Part B: Reviews*. https://doi.org/10.1089/ten.teb.2021.0114.

[30] Li, J. *et al.* (2023). Procedural Promotion of Multiple Stages in the Wound Healing Process by Graphene-Spiky Silica Heterostructured Nanoparticles. *International Journal of Nanomedicine*. https://doi.org/10.2147/IJN.S426552.

[31] Rodrigues, M. *et al.* (2019). Wound Healing: A Cellular Perspective. *Physiol Rev*. https://doi.org/10.1152/physrev.00067.2017.-Wound.

[32] Rousselle, P. *et al.* (2019). Re-epithelialization of adult skin wounds: Cellular mechanisms and therapeutic strategies. *Advanced Drug Delivery Reviews*. https://doi.org/https://doi.org/10.1016/j.addr.2018.06.019.

[33] Peña, O.A. and Martin, P. (2024). Cellular and molecular mechanisms of skin wound healing. *Nature Reviews Molecular Cell Biology*. https://doi.org/10.1038/s41580-024-00715-1.

[34] Chen, G. *et al.* (2023). Living microecological hydrogels for wound healing. *Science Advances*. https://doi.org/10.1126/sciadv.adg3478.

[35] Asadi, N. *et al.* (2021). Multifunctional hydrogels for wound healing: Special focus on biomacromolecular based hydrogels. *International Journal of Biological Macromolecules*. https://doi.org/https://doi.org/10.1016/j.ijbiomac.2020.12.202.

[36] Patenall, B.L. *et al.* (2024). Kick-Starting Wound Healing: A Review of Pro-Healing Drugs. *International Journal of Molecular Sciences*. https://doi.org/10.3390/ijms25021304.

[37] Luo, R. *et al.* (2021). Accelerated Skin Wound Healing by Electrical Stimulation. *Advanced Healthcare Materials*. https://doi.org/10.1002/adhm.202100557.

[38] Luo, R. *et al.* (2023). Reshaping the Endogenous Electric Field to Boost Wound Repair via Electrogenerative Dressing. *Advanced Materials*. https://doi.org/10.1002/adma.202208395.

[39] Yan, Y. *et al.* (2024). Reconfiguring the endogenous electric field of a wound through a conductive hydrogel for effective exudate management to enhance skin wound healing. *Journal of Materials Chemistry B*. https://doi.org/10.1039/d4tb01349b.

[40] Zhao, M. *et al.* (2022). Bioelectric Signaling: Role of Bioelectricity in Directional Cell Migration in Wound Healing. *Cold Spring Harbor Perspectives in Biology*. https://doi.org/10.1101/cshperspect.a041236.

[41] Nuccitelli, R. (2003). A Role for Endogenous Electric Fields in Wound Healing, in *Current Topics in Developmental Biology*, vol. 58, Academic Press, pp. 1–26.

[42] Korupalli, C. *et al.* (2021). Conductive Materials for Healing Wounds: Their Incorporation in Electroactive Wound Dressings, Characterization, and Perspectives. *Advanced Healthcare Materials*. https://doi.org/10.1002/adhm.202001384.

[43] Yang, J. *et al.* (2022). Bioelectric fields coordinate wound contraction and re-epithelialization process to accelerate wound healing via promoting myofibroblast transformation. *Bioelectrochemistry*. https://doi.org/https://doi.org/10.1016/j.bioelechem.2022.108247.

[44] Kamalov, A. *et al.* (2022). Influence of Electric Field on Proliferation Activity of Human Dermal Fibroblasts. *Journal of Functional Biomaterials*. https://doi.org/10.3390/jfb13030089.

[45] Chen, Y. *et al.* (2021). Optimizing microenvironment by integrating negative pressure and exogenous electric fields: Via a flexible porous conductive dressing to accelerate wound healing. *Biomaterials Science*. https://doi.org/10.1039/d0bm01172j.

[46] Opt Veld, R.C. *et al.* (2020). Design Considerations for Hydrogel Wound Dressings: Strategic and Molecular Advances. *Tissue Engineering - Part B: Reviews*. https://doi.org/10.1089/ten.teb.2019.0281.

[47] Bahram, M. *et al.* (2016). An Introduction to Hydrogels and Some Recent Applications, in *Emerging Concepts in Analysis and Applications of Hydrogels*, InTech.

[48] Liang, Y. *et al.* (2021). Functional Hydrogels as Wound Dressing to Enhance Wound Healing. *ACS Nano*. https://doi.org/10.1021/acsnano.1c04206.

[49] Chen, J. *et al.* (2022). Antibacterial adhesive self-healing hydrogels to promote diabetic wound healing. *Acta Biomaterialia*. https://doi.org/https://doi.org/10.1016/j.actbio.2022.04.041.

[50] Hu, H. and Xu, F.J. (2020). Rational design and latest advances of polysaccharide-based hydrogels for wound healing. *Biomaterials Science*. https://doi.org/10.1039/d0bm00055h.

[51] Rop, K. *et al.* (2019). Biodegradable water hyacinth cellulose-graft-poly(ammonium acrylate-co-acrylic acid) polymer hydrogel for potential agricultural application. *Heliyon*. https://doi.org/10.1016/j.heliyon.2019.e01416.

[52] Zain, G. *et al.* (2018). Superabsorbent hydrogel based on sulfonated-starch for improving water and saline absorbency. *International Journal of Biological Macromolecules*. https://doi.org/https://doi.org/10.1016/j.ijbiomac.2018.04.032.

[53] Luo, M. *et al.* (2022). Multiple Coordination-Derived Bioactive Hydrogel with Proangiogenic Hemostatic Capacity for Wound Repair. *Advanced Healthcare Materials*. https://doi.org/10.1002/adhm.202200722.

[54] Firlar, I. *et al.* (2022). Functional Hydrogels for Treatment of Chronic Wounds. *Gels*. https://doi.org/10.3390/gels8020127.

[55] Katiyar, S. *et al.* (2022). Novel strategies for designing regenerative skin products for accelerated wound healing. *3 Biotech*. https://doi.org/10.1007/s13205-022-03331-y.

[56] Olteanu, G. *et al.* (2024). Advancements in Regenerative Hydrogels in Skin Wound Treatment: A Comprehensive Review. *International Journal of Molecular Sciences*. https://doi.org/10.3390/ijms25073849.

[57] Sharma, S. and Tiwari, S. (2020). A review on biomacromolecular hydrogel classification and its applications. *International Journal of Biological Macromolecules*. https://doi.org/10.1016/J.IJBIOMAC.2020.06.110.

[58] Fletes-Vargas, G. *et al.* (2023). Natural Hydrogels as Wound Dressing for Skin Wound-Healing Applications, in *Interaction of Nanomaterials with Living Cells*, Springer Nature, pp. 439–469.

[59] Guamba, E. *et al.* (2023). Cellulose-based hydrogels towards an antibacterial wound dressing. *Biomaterials Science*. https://doi.org/10.1039/D2BM01369J.

[60] Isobe, N. *et al.* (2018). Cellulose hydrogel with tunable shape and mechanical properties: From rigid cylinder to soft scaffold. *International Journal of Biological Macromolecules*. https://doi.org/https://doi.org/10.1016/j.ijbiomac.2018.05.071.

[61] Yang, Y. *et al.* (2024). Chitosan-based hydrogel dressings with antibacterial and antioxidant for wound healing. *International Journal of Biological Macromolecules*. https://doi.org/https://doi.org/10.1016/j.ijbiomac.2024.135939.

[62] Tan, Y. *et al.* (2024). Sprayable and self-healing chitosan-based hydrogels for promoting healing of infected wound via anti-bacteria, anti-inflammation and angiogenesis. *Carbohydrate Polymers*. https://doi.org/https://doi.org/10.1016/j.carbpol.2024.122147.

[63] Mohammed Kassim. Al-Hussainawy *et al.* (2024). New Synthesis Method of Biopolymer Composites Based on Alginate, Carrageenan and ZnONPS for Wound Healing Applications. *Iraqi Journal of Pharmaceutical Sciences*. https://doi.org/10.31351/vol33iss4pp195-207.

[64] González, L. *et al.* (2024). Innovative Approach to Accelerate Wound Healing: Synthesis and Validation of Enzymatically Cross-Linked COL–rGO Biocomposite Hydrogels. *Gels*. https://doi.org/10.3390/gels10070448.

[65] Peña, B. *et al.* (2018). Injectable Hydrogels for Cardiac Tissue Engineering. *Macromolecular Bioscience*. https://doi.org/10.1002/mabi.201800079.

[66] Khan, F. *et al.* (2022). Synthesis, classification and properties of hydrogels: their applications in drug delivery and agriculture. *Journal of Materials Chemistry B*. https://doi.org/10.1039/D1TB01345A.

[67] Gradinaru, V. *et al.*Hydrogel-Tissue Chemistry: Principles and Applications. https://doi.org/https://doi.org/10.1146/annurev-biophys-070317-032905.

[68] Bustamante-Torres, M. *et al.* (2021). Hydrogels classification according to the physical or chemical interactions and as stimuli-sensitive materials. *Gels*. https://doi.org/10.3390/gels7040182.

[69] Bashir, S. *et al.* (2020). Fundamental concepts of hydrogels: Synthesis, properties, and their applications. *Polymers*. https://doi.org/10.3390/polym12112702.

[70] Benwood, C. *et al.* (2021). Natural biomaterials and their use as bioinks for printing tissues. *Bioengineering*. https://doi.org/10.3390/bioengineering8020027.

[71] Zhang, Y. and Huang, Y. (2021). Rational Design of Smart Hydrogels for Biomedical Applications. *Frontiers in Chemistry*. https://doi.org/10.3389/fchem.2020.615665.

[72] Vasile, C. *et al.* (2020). New developments in medical applications of hybrid hydrogels containing natural polymers. *Molecules*. https://doi.org/10.3390/molecules25071539.

[73] Vijayavenkataraman, S. *et al.* (2019). Conductive collagen/polypyrrole-b-polycaprolactone hydrogel for bioprinting of neural tissue constructs. *International Journal of Bioprinting*. https://doi.org/10.18063/ijb.v5i2.1.229.

[74] Liang, Y. *et al.* (2025). A highly adhesive and melatonin-loaded PEG hydrogel prevents tumor recurrence and promotes wound healing for tumor-resection wound management of liposarcoma. *Materials Today Bio*. https://doi.org/https://doi.org/10.1016/j.mtbio.2025.101842.

[75] Li, Y. *et al.* (2025). A 3R (remove-remodel-repair)-integrated self-assembled Chlorella-gelatin-PEG hydrogel for diabetic wound healing. *Materials Today Bio*. https://doi.org/https://doi.org/10.1016/j.mtbio.2025.101935.

[76] Gu, L. *et al.* (2025). AIE-active PVA/berberine antibacterial hydrogel for wound healing, visual monitoring pH and dehydration. *Biomaterials*. https://doi.org/https://doi.org/10.1016/j.biomaterials.2025.123432.

[77] Abbasi, Y.F. *et al.* (2025). High molecular weight laminarin/AgNPs-impregnated PVA based in situ hydrogels accelerated diabetic wound healing. *Carbohydrate Polymers*. https://doi.org/https://doi.org/10.1016/j.carbpol.2025.123991.

[78] Ashrafi, F. *et al.* (2025). Accelerated healing of full-thickness skin wounds by multifunctional exosome-loaded scaffolds of alginate hydrogel/PCL nanofibers with hemostatic efficacy. *International Journal of Biological Macromolecules*. https://doi.org/https://doi.org/10.1016/j.ijbiomac.2025.142271.

[79] Nazemoroaia, M. *et al.* (2025). Asymmetric natural wound dressing based on porous chitosan-alginate hydrogel/electrospun PCL-silk sericin loaded by 10-HDA for skin wound healing: In vitro and in vivo studies. *International Journal of Pharmaceutics*. https://doi.org/https://doi.org/10.1016/j.ijpharm.2024.124976.

[80] Kamel, A.M. *et al.* (2025). Smart hydrogels for rapid wound repair: Chitosan-PVP matrices empowered by bimetallic MOF nanocages. *International Journal of Biological Macromolecules*. https://doi.org/https://doi.org/10.1016/j.ijbiomac.2024.138672.

[81] Wang, Z. *et al.* (2025). Tannic acid-etched PAN/PVP nanofibers loaded with Cu-MOFs enhance antibacterial efficacy and accelerate wound healing. *Colloids and Surfaces B: Biointerfaces*. https://doi.org/https://doi.org/10.1016/j.colsurfb.2025.114719.

[82] Hozjan, N.A. *et al.* (2025). Oxygen-generating and antibacterial xanthan gum/PLA aerogels loaded with dexamethasone for potential wound healing. *International Journal of Biological Macromolecules*. https://doi.org/https://doi.org/10.1016/j.ijbiomac.2025.143314.

[83] Alharthi, N.S. (2025). Fabrication of curcumin-incorporated poly glycerol sebacate/poly lactide acid (PGS/PLA) hydrogel to enhance full-thickness wound healing in diabetic rats. *Tissue and Cell*. https://doi.org/https://doi.org/10.1016/j.tice.2025.102856.

[84] Mondal, S. *et al.* (2020). A review on recent advances in polymer and peptide hydrogels. *Soft Matter*. https://doi.org/10.1039/C9SM02127B.

[85] Gačanin, J. *et al.* (2020). Biomedical Applications of DNA-Based Hydrogels. *Advanced Functional Materials*. https://doi.org/10.1002/adfm.201906253.

[86] Wang, D. *et al.* (2023). Stimuli-Responsive Self-Degradable DNA Hydrogels: Design, Synthesis, and Applications. *Advanced Healthcare Materials*. https://doi.org/10.1002/adhm.202203031.

[87] Ma, Y. *et al.* (2024). DNA Hydrogels as Functional Materials and Their Biomedical Applications. *Advanced Functional Materials*. https://doi.org/10.1002/adfm.202309070.

[88] Pan, H. *et al.* (2024). Fully Biobased High-Strength and High-Toughness Double Cross-Linked Cellulose Hydrogel for Flexible Electrolytes. *ACS Sustainable Chemistry & Engineering*. https://doi.org/10.1021/acssuschemeng.4c07758.

[89] Lee, J.H. and Kim, H.W. (2018). Emerging properties of hydrogels in tissue engineering. . *Journal of tissue engineering*.

[90] Tian, B. *et al.* (2020). Chemical and physical chitosan hydrogels as prospective carriers for drug delivery: a review. *Journal of Materials Chemistry B*. https://doi.org/10.1039/D0TB01869D.

[91] Li, X. *et al.* (2018). Integrated Functional High-Strength Hydrogels with Metal-Coordination Complexes and H-Bonding Dual Physically Cross-linked Networks. *Macromolecular Rapid Communications*. https://doi.org/10.1002/marc.201800400.

[92] Zhang, Y.S. and Khademhosseini, A. (2017). Advances in engineering hydrogels. *Science (New York, N.Y.)*. https://doi.org/https://doi.org/10.1126/science.aaf3627.

[93] Ye, D. *et al.* (2019). High-Strength and Tough Cellulose Hydrogels Chemically Dual Cross-Linked by Using Low- and High-Molecular-Weight Cross-Linkers. *Biomacromolecules*. https://doi.org/10.1021/acs.biomac.9b00204.

[94] Mitura, S. *et al.* (2020). Biopolymers for hydrogels in cosmetics: review. *Journal of Materials Science: Materials in Medicine*. https://doi.org/10.1007/s10856-020-06390-w.

[95] Hou, Y. *et al.* (2020). Surface Roughness Gradients Reveal Topography-Specific Mechanosensitive Responses in Human Mesenchymal Stem Cells. *Small*. https://doi.org/10.1002/smll.201905422.

[96] Moxon, S.R. *et al.* (2022). Regulation of Mesenchymal Stem Cell Morphology Using Hydrogel Substrates with Tunable Topography and Photoswitchable Stiffness. *Polymers*. https://doi.org/10.3390/polym14245338.

[97] Hosseini, S.A. *et al.* (2025). Hydrogel-based dressing for wound healing: A systematic review of clinical trials. *International Journal of Biological Macromolecules*. https://doi.org/https://doi.org/10.1016/j.ijbiomac.2025.142322.

[98] Shan, Z. *et al.* (2025). Emerging role and potential of lignin in antibacterial hydrogel applications for wound healing: A review. *International Journal of Biological Macromolecules*. https://doi.org/https://doi.org/10.1016/j.ijbiomac.2025.144976.

[99] Deng, H. *et al.* (2025). Biosynthesis of a dual growth factors (GFs) functionalized silk sericin hydrogel to promote chronic wound healing in diabetic mice. *Bioactive Materials*. https://doi.org/https://doi.org/10.1016/j.bioactmat.2025.06.017.

[100] Zhang, Y. *et al.* (2025). Programmable hierarchical hydrogel dressing for sequential release of growth factor and DNase to accelerate diabetic wound healing. *Journal of Controlled Release*. https://doi.org/https://doi.org/10.1016/j.jconrel.2025.113825.

[101] Zhang, S. *et al.* (2025). C-phycocyanin and quaternized chitosan based antibiotic-free hydrogels with antioxidant and antibacterial activity for wound healing. *International Journal of Biological Macromolecules*. https://doi.org/https://doi.org/10.1016/j.ijbiomac.2025.140647.

[102] Tao, Q. *et al.* (2025). Multi-functional bioactive hydrogel based on CCM-Co-ZIF-8 nanoparticles for chronic wound healing: Synergistic antibacterial, antioxidant, and anti-inflammatory therapy. *European Polymer Journal*. https://doi.org/https://doi.org/10.1016/j.eurpolymj.2025.113824.

[103] Lin, J. *et al.* (2025). Effects of a PDGF-stem cell-hydrogel compound on skin wound healing in mice. *Cytotherapy*. https://doi.org/https://doi.org/10.1016/j.jcyt.2025.01.001.

[104] Xing, C. *et al.* (2025). Injectable polypeptide/chitosan hydrogel with loaded stem cells and rapid gelation promoting angiogenesis for diabetic wound healing. *International Journal of Biological Macromolecules*. https://doi.org/https://doi.org/10.1016/j.ijbiomac.2025.141578.

[105] She, Y. *et al.* (2025). Polysaccharides, proteins and DNA based stimulus responsive hydrogels promoting wound healing and repair: A review. *International Journal of Biological Macromolecules*. https://doi.org/https://doi.org/10.1016/j.ijbiomac.2025.140961.

[106] Gao, J. *et al.* (2025). Synthesis of stimuli-responsive copolymeric hydrogels for temperature, reduction and pH-controlled drug delivery. *Journal of Industrial and Engineering Chemistry*. https://doi.org/https://doi.org/10.1016/j.jiec.2024.08.027.

[107] Yang, J. *et al.* (2025). Polyvinyl alcohol/graphene oxide/dextran hydrogel doped copper oxide modified biochar with nano-enzymatic activity and multiple synergistic effects for accelerated diabetic wound healing. *International Journal of Biological Macromolecules*. https://doi.org/https://doi.org/10.1016/j.ijbiomac.2025.144480.

[108] Afruzi, F.H. *et al.* (2025). Metal-organic framework-hydrogel composites as emerging platforms for enhanced wound healing applications: Material design, therapeutic strategies, and future prospects. *Coordination Chemistry Reviews*. https://doi.org/https://doi.org/10.1016/j.ccr.2024.216330.

[109] Xiao, L. *et al.* (2021). A Novel Conductive Antibacterial Nanocomposite Hydrogel Dressing for Healing of Severely Infected Wounds. *Frontiers in Chemistry*. https://doi.org/10.3389/fchem.2021.787886.

[110] Guoyingy, P. *et al.* (2023). Latest Findings on Stimuli-Responsive Hydrogel Wound Dressings Applied in Diabetic Chronic Wound Repair. *Journal of Sichuan University (Medical Science)*. https://doi.org/10.12182/20230760206.

[111] Guo, B. *et al.* (2021). Haemostatic materials for wound healing applications. *Nature Reviews Chemistry*. https://doi.org/10.1038/s41570-021-00323-z.

[112] Zhang, B. *et al.* (2020). Injectable self-healing supramolecular hydrogels with conductivity and photo-thermal antibacterial activity to enhance complete skin regeneration. *Chemical Engineering Journal*. https://doi.org/10.1016/J.CEJ.2020.125994.

[113] Vecin, N.M. and Kirsner, R.S. (2023). Skin substitutes as treatment for chronic wounds: current and future directions. *Frontiers in Medicine*. https://doi.org/10.3389/fmed.2023.1154567.

[114] Mandal, A. *et al.* (2020). Hydrogels in the clinic. *Bioengineering and Translational Medicine*. https://doi.org/10.1002/btm2.10158.

[115] Choi, S.W. *et al.* (2021). Basic principles of hydrogel-based tissue transformation technologies and their applications. *Cell*. https://doi.org/10.1016/j.cell.2021.07.009.

[116] Zhao, Y. *et al.* (2023). Chitosan derivative-based mussel-inspired hydrogels used as dressings for infectious wound healing. *European Polymer Journal*. https://doi.org/10.1016/j.eurpolymj.2023.112315.

[117] Cuéllar-Gaona, C.G. *et al.* (2021). Obtención de hidrogeles de quitosano/Rosmarinus officinalis modificados con plasma. *Pädi Boletín Científico de Ciencias Básicas e Ingenierías del ICBI*. https://doi.org/10.29057/icbi.v9iespecial2.8002.

[118] Abbas, M. *et al.* (2019). Wound healing potential of curcumin cross-linked chitosan/polyvinyl alcohol. *International journal of biological macromolecules*. https://doi.org/10.1016/j.ijbiomac.2019.08.153.

[119] Bagher, Z. *et al.* (2020). Wound healing with alginate/chitosan hydrogel containing hesperidin in rat model. *Journal of Drug Delivery Science and Technology*. https://doi.org/10.1016/J.JDDST.2019.101379.

[120] Zidan, T.A. *et al.* (2020). N-Aminorhodanine modified chitosan hydrogel for antibacterial and copper ions removal from aqueous solutions. *International Journal of Biological Macromolecules*. https://doi.org/10.1016/J.IJBIOMAC.2020.04.180.

[121] Chenite, A. *et al.* (2000). Novel injectable neutral solutions of chitosan form biodegradable gels in situ. *Biomaterials*. https://doi.org/10.1016/S0142-9612(00)00116-2.

[122] Li, A. *et al.* (2024). Chitosan-based injectable hydrogel with multifunction for wound healing: A critical review. *Carbohydrate polymers*. https://doi.org/10.1016/j.carbpol.2024.121952.

[123] Matica, M. *et al.* (2019). Chitosan as a Wound Dressing Starting Material: Antimicrobial Properties and Mode of Action. *International Journal of Molecular Sciences*. https://doi.org/10.3390/ijms20235889.

[124] Guo, W. *et al.* (2024). Self-adhesive and self-healing hydrogel dressings based on quaternary ammonium chitosan and host-guest interacted silk fibroin. *Colloids and Surfaces A: Physicochemical and Engineering Aspects*. https://doi.org/10.1016/j.colsurfa.2024.133145.

[125] Bai, Q. *et al.* (2023). Chitosan and hyaluronic-based hydrogels could promote the infected wound healing. *International journal of biological macromolecules*. https://doi.org/10.1016/j.ijbiomac.2023.123271.

[126] López, H. (2022). "Síntesis y aplicación de un nanocompósito de quitosano-glicidil metacrilato-colágeno tipo I y nanopartículas de oro sobre la cicatrización de heridas cutáneas."

[127] Yuan, N. *et al.* (2023). Chitosan, alginate, hyaluronic acid and other novel multifunctional hydrogel dressings for wound healing: A review. *International Journal of Biological Macromolecules*. https://doi.org/https://doi.org/10.1016/j.ijbiomac.2023.124321.

[128] Li, A. *et al.* (2024). Chitosan-based injectable hydrogel with multifunction for wound healing: A critical review. *Carbohydrate Polymers*. https://doi.org/https://doi.org/10.1016/j.carbpol.2024.121952.

[129] Bellier, N. *et al.* (2022). Recent biomedical advancements in graphene oxide- and reduced graphene oxide-based nanocomposite nanocarriers. *Biomaterials Research*. https://doi.org/10.1186/s40824-022-00313-2.

[130] Ghawanmeh, A.A. *et al.* (2019). Graphene oxide-based hydrogels as a nanocarrier for anticancer drug delivery. *Nano Research*. https://doi.org/10.1007/s12274-019-2300-4.

[131] Chiticaru, E.A. and Ionita, M. (2022). Graphene toxicity and future perspectives in healthcare and biomedicine. *FlatChem*. https://doi.org/https://doi.org/10.1016/j.flatc.2022.100417.

[132] Cebadero-Domínguez, O. *et al.* (2022). In vitro toxicity evaluation of graphene oxide and reduced graphene oxide on Caco-2 cells. *Toxicology Reports*. https://doi.org/https://doi.org/10.1016/j.toxrep.2022.05.010.

[133] Mohammed, H. *et al.* (2020). Antimicrobial Mechanisms and Effectiveness of Graphene and Graphene-Functionalized Biomaterials. A Scope Review. *Frontiers in Bioengineering and Biotechnology*. https://doi.org/10.3389/fbioe.2020.00465.

[134] Shariati, A. *et al.* (2023). Graphene-Based Materials for Inhibition of Wound Infection and Accelerating Wound Healing. *Biomedicine & Pharmacotherapy*. https://doi.org/https://doi.org/10.1016/j.biopha.2022.114184.

[135] Guo, B. and Ma, P.X. (2018). Conducting Polymers for Tissue Engineering. *Biomacromolecules*. https://doi.org/10.1021/acs.biomac.8b00276.

[136] Liao, C. *et al.* (2018). Graphene nanomaterials: Synthesis, biocompatibility, and cytotoxicity. *International Journal of Molecular Sciences*. https://doi.org/10.3390/ijms19113564.

[137] Bai, R.G. and Tuvikene, R. (2021). Chapter 12 - Biomedical applications of graphene, in *Handbook of Carbon-Based Nanomaterials* (eds.Thomas, S. *et al.*), Elsevier, pp. 551–571.

[138] Hummers, W.S.Jr. and Offeman, R.E. (1958). Preparation of Graphitic Oxide. *Journal of the American Chemical Society*. https://doi.org/10.1021/ja01539a017.

[139] Marcano, D.C. *et al.* (2010). Improved Synthesis of Graphene Oxide. *ACS Nano*. https://doi.org/10.1021/nn1006368.

[140] Qun Xu, L. *et al.* (2010). Dopamine-Induced Reduction and Functionalization of Graphene Oxide Nanosheets. *Macromolecules*. https://doi.org/10.1021/ma101526k.

[141] Almoshari, Y. *et al.* (2020). GSK3 inhibitor-loaded osteotropic Pluronic hydrogel effectively mitigates periodontal tissue damage associated with experimental periodontitis. *Biomaterials*. https://doi.org/10.1016/J.BIOMATERIALS.2020.120293.

[142] Rahdar, A. *et al.* (2018). Pluronic as nano-carier platform for drug delivery systems. *Nanomedicine Research Journal*. https://doi.org/10.22034/NMRJ.2018.04.001.

[143] Alexandridis, P. and Alan Hatton, T. (1995). Poly(ethylene oxide)□poly(propylene oxide)□poly(ethylene oxide) block copolymer surfactants in aqueous solutions and at interfaces: thermodynamics, structure, dynamics, and modeling. *Colloids and Surfaces A: Physicochemical and Engineering Aspects*. https://doi.org/https://doi.org/10.1016/0927-7757(94)03028-X.

[144] Li, S. *et al.* (2023). Progress in Pluronic F127 Derivatives for Application in Wound Healing and Repair. *International Journal of Nanomedicine*. https://doi.org/10.2147/IJN.S418534.

[145] Chen, Y. *et al.* (2025). Preparation of antibacterial tellurium nanorod-incorporated thermosensitive pluronic F-127 hydrogels for wound healing applications. *Journal of Drug Delivery Science and Technology*. https://doi.org/https://doi.org/10.1016/j.jddst.2025.107107.

[146] Kumari, P. *et al.* (2024). Formulation, characterization, in vitro and in vivo evaluation of thermoresponsive lawsone-based Pluronic F-127 nanogels for wound healing. *Journal of Drug Delivery Science and Technology*. https://doi.org/https://doi.org/10.1016/j.jddst.2024.105451.

[147] Dumortier, G. *et al.* (2006). A review of poloxamer 407 pharmaceutical and pharmacological characteristics. *Pharmaceutical Research*. https://doi.org/10.1007/s11095-006-9104-4.

[148] Luo, F. *et al.* (2017). Green reduction of graphene oxide by polydopamine to a construct flexible film: superior flame retardancy and high thermal conductivity. *Journal of Materials Chemistry A*. https://doi.org/10.1039/C7TA04740A.

[149] Liu, Y. *et al.* (2019). A highly sensitive and selective electrochemical sensor based on polydopamine functionalized graphene and molecularly imprinted polymer for the 2,4-dichlorophenol recognition and detection. *Talanta*. https://doi.org/10.1016/j.talanta.2018.11.052.

[150] Malli, S. *et al.* (2017). In situ forming pluronic® F127/chitosan hydrogel limits metronidazole transmucosal absorption. *European Journal of Pharmaceutics and Biopharmaceutics*. https://doi.org/https://doi.org/10.1016/j.ejpb.2016.11.024.

[151] Pelegrino, M.T. *et al.* (2018). Biocompatible and Antibacterial Nitric Oxide-Releasing Pluronic F-127/Chitosan Hydrogel for Topical Applications. *Polymers*. https://doi.org/10.3390/polym10040452.

[152] Luo, R. *et al.* (2021). Accelerated Skin Wound Healing by Electrical Stimulation. *Advanced Healthcare Materials*. https://doi.org/10.1002/adhm.202100557.

[153] Fernández, K. *et al.* (2023). Self-Assembled CNF/rGO/Tannin Composite: Study of the Physicochemical and Wound Healing Properties. *Polymers*. https://doi.org/10.3390/polym15122752.

[154] Ruiz, I. *et al.* (2024). Inclusion of Reduced Graphene Oxide to Silk Fibroin Hydrogels Improve the Conductive, Swelling and Wound Healing Capacity. *ChemistrySelect*. https://doi.org/10.1002/slct.202402444.

[155] Safarzadeh Kozani, P. *et al.* (2022). Polysaccharide-based hydrogels: properties, advantages, challenges, and optimization methods for applications in regenerative medicine. *International Journal of Polymeric Materials and Polymeric Biomaterials*. https://doi.org/10.1080/00914037.2021.1962876.

[156] Lu, H. *et al.* (2019). Electroconductive hydrogels for biomedical applications. *Wiley Interdisciplinary Reviews: Nanomedicine and Nanobiotechnology*. https://doi.org/10.1002/wnan.1568.

[157] Fathi, A. *et al.* (2024). Thermoresponsive in situ forming and self-healing double-network hydrogels as injectable dressings for silymarin/levofloxacin delivery for treatment of third-degree burn wounds. *Carbohydrate Polymers*. https://doi.org/10.1016/j.carbpol.2024.121856.

[158] Feng, P. *et al.* (2021). Chitosan-Based Functional Materials for Skin Wound Repair: Mechanisms and Applications. *Frontiers in Bioengineering and Biotechnology*.

[159] Rajinikanth B, S. *et al.* (2024). Chitosan-Based Biomaterial in Wound Healing: A Review. *Cureus*. https://doi.org/10.7759/cureus.55193.

[160] Gegel', N.O. *et al.* (2022). Influence of Chitosan on Orientation–Micellar Ordering of the Pluronic F-127 Gel Phase in an Aqueous Medium. *Optics and Spectroscopy*. https://doi.org/10.1134/S0030400X22040051.

[161] Mattevi, C. *et al.* (2009). Evolution of electrical, chemical, and structural properties of transparent and conducting chemically derived graphene thin films. *Advanced Functional Materials*. https://doi.org/10.1002/adfm.200900166.

[162] Emmanuel Ibukun, A. *et al.* (2024). Recent developments in synthesis and characterisation of graphene oxide modified with deep eutectic solvents for dispersive and magnetic solid-phase extractions. *Microchemical Journal*. https://doi.org/10.1016/j.microc.2024.110111.

[163] Abdillah, O.B. *et al.* (2023). Recent progress on reduced graphene oxide and polypyrrole composites for high performance supercapacitors: A review. *Journal of Energy Storage*. https://doi.org/10.1016/j.est.2023.109300.

[164] AL-Salman, H.N.K. *et al.* (2023). Graphene oxide-based biosensors for detection of lung cancer: A review. *Results in Chemistry*. https://doi.org/10.1016/j.rechem.2023.101300.

[165] Xu, L.Q. *et al.* (2010). Dopamine-Induced Reduction and Functionalization of Graphene Oxide Nanosheets. *Macromolecules*. https://doi.org/10.1021/ma101526k.

[166] Liang, Y. *et al.* (2019). Adhesive Hemostatic Conducting Injectable Composite Hydrogels with Sustained Drug Release and Photothermal Antibacterial Activity to Promote Full-Thickness Skin Regeneration During Wound Healing. *Small*. https://doi.org/10.1002/smll.201900046.

[167] Nowroozi, N. *et al.* (2021). Biological and structural properties of graphene oxide/curcumin nanocomposite incorporated chitosan as a scaffold for wound healing application. *Life Sciences*. https://doi.org/https://doi.org/10.1016/j.lfs.2020.118640.

[168] Elhami, N. *et al.* (2024). Development of nanocomposites based on chitosan/reduced graphene oxide for wound healing application. *International Journal of Biological Macromolecules*. https://doi.org/https://doi.org/10.1016/j.ijbiomac.2023.128832.

[169] Zheng, F. *et al.* (2020). The electrostimulation and scar inhibition effect of chitosan/oxidized hydroxyethyl cellulose/reduced graphene oxide/asiaticoside liposome based hydrogel on peripheral nerve regeneration in vitro. *Materials Science and Engineering C*. https://doi.org/10.1016/j.msec.2019.110560.

[170] Camana, G. *et al.* (2023). Design of Functional Pluronic-Based Precursors for Tailoring Hydrogel Thermoresponsiveness and Cell-Adhesive Properties. *Materials*. https://doi.org/10.3390/ma16072749.

[171] García-Couce, J. *et al.* (2022). Chitosan/Pluronic F127 Thermosensitive Hydrogel as an Injectable Dexamethasone Delivery Carrier. *Gels*. https://doi.org/10.3390/gels8010044.

[172] Saravanan, S. *et al.* (2018). Chitosan based thermoresponsive hydrogel containing graphene oxide for bone tissue repair. *Biomedicine & Pharmacotherapy*. https://doi.org/10.1016/J.BIOPHA.2018.08.072.

[173] Saravanan, S. *et al.* (2013). Chitosan scaffolds containing chicken feather keratin nanoparticles for bone tissue engineering. *International Journal of Biological Macromolecules*. https://doi.org/10.1016/J.IJBIOMAC.2013.09.034.

[174] Saravanan, S. *et al.* (2019). A review on injectable chitosan/beta glycerophosphate hydrogels for bone tissue regeneration. *International Journal of Biological Macromolecules*. https://doi.org/10.1016/J.IJBIOMAC.2018.10.014.

[175] Wei, J. *et al.* (2021). Bioinspired 3D Printable, Self-Healable, and Stretchable Hydrogels with Multiple Conductivities for Skin-like Wearable Strain Sensors. *ACS Applied Materials & Interfaces*. https://doi.org/10.1021/acsami.0c19512.

[176] Kokubo, T. *et al.* (1990). Soluciones capaces de reproducir cambios en la estructura de la superficie en vivo en vitrocerámica bioactiva A-W3. *Revista de investigación de materiales biomédicos*.

[177] Schuhladen, K. *et al.* (2021). Production of a novel poly(ε-caprolactone)-methylcellulose electrospun wound dressing by incorporating bioactive glass and Manuka honey. *Journal of Biomedical Materials Research - Part B Applied Biomaterials*. https://doi.org/10.1002/jbm.b.34690.

[178] Leyva-Gómez, G. *et al.* (2017). A novel hydrogel of poloxamer 407 and chitosan obtained by gamma irradiation exhibits physicochemical properties for wound management. *Materials Science and Engineering: C*. https://doi.org/https://doi.org/10.1016/j.msec.2016.12.127.

[179] Wang, X. *et al.* (2021). Photothermally triggered biomimetic drug delivery of Teriparatide via reduced graphene oxide loaded chitosan hydrogel for osteoporotic bone regeneration. *Chemical Engineering Journal*. https://doi.org/https://doi.org/10.1016/j.cej.2020.127413.

[180] Cao, N. *et al.* (2017). Facile synthesis of fluorinated polydopamine/chitosan/reduced graphene oxide composite aerogel for efficient oil/water separation. *Chemical Engineering Journal*. https://doi.org/https://doi.org/10.1016/j.cej.2017.05.117.

[181] Salimiyan, N. *et al.* (2023). Preparation of degradable, biocompatible, conductive and multifunctional chitosan/thiol-functionalized graphene nanocomposite hydrogel via click chemistry for human motion sensing. *Chemical Engineering Journal*. https://doi.org/https://doi.org/10.1016/j.cej.2023.144648.

[182] Figueroa, T. *et al.* (2020). Design and characterization of chitosan-graphene oxide nanocomposites for the delivery of proanthocyanidins. *International Journal of Nanomedicine*. https://doi.org/10.2147/IJN.S240305.

[183] Ahmed, J. *et al.* (2020). Rheological and Dielectric Behavior of 3D-Printable Chitosan/Graphene Oxide Hydrogels. *ACS Biomaterials Science & Engineering*. https://doi.org/10.1021/acsbiomaterials.9b00201.

[184] Tang, Y. *et al.* (2024). A mild one-step method to fabricate graphene oxide cross-linked with dopamine/polyethyleneimine (GO@DA/PEI) composite membranes with an ultrahigh flux for heavy metal ion removal. *Separation and Purification Technology*. https://doi.org/https://doi.org/10.1016/j.seppur.2024.126618.

[185] Kaminska, I. *et al.* (2012). Reduction and Functionalization of Graphene Oxide Sheets Using Biomimetic Dopamine Derivatives in One Step. *ACS Applied Materials & Interfaces*. https://doi.org/10.1021/am201664n.

[186] Luo, F. *et al.* (2017). Green reduction of graphene oxide by polydopamine to a construct flexible film: superior flame retardancy and high thermal conductivity. *Journal of Materials Chemistry A*. https://doi.org/10.1039/C7TA04740A.

[187] AL-Rajabi, M.M. and Teow, Y.H. (2023). Synthesis of thermoresponsive composite hydrogel from Pluronic F127 reinforced by oil palm empty fruit bunches-extracted cellulose for silver sulfadiazine drug delivery. *Sustainable Chemistry and Pharmacy*. https://doi.org/https://doi.org/10.1016/j.scp.2022.100939.

[188] Wu, T.-Y. *et al.* (2024). Mucin-mediated mucosal retention via end-terminal modified Pluronic F127-based hydrogel to increase drug accumulation in the lungs. *Biomaterials Advances*. https://doi.org/https://doi.org/10.1016/j.bioadv.2023.213722.

[189] Dang, Q. *et al.* (2019). Decanoic acid functionalized chitosan: Synthesis, characterization, and evaluation as potential wound dressing material. *International Journal of Biological Macromolecules*. https://doi.org/https://doi.org/10.1016/j.ijbiomac.2019.08.083.

[190] Ji, C.-C. *et al.* (2013). Self-assembly of three-dimensional interconnected graphene-based aerogels and its application in supercapacitors. *Journal of Colloid and Interface Science*. https://doi.org/https://doi.org/10.1016/j.jcis.2013.06.054.

[191] Cao, N. *et al.* (2017). Facile synthesis of fluorinated polydopamine/chitosan/reduced graphene oxide composite aerogel for efficient oil/water separation. *Chemical Engineering Journal*. https://doi.org/https://doi.org/10.1016/j.cej.2017.05.117.

[192] Suhail, M. *et al.* (2023). Xanthan-Gum/Pluronic-F-127-Based-Drug-Loaded Polymeric Hydrogels Synthesized by Free Radical Polymerization Technique for Management of Attention-Deficit/Hyperactivity Disorder. *Gels*. https://doi.org/10.3390/gels9080640.

[193] Mansoor, S. *et al.* (2023). A Closed Loop Stimuli-Responsive Concanavalin A-Loaded Chitosan–Pluronic Hydrogel for Glucose-Responsive Delivery of Short-Acting Insulin Prototyped in RIN-5F Pancreatic Cells. *Biomedicines*. https://doi.org/10.3390/biomedicines11092545.

[194] Wang, Y. *et al.* (2023). Agarose hydrogel doped with soluble Se-chitosan for Se-enriched cultivation of sprouts. *Advanced Agrochem*. https://doi.org/https://doi.org/10.1016/j.aac.2023.09.001.

[195] Nasir, N. *et al.*pH-responsive smart gels of block copolymer [pluronic F127-co-poly(acrylic acid)] for controlled delivery of Ivabradine hydrochloride: its toxicological evaluation. https://doi.org/10.1007/s10965-019-1872-8/Published.

[196] Naeem, S. *et al.* (2022). Fabrication of pH responsive hydrogel blends of chondroitin sulfate/pluronic F-127 for the controlled release of ketorolac: its characterization and acute oral toxicity study. *Drug Development and Industrial Pharmacy*. https://doi.org/10.1080/03639045.2022.2150773.

[197] Suneetha, M. *et al.* (2023). Antibacterial, biocompatible, hemostatic, and tissue adhesive hydrogels based on fungal-derived carboxymethyl chitosan-reduced graphene oxide-polydopamine for wound healing applications. *International Journal of Biological Macromolecules*. https://doi.org/10.1016/J.IJBIOMAC.2023.124641.

[198] Vandenhaute, M. *et al.* (2014). Cross-linkable, thermo-responsive Pluronic® building blocks for biomedical applications: Synthesis and physico-chemical evaluation. *European Polymer Journal*. https://doi.org/https://doi.org/10.1016/j.eurpolymj.2014.01.016.

[199] Oliveira, S.M. *et al.* (2014). Cell interactions with superhydrophilic and superhydrophobic surfaces. *Journal of Adhesion Science and Technology*. https://doi.org/10.1080/01694243.2012.697776.

[200] Graça, M.F.P. *et al.* (2023). Reduced graphene oxide-enriched chitosan hydrogel/cellulose acetate-based nanofibers application in mild hyperthermia and skin regeneration. *International Journal of Biological Macromolecules*. https://doi.org/10.1016/J.IJBIOMAC.2022.12.291.

[201] Wu, B. *et al.* (2018). Pluronic F127 blended polycaprolactone scaffolds via e-jetting for esophageal tissue engineering. *Journal of Materials Science: Materials in Medicine*. https://doi.org/10.1007/s10856-018-6148-z.

[202] Peters, M.J. *et al.* (2001). Estimation of the electrical conductivity of human tissue. *Electromagnetics*. https://doi.org/10.1080/027263401752246199.

[203] Zhao, X. *et al.* (2017). Antibacterial anti-oxidant electroactive injectable hydrogel as self-healing wound dressing with hemostasis and adhesiveness for cutaneous wound healing. *Biomaterials*. https://doi.org/10.1016/J.BIOMATERIALS.2017.01.011.

[204] Li, M. *et al.* (2020). Toward Controlled Electrical Stimulation for Wound Healing Based on a Precision Layered Skin Model. *ACS Applied Bio Materials*. https://doi.org/10.1021/acsabm.0c01190.

[205] Babaluei, M. *et al.* (2023). Injectable hydrogel based on silk fibroin/carboxymethyl cellulose/agarose containing polydopamine functionalized graphene oxide with conductivity, hemostasis, antibacterial, and anti-oxidant properties for full-thickness burn healing. *International Journal of Biological Macromolecules*. https://doi.org/10.1016/j.ijbiomac.2023.126051.

[206] Jing, X. *et al.* (2017). Mussel-inspired electroactive chitosan/graphene oxide composite hydrogel with rapid self-healing and recovery behavior for tissue engineering. *Carbon*. https://doi.org/10.1016/J.CARBON.2017.09.071.

[207] Liang, Y. *et al.* (2020). Injectable Antimicrobial Conductive Hydrogels for Wound Disinfection and Infectious Wound Healing. *Biomacromolecules*. https://doi.org/10.1021/acs.biomac.9b01732.

[208] Ulutürk, C. and Alemdar, N. (2019). Production of reduced graphene oxide-based electrically conductive hydrogel by using modified chitosan. *Journal of Applied Polymer Science*. https://doi.org/10.1002/app.48008.

[209] Xiong, D. *et al.* (2015). Oxygen-containing Functional Groups Enhancing Electrochemical Performance of Porous Reduced Graphene Oxide Cathode in Lithium Ion Batteries. *ACS nano*. https://doi.org/https://doi.org/10.1016/j.electacta.2015.06.041.

[210] Wang, J. *et al.* (2015). Facile self-assembly of magnetite nanoparticles on three-dimensional graphene oxide–chitosan composite for lipase immobilization. *Biochemical Engineering Journal*. https://doi.org/https://doi.org/10.1016/j.bej.2014.11.013.

[211] Escalona-Rayo, C.F. *et al.* (2020). Optimization of Unidirectional Mucoadhesive Buccal Patches Based on Chitosan and Pluronic® F-127 for Metoprolol Controlled Release: In Vitro and Ex Vivo Evaluations. *Journal of Pharmaceutical Innovation*. https://doi.org/10.1007/s12247-019-09401-8.

[212] Yavari, N. and Azizian, S. (2022). Mixed diffusion and relaxation kinetics model for hydrogels swelling. *Journal of Molecular Liquids*. https://doi.org/10.1016/J.MOLLIQ.2022.119861.

[213] Kosowska, K. *et al.* (2019). Synthesis and characterization of chitosan/reduced graphene oxide hybrid composites. *Materials*. https://doi.org/10.3390/ma12132077.

[214] Rokhade, A. *et al.* (2007). Novel hydrogel microspheres of chitosan and pluronic F-127 for controlled release of 5-fluorouracil. *Journal of Microencapsulation*. https://doi.org/10.1080/02652040701281365.

[215] Song, Y. *et al.* (2024). A chitosan-based conductive double network hydrogel doped by tannic acid-reduced graphene oxide with excellent stretchability and high sensitivity for wearable strain sensors. *International Journal of Biological Macromolecules*. https://doi.org/https://doi.org/10.1016/j.ijbiomac.2023.128861.

[216] Scanga, V.I. *et al.* (2010). Biomaterials for neural-tissue engineering - Chitosan supports the survival, migration, and differentiation of adult-derived neural stem and progenitor cells. *Canadian Journal of Chemistry*. https://doi.org/10.1139/V09-171.

[217] Kwon, J.S. *et al.* (2012). Chitosan-based hydrogels to induce neuronal differentiation of rat muscle-derived stem cells. *International Journal of Biological Macromolecules*. https://doi.org/https://doi.org/10.1016/j.ijbiomac.2012.08.007.

[218] Wang, Y. *et al.* (2017). Conductive graphene oxide hydrogels reduced and bridged by l-cysteine to support cell adhesion and growth. *Journal of Materials Chemistry B*. https://doi.org/10.1039/c6tb02333a.

[219] Sayyar, S. *et al.* (2015). Processable conducting graphene/chitosan hydrogels for tissue engineering. *Journal of Materials Chemistry B*. https://doi.org/10.1039/c4tb01636j.

[220] Guo, S. *et al.* (2022). Injectable Self-Healing Adhesive Chitosan Hydrogel with Antioxidative, Antibacterial, and Hemostatic Activities for Rapid Hemostasis and Skin Wound Healing. *ACS Applied Materials & Interfaces*. https://doi.org/10.1021/acsami.2c08870.

[221] Masood, N. *et al.* (2019). Silver nanoparticle impregnated chitosan-PEG hydrogel enhances wound healing in diabetes induced rabbits. *International Journal of Pharmaceutics*. https://doi.org/10.1016/J.IJPHARM.2019.01.019.

[222] Omran, B. and Baek, K.H. (2022). Graphene-derived antibacterial nanocomposites for water disinfection: Current and future perspectives. *Environmental Pollution*. https://doi.org/10.1016/J.ENVPOL.2022.118836.

[223] Yaragalla, S. *et al.* (2021). A review on graphene based materials and their antimicrobial properties. *Coatings*. https://doi.org/10.3390/coatings11101197.

[224] Sengupta, I. *et al.* (2019). Bactericidal effect of graphene oxide and reduced graphene oxide: Influence of shape of bacteria. *Colloid and Interface Science Communications*. https://doi.org/10.1016/J.COLCOM.2018.12.001.

[225] Akhavan, O. and Ghaderi, E. (2010). Toxicity of Graphene and Graphene Oxide Nanowalls Against Bacteria. *ACS Nano*. https://doi.org/10.1021/nn101390x.

[226] Suneetha, M. *et al.* (2023). Antibacterial, biocompatible, hemostatic, and tissue adhesive hydrogels based on fungal-derived carboxymethyl chitosan-reduced graphene oxide-polydopamine for wound healing applications. *International Journal of Biological Macromolecules*. https://doi.org/10.1016/J.IJBIOMAC.2023.124641.

[227] Xiong, S. *et al.* (2023). Polyvinyl-alcohol, chitosan and graphene-oxide composed conductive hydrogel for electrically controlled fluorescein sodium transdermal release. *Carbohydrate Polymers*. https://doi.org/10.1016/J.CARBPOL.2023.121172.

[228] Hosseini, S. *et al.* (2023). Self-healing nanocomposite hydrogels based on chitosan/ modified polyethylene glycol/graphene. *Materials Today Communications*. https://doi.org/10.1016/J.MTCOMM.2023.107417.

[229] Qureshi, M.A. ur R. *et al.* (2023). Graphene oxide reinforced biopolymeric (chitosan) hydrogels for controlled cephradine release. *International Journal of Biological Macromolecules*. https://doi.org/10.1016/J.IJBIOMAC.2023.124948.

[230] Gegel, N.O. *et al.* (2022). Thermosensitive Chitosan-Containing Hydrogels: Their Formation, Properties, Antibacterial Activity, and Veterinary Usage. *Gels*. https://doi.org/10.3390/gels8020093.

[231] Morsi, R.E. *et al.* (2023). Cellulose acetate membranes loaded with combinations of tetraphenylporphyrin, graphene oxide and Pluronic F-127 as responsive materials with antibacterial photodynamic activity. *RSC Advances*. https://doi.org/10.1039/d3ra04193j.

[232] Qu, J. *et al.* (2018). Antibacterial adhesive injectable hydrogels with rapid self-healing, extensibility and compressibility as wound dressing for joints skin wound healing. *Biomaterials*. https://doi.org/https://doi.org/10.1016/j.biomaterials.2018.08.044.

[233] Yap, L.-S. and Yang, M.-C. (2016). Evaluation of hydrogel composing of Pluronic F127 and carboxymethyl hexanoyl chitosan as injectable scaffold for tissue engineering applications. *Colloids and Surfaces B: Biointerfaces*. https://doi.org/https://doi.org/10.1016/j.colsurfb.2016.05.094.

[234] Lima-Sousa, R. *et al.* (2021). Poly(2-ethyl-2-oxazoline) functionalized reduced graphene oxide: Optimization of the reduction process using dopamine and application in cancer photothermal therapy. *Materials Science and Engineering: C*. https://doi.org/https://doi.org/10.1016/j.msec.2021.112468.

[235] Kosowska, K. *et al.* (2020). Gradient chitosan hydrogels modified with graphene derivatives and hydroxyapatite: Physiochemical properties and initial cytocompatibility evaluation. *International Journal of Molecular Sciences*. https://doi.org/10.3390/ijms21144888.

[236] Thangavel, P. *et al.* (2018). Development of reduced graphene oxide (rGO)-isabgol nanocomposite dressings for enhanced vascularization and accelerated wound healing in normal and diabetic rats. *Journal of Colloid and Interface Science*. https://doi.org/https://doi.org/10.1016/j.jcis.2018.01.110.

[237] Esmaeili, E. *et al.* (2020). The biomedical potential of cellulose acetate/polyurethane nanofibrous mats containing reduced graphene oxide/silver nanocomposites and curcumin: Antimicrobial performance and cutaneous wound healing. *International Journal of Biological Macromolecules*. https://doi.org/https://doi.org/10.1016/j.ijbiomac.2020.02.295.

[238] Cifuentes, J. *et al.* (2022). Reduced Graphene Oxide-Extracellular Matrix Scaffolds as a Multifunctional and Highly Biocompatible Nanocomposite for Wound Healing: Insights into Characterization and Electroconductive Potential. *Nanomaterials*. https://doi.org/10.3390/nano12162857.

[239] Fu, J. *et al.* (2019). Reduced Graphene Oxide Incorporated Acellular Dermal Composite Scaffold Enables Efficient Local Delivery of Mesenchymal Stem Cells for Accelerating Diabetic Wound Healing. *ACS Biomaterials Science & Engineering*. https://doi.org/10.1021/acsbiomaterials.9b00485.

[240] Van De Vyver, M. *et al.* (2021). Histology Scoring System for Murine Cutaneous Wounds. *Stem Cells and Development*. https://doi.org/10.1089/scd.2021.0124.

[241] Zhang, J.-Y. *et al.* (2022). Recent advances in electrocatalytic oxygen reduction for on-site hydrogen peroxide synthesis in acidic media. *Journal of Energy Chemistry*. https://doi.org/https://doi.org/10.1016/j.jechem.2021.10.013.

[242] Deng, X. *et al.* (2022). A review of current advancements for wound healing: Biomaterial applications and medical devices. *Journal of Biomedical Materials Research - Part B Applied Biomaterials*. https://doi.org/10.1002/jbm.b.35086.

[243] Jabeen, S. *et al.* (2019). Partial thickness wound: Does mechanism of injury influence healing? *Burns*. https://doi.org/https://doi.org/10.1016/j.burns.2018.08.010.

[244] Park, S.J. *et al.* (2018). Substance-P and transforming growth factor-β in chitosan microparticle-pluronic hydrogel accelerates regenerative wound repair of skin injury by local ionizing radiation. *Journal of Tissue Engineering and Regenerative Medicine*. https://doi.org/10.1002/term.2445.

[245] Liang, Y. *et al.* (2021). Functional Hydrogels as Wound Dressing to Enhance Wound Healing. *ACS Nano*. https://doi.org/10.1021/acsnano.1c04206.

[246] Xiang, J. *et al.* (2020). Status and future scope of hydrogels in wound healing: Synthesis, materials and evaluation. *European Polymer Journal*. https://doi.org/10.1016/j.eurpolymj.2020.109609.

[247] Yang, Z. *et al.* (2021). Highly Stretchable, Adhesive, Biocompatible, and Antibacterial Hydrogel Dressings for Wound Healing. *Advanced Science*. https://doi.org/10.1002/advs.202003627.

[248] Bano, I. *et al.* (2017). Chitosan: A potential biopolymer for wound management. *International journal of biological macromolecules*. https://doi.org/10.1016/j.ijbiomac.2017.04.047.

[249] Moeini, A. *et al.* (2020). Wound healing and antimicrobial effect of active secondary metabolites in chitosan-based wound dressings: A review. *Carbohydrate polymers*. https://doi.org/10.1016/j.carbpol.2020.115839.

[250] Liu, H. *et al.* (2018). A functional chitosan-based hydrogel as a wound dressing and drug delivery system in the treatment of wound healing. *RSC Advances*. https://doi.org/10.1039/c7ra13510f.

[251] Gutha, Y. *et al.* (2017). Antibacterial and wound healing properties of chitosan/poly(vinyl alcohol)/zinc oxide beads (CS/PVA/ZnO). *International journal of biological macromolecules*. https://doi.org/10.1016/j.ijbiomac.2017.05.020.

[252] Dumont, M. *et al.* (2018). Processing and antibacterial properties of chitosan-coated alginate fibers. *Carbohydrate Polymers*. https://doi.org/https://doi.org/10.1016/j.carbpol.2017.11.088.

[253] Chiticaru, E.A. and Ionita, M. (2022). Graphene toxicity and future perspectives in healthcare and biomedicine. *FlatChem*. https://doi.org/https://doi.org/10.1016/j.flatc.2022.100417.

[254] Graça, M. *et al.* (2022). Reduced graphene oxide-enriched chitosan hydrogel/cellulose acetate-based nanofibers application in mild hyperthermia and skin regeneration. *International journal of biological macromolecules*. https://doi.org/10.1016/j.ijbiomac.2022.12.291.

[255] Xu, Z. *et al.* (2020). Advances and Impact of Antioxidant Hydrogel in Chronic Wound Healing. *Advanced Healthcare Materials*. https://doi.org/10.1002/adhm.201901502.

[256] Stefanov, I. *et al.* (2017). Multifunctional Enzymatically Generated Hydrogels for Chronic Wound Application. *Biomacromolecules*. https://doi.org/10.1021/acs.biomac.7b00111.

[257] Rocasalbas Lozano, G. *Development of multifunctional biopolymeric materials for treatment of decubitus ulcers*.

[258] Helaehil, J.V. *et al.* (2023). Electrical Stimulation Therapy and HA/TCP Composite Scaffolds Modulate the Wnt Pathways in Bone Regeneration of Critical-Sized Defects. *Bioengineering*. https://doi.org/10.3390/bioengineering10010075.

[259] Biswal, A. *et al.* (2025). Nano CaCO3 mediated in vitro and in vivo wound healing characteristics of chitosan films without added drugs. *International Journal of Biological Macromolecules*. https://doi.org/https://doi.org/10.1016/j.ijbiomac.2025.142057.

[260] Li, H. *et al.* (2025). Novel injectable self-healing bifunctionalized chitosan hydrogel with cell proliferation and antibacterial activity for promoting wound healing. *International Journal of Biological Macromolecules*. https://doi.org/https://doi.org/10.1016/j.ijbiomac.2025.141259.

[261] Smeriglio, A. *et al.* (2017). Proanthocyanidins and hydrolysable tannins: occurrence, dietary intake and pharmacological effects. *British Journal of Pharmacology*. https://doi.org/https://doi.org/10.1111/bph.13630.

[262] Ke, C.L. *et al.* (2021). Antimicrobial actions and applications of Chitosan. *Polymers*. https://doi.org/10.3390/polym13060904.

[263] Guo, X. and Mei, N. (2014). Assessment of the toxic potential of graphene family nanomaterials. *Journal of Food and Drug Analysis*. https://doi.org/https://doi.org/10.1016/j.jfda.2014.01.009.

[264] Fernández, K. *et al.* (2023). Self-Assembled CNF/rGO/Tannin Composite: Study of the Physicochemical and Wound Healing Properties. *Polymers*. https://doi.org/10.3390/polym15122752.

[265] Zuo, L. *et al.* (2023). Preparation and characterization of tannin-maltodextrin-polyvinyl alcohol hydrogel based on hydrogen bonding for wound healing. *Journal of the Mechanical Behavior of Biomedical Materials*. https://doi.org/https://doi.org/10.1016/j.jmbbm.2023.105942.

[266] Li, D. *et al.* (2024). Cellulose nanofibers embedded chitosan/tannin hydrogel with high antibacterial activity and hemostatic ability for drug-resistant bacterial infected wound healing. *Carbohydrate Polymers*. https://doi.org/10.1016/j.carbpol.2023.121687.

[267] Su, X. *et al.* (2017). Wound-healing promoting effect of total tannins from Entada phaseoloides (L.) Merr. in rats. *Burns*. https://doi.org/https://doi.org/10.1016/j.burns.2016.10.010.

[268] Sun, W. *et al.* (2024). Quaternary ammonium grafted chitosan hydrogel with enhanced antibacterial performance as tannin acid and deferoxamine carrier to promote diabetic

wound healing. *Colloids and Surfaces B: Biointerfaces*. https://doi.org/https://doi.org/10.1016/j.colsurfb.2024.114160.

[269] Hernandes, L. *et al.* (2010). Wound-healing evaluation of ointment from Stryphnodendron adstringens (barbatimão) in rat skin. *Article Brazilian Journal of Pharmaceutical Sciences*.

[270] Elhami, N. *et al.* (2024). Development of nanocomposites based on chitosan/reduced graphene oxide for wound healing application. *International Journal of Biological Macromolecules*. https://doi.org/https://doi.org/10.1016/j.ijbiomac.2023.128832.

[271] Pinto, S.C.G. *et al.* (2015). Stryphnodendron adstringens: Clarifying Wound Healing in Streptozotocin-Induced Diabetic Rats. *Planta Medica*. https://doi.org/10.1055/s-0035-1546209.

[272] Li, L. *et al.* (2023). Pilose antler extract restores type I and III collagen to accelerate wound healing. *Biomedicine & Pharmacotherapy*. https://doi.org/https://doi.org/10.1016/j.biopha.2023.114510.

[273] Kumar, T. *et al.* (2015). HERBAL PLANTS WITH POTENTIAL OF WOUND HEALING ACTIVITY: A REVIEW ARTICLE. *www.wjpps.com* |. https://doi.org/10.20959/wjpps20233-24260.

[274] Vitale, S. *et al.* (2022). Phytochemistry and Biological Activity of Medicinal Plants in Wound Healing: An Overview of Current Research. *Molecules*. https://doi.org/10.3390/molecules27113566.

[275] Mathew-Steiner, S.S. *et al.* (2021). Collagen in wound healing. *Bioengineering*. https://doi.org/10.3390/bioengineering8050063.

[276] Merkel, J.R. *et al.* (1988). Type I and type III collagen content of healing wounds in fetal and adult rats. *Proceedings of the Society for Experimental Biology and Medicine. Society for Experimental Biology and Medicine (New York, N.Y.)*. https://doi.org/10.3181/00379727-187-42694.

[277] Rodrigues, D.F. *et al.* (2017). Treatment of excisional wound in rabbits with barbatiman extracts associated with autologous bone marrow mononuclear cells. *SCielo*. https://doi.org/10.1590/1678-4162-9301.

[278] Arranz-Valsero, I. *et al.* (2014). IL-6 as a corneal wound healing mediator in an in vitro scratch assay. *Experimental Eye Research*. https://doi.org/https://doi.org/10.1016/j.exer.2014.06.012.

[279] Sato, Y. *et al.* (1999). Regulatory Role of Endogenous Interleukin-10 in Cutaneous Inflammatory Response of Murine Wound Healing. *Biochemical and Biophysical Research Communications*. https://doi.org/https://doi.org/10.1006/bbrc.1999.1455.

[280] Shen, T.N.Y. *et al.* (2017). Interleukin-6 stimulates Akt and p38 MAPK phosphorylation and fibroblast migration in non-diabetic but not diabetic mice. *PLoS ONE*. https://doi.org/10.1371/journal.pone.0178232.

[281] Short, W.D. *et al.* (2022). IL-10 promotes endothelial progenitor cell infiltration and wound healing via STAT3. *FASEB Journal*. https://doi.org/10.1096/fj.201901024RR.

[282] Vaidyanathan, L. (2021). Growth factors in wound healing ⇓ a review. *Biomedical and Pharmacology Journal*. https://doi.org/10.13005/bpj/2249.

[283] Bao, P. *et al.* (2009). The Role of Vascular Endothelial Growth Factor in Wound Healing. *Journal of Surgical Research*. https://doi.org/10.1016/j.jss.2008.04.023.

[284] Liu, F. *et al.* (2024). Vascular endothelial growth factor accelerates healing of foot ulcers in diabetic rats via promoting M2 macrophage polarization. *Diabetic Medicine*. https://doi.org/10.1111/dme.15388.

[285] Hwang, J. *et al.* (2023). VEGF-Encoding, Gene-Activated Collagen-Based Matrices Promote Blood Vessel Formation and Improved Wound Repair. *ACS Applied Materials and Interfaces*. https://doi.org/10.1021/acsami.2c23022.

[286] Shams, F. *et al.* (2022). Overexpression of VEGF in dermal fibroblast cells accelerates the angiogenesis and wound healing function: in vitro and in vivo studies. *Scientific Reports*. https://doi.org/10.1038/s41598-022-23304-8.

[287] Lopes, G.C. *et al.* (2005). Influence of extracts of Stryphnodendron polyphyllum Mart. and Stryphnodendron obovatum Benth. on the cicatrisation of cutaneous wounds in rats. *Journal of Ethnopharmacology*. https://doi.org/https://doi.org/10.1016/j.jep.2005.02.019.

[288] Butin-Israeli, V. *et al.* (2019). Neutrophil-induced genomic instability impedes resolution of inflammation and wound healing. *Journal of Clinical Investigation*. https://doi.org/10.1172/JCI122085.

[289] Slater, T.W. *et al.* (2017). Neutrophil Microparticles Deliver Active Myeloperoxidase to Injured Mucosa To Inhibit Epithelial Wound Healing. *The Journal of Immunology*. https://doi.org/10.4049/jimmunol.1601810.

[290] Dzik, J.M. (2014). Evolutionary roots of arginase expression and regulation. *Frontiers in Immunology*. https://doi.org/10.3389/fimmu.2014.00544.

[291] Paduch, K. *et al.* (2019). Resolution of Cutaneous Leishmaniasis and Persistence of Leishmania major in the Absence of Arginase 1 . *The Journal of Immunology*. https://doi.org/10.4049/jimmunol.1801249.

[292] Crompton, R.A. *et al.* (2022). An Epidermal-Specific Role for Arginase1 during Cutaneous Wound Repair. *Journal of Investigative Dermatology*. https://doi.org/10.1016/j.jid.2021.09.009.

[293] Yan, C. *et al.* (2016). Targeting Imbalance between IL-1β and IL-1 Receptor Antagonist Ameliorates Delayed Epithelium Wound Healing in Diabetic Mouse Corneas. *The American Journal of Pathology*. https://doi.org/https://doi.org/10.1016/j.ajpath.2016.01.019.

[294] Chamberlain, C.S. *et al.* (2013). Interleukin Expression after Injury and the Effects of Interleukin-1 Receptor Antagonist. *PLoS ONE*. https://doi.org/10.1371/journal.pone.0071631.

[295] Perrault, D.P. *et al.* (2018). Local Administration of Interleukin-1 Receptor Antagonist Improves Diabetic Wound Healing. *Annals of plastic surgery*. https://doi.org/10.1097/SAP.0000000000001417.

[296] Nicolli, Elizabeth A *et al.* (2015). IL-1 Receptor Antagonist Inhibits Early Granulation Formation. *Annals of Otology, Rhinology & Laryngology*. https://doi.org/10.1177/0003489415610588.

[297] Murray, P.J. and Wynn, T.A. (2011). Protective and pathogenic functions of macrophage subsets. *Nature Reviews Immunology*. https://doi.org/10.1038/nri3073.

[298] Qian, J. *et al.* (2024). GelMA loaded with exosomes from human minor salivary gland organoids enhances wound healing by inducing macrophage polarization. *Journal of Nanobiotechnology* . https://doi.org/10.1186/s12951-024-02811-y.

[299] Gandolfi, S. *et al.* (2024). The role of adipose tissue-derived stromal cells, macrophages and bioscaffolds in cutaneous wound repair. *Biology direct*. https://doi.org/10.1186/s13062-024-00534-6.

[300] Song, X. *et al.* (2023). Exosomes from tannic acid-stimulated macrophages accelerate wound healing through miR-221-3p mediated fibroblasts migration by targeting CDKN1b. *International Journal of Biological Macromolecules*. https://doi.org/https://doi.org/10.1016/j.ijbiomac.2023.125088.

[301] Utpal, B.K. *et al.* (2024). Polyphenols in wound healing: unlocking prospects with clinical applications. *Naunyn-Schmiedeberg's Archives of Pharmacology*. https://doi.org/10.1007/s00210-024-03538-1.

[302] Trinh, X.T. *et al.* (2022). A Comprehensive Review of Natural Compounds for Wound Healing: Targeting Bioactivity Perspective. *International Journal of Molecular Sciences*. https://doi.org/10.3390/ijms23179573.

[303] Kim, S.J. *et al.* (2003). Swelling kinetics of interpenetrating polymer hydrogels composed of poly(vinyl alcohol)/chitosan. *Journal of Macromolecular Science - Pure and Applied Chemistry*. https://doi.org/10.1081/MA-120019888.

[304] Ostrowska-Czubenko, J. *et al.* (2015). pH-responsive hydrogel membranes based on modified chitosan: water transport and kinetics of swelling. *Journal of Polymer Research*. https://doi.org/10.1007/s10965-015-0786-3.

[305] Ghani, S.M.M. *et al.* (2023). Amine Infused Fly Ash Grafted Acrylic Acid/Acrylamide Hydrogel for Carbon Dioxide (CO2) Adsorption and Its Kinetic Analysis. *Gels*. https://doi.org/10.3390/gels9030229.

[306] Kipcak, A.S. *et al.* (2014). Modeling and Investigation of the Swelling Kinetics of Acrylamide-Sodium Acrylate Hydrogel. *Journal of Chemistry*. https://doi.org/10.1155/2014/281063.

[307] Grigoraș, C.G. *et al.* (2023). Exploration of Reactive Black 5 Dye Desorption from Composite Hydrogel Beads—Adsorbent Reusability, Kinetic and Equilibrium Isotherms. *Gels*. https://doi.org/10.3390/gels9040299.

[308] Bocalandro, C. *et al.* (2012). Comparison of the composition of Pinus radiata bark extracts obtained at bench- and pilot-scales. *Industrial Crops and Products*. https://doi.org/https://doi.org/10.1016/j.indcrop.2012.01.001.